

Electronic Thesis and Dissertation Repository

12-8-2017 10:00 AM

Evaluating Small Airways Disease in Asthma and COPD using the Forced Oscillation Technique and Magnetic Resonance Imaging

Heather M. Young
The University of Western Ontario

Supervisor
Parraga, Grace E.
The University of Western Ontario

Graduate Program in Medical Biophysics
A thesis submitted in partial fulfillment of the requirements for the degree in Master of Science
© Heather M. Young 2017

Follow this and additional works at: <https://ir.lib.uwo.ca/etd>



Part of the [Medical Biophysics Commons](#)

Recommended Citation

Young, Heather M., "Evaluating Small Airways Disease in Asthma and COPD using the Forced Oscillation Technique and Magnetic Resonance Imaging" (2017). *Electronic Thesis and Dissertation Repository*. 5084.
<https://ir.lib.uwo.ca/etd/5084>

This Dissertation/Thesis is brought to you for free and open access by Scholarship@Western. It has been accepted for inclusion in Electronic Thesis and Dissertation Repository by an authorized administrator of Scholarship@Western. For more information, please contact wlsadmin@uwo.ca.

Abstract

Obstructive lung disease, including asthma and chronic obstructive pulmonary disease (COPD), is characterized by heterogeneous ventilation. Unfortunately, the underlying structure-function relationships and the relationships between measurements of heterogeneity and patient quality-of-life in obstructive lung disease are not well understood. Hyperpolarized noble gas MRI is used to visualize and quantify ventilation distribution and the forced oscillation technique (FOT) applies a multi-frequency pressure oscillation at the mouth to measure respiratory impedance to airflow (including resistance and reactance). My objective was to use FOT, ventilation MRI and computational airway tree modeling to better understand ventilation heterogeneity in asthma and COPD. FOT-measured respiratory system impedance was correlated with MRI ventilation heterogeneity and both were related to quality-of-life in asthma and COPD. FOT-measurements and model-predictions of reactance and small-airways resistance were correlated in asthma and COPD respectively. This study is the first to demonstrate the relationships between FOT-measured impedance, MRI ventilation heterogeneity, and patient quality-of-life.

Keywords

Obstructive Lung Disease, Asthma, Chronic Obstructive Pulmonary Disease, Forced Oscillation Technique, Lung Biomechanics, Magnetic Resonance Imaging, Hyperpolarized ^3He , Pulmonary Imaging, Imaging Biomarkers

Co-Authorship Statement

The following thesis contains one manuscript that has been submitted for publication. As the first author of this manuscript, I was a significant contributor to all aspects of the study as well as the manuscript preparation and submission. Specific tasks included: organization and management of patient study visits, acquisition of pulmonary function test and noble gas MRI data. Following data acquisition, tasks included: image analysis, statistical analysis and interpretation, clinical/physiological interpretation of the data, drafting and final approval of the manuscript. Dr. Grace Parraga, as the Principal Investigator and Supervisor, provided ongoing guidance and was responsible for study conception and experimental design, data analysis and interpretation, drafting and approval of the manuscripts. She was also the guarantor of integrity of the data and responsible for Good Clinical Practice. Patient study visits and acquisition of pulmonary function data was performed under the supervision of Sandra Blamires and Lyndsey Reid-Jones. Polarization of the ^3He gas was performed by Andrew Wheatley, Dante PI Capaldi and me. MRI acquisition was performed by Trevor Szekeres and David Reese. Listed below are the specific contributions for all other co-authors for the manuscript contained in this thesis.

Chapter 2 is an original research article entitled “Oscillometry and Pulmonary MRI of Ventilation Heterogeneity in Obstructive Lung Disease: Relationship to Quality of Life and Disease Control” and it was submitted to the Journal of Applied Physiology on November 15, 2017. The manuscript was co-authored by Heather M Young, Dr. Fumin Guo, Rachel L Eddy, Dr. Geoffrey Maksym, and Dr. Grace Parraga. As first author I collected, analyzed and interpreted the data, and I prepared the written manuscript. Dr. Fumin Guo assisted with data analysis and interpretation and Rachel L Eddy assisted with data collection and interpretation. Dr. Geoffrey Maksym assisted with data interpretation and revisions to the manuscript.

Acknowledgments

I would like to first thank my supervisor, Dr. Grace Parraga. You provided me with countless opportunities to conduct innovative research, to work directly with patients and to develop many new skills that will benefit me for years to come. You pushed me to work hard, be assertive and to push myself to do my very best work. The experience you provided to me as a trainee has been invaluable.

I would also like to thank the members of my advisory committee: Dr. Geoffrey Maksym, Dr. Maria Drangova, and Dr. Hanif Ladak. Your support and advice made my research stronger, and I am grateful for the time you took to provide feedback and direction as I navigated my degree.

To all the other members of the Parraga lab, you are an outstanding team and your support made this work possible. After all, team work makes the dream work! To Lyndsey Reid-Jones, thank you for your clinical insight and for reminding me that everyone just wants to have a conversation like a human. To Dave Reese, thank you for your help and co-operation with all of our imaging needs, and for your commitment to helping us acquire the best images we can. To Dr. Alexei Ouriadov, thank you for teaching me about diffusion imaging and about MRI physics. To Khadija, thank you for being such a strong role model and for teaching me so much when I joined the lab. You provided endless patience and support, and it made a world of difference in tackling the steep learning curve I faced. To Fumin, thank you for your help with image processing and for the evening chats at Robarts. To Dante, thank you for teaching me about polarization, image processing and MRI. Thank you for the many interesting conversations about MRI, research, careers and more. To Rachel, thank you for teaching me about working with patients and collecting data, and for your critical eye for my writing. To Eric, thank you for your encouragement, for teaching me about diffusion imaging and for your bad jokes- they still made me laugh. To Andrew, thank you for the positive attitude you bring every day and for asking questions that make me think more deeply about my research. Thank you to the other past and present members of the lab who help make our research possible: Anurag Bhalla, Sarah Svenningsen, Andrea Kassay, Robert DiCesare and Matthew Schweers.

There are many other students and staff at Robarts who I want to thank for their support. Olivia, thank you for sharing in lots of good food and conversations about MRI, research, sanity, and your latest crazy book. Megan, thanks for the great conversations over coffee and lunch. Thanks also to Amanda, Amy, Dickson, Derek, Tomi, and my fellow Robarts trainees. The strong research community at Robarts is an important part of what made this experience so memorable.

Finally, I want to express my gratitude to Brandon, my family and my friends. Brandon, thank you for your partnership in facing new challenges, and for always providing a positive attitude and perspective. To my parents, thank you for the constant support of my goals, and for checking in to make sure I am eating well. To Sarah, thanks for the visits and all our laughs. The support of family and friends has made this possible.

Table of Contents

Abstract	i
Co-Authorship Statement	ii
Acknowledgments	iii
Table of Contents	v
List of Tables	viii
List of Figures	ix
List of Appendices	xi
List of Abbreviations	xii
CHAPTER 1	1
1 INTRODUCTION	1
1.1 Motivation and Rationale	1
1.2 Lung Structure, Function, and Biomechanics	4
1.2.1 The Conducting Airways	4
1.2.2 The Peripheral Airways and Alveoli.....	5
1.2.3 Ventilation.....	7
1.3 Pathophysiology of Obstructive Lung Disease	7
1.3.1 Asthma	8
1.3.2 COPD	8
1.4 Clinical Measurements of Lung Function	9
1.4.1 Spirometry.....	10
1.4.2 Plethysmography.....	11
1.4.3 Diffusing Capacity of the Lung	12
1.4.4 Disease Control and Quality of Life	12
1.4.5 Obstructive Lung Disease	12

1.5 Emerging Clinical Measurements of Lung Function	13
1.5.1 Mechanical Properties of the Lung	13
1.5.2 The Forced Oscillation Technique.....	14
1.6 Imaging Measurements of Lung Structure and Function	16
1.6.1 Structural and Anatomical Imaging.....	17
1.6.2 Functional Imaging.....	20
1.6.3 Inhaled Noble Gas Magnetic Resonance Imaging.....	21
1.7 Biomechanical Modeling of the Lung	24
1.7.1 Inverse Modeling	24
1.7.2 Forward Modeling	26
1.7.3 Pulmonary Imaging and Biomechanical Modeling	27
1.8 Thesis Objectives and Hypotheses	28
1.9 References	29
CHAPTER 2	36
2 OSCILLOMETRY AND PULMONARY MRI OF VENTILATION HETEROGENEITY IN OBSTRUCTIVE LUNG DISEASE: RELATIONSHIP TO QUALITY OF LIFE AND DISEASE CONTROL	36
2.1 Introduction	36
2.2 Materials and Methods	38
2.2.1 Study Design.....	38
2.2.2 Image Acquisition and Analysis	39
2.2.3 Computational Modeling	40
2.2.4 Statistics	42
2.3 Results	43
2.3.1 Participant Demographics.....	43
2.3.2 FOT and ³ He MRI VDP Relationships.....	46
2.3.3 Relationships with Disease Control and Quality of Life Scores.....	48

2.3.4	Experimental and Model Impedance Measurements	52
2.4	Discussion	52
2.4.1	FOT and ³ He MRI Ventilation Heterogeneity	53
2.4.2	FOT, Disease Control and Quality of Life.....	54
2.4.3	Measured Impedance and Image Functional Modeling.....	55
2.4.4	Limitations	55
2.4.5	Conclusions.....	56
2.5	References	57
CHAPTER 3	64
3	CONCLUSIONS AND FUTURE DIRECTIONS	64
3.1	Overview and Research Questions	64
3.2	Summary and Conclusions	64
3.3	Limitations	65
3.4	Future Directions	66
3.4.1	FOT Biomarkers in Severe Asthmatics Undergoing Bronchial Thermoplasty	66
3.4.2	FOT Biomarkers and Higher-Order Image Features in ³ He MRI.....	67
3.4.3	Image Functional Modeling Incorporating all MRI Ventilation.....	68
3.5	Significance and Impact	68
3.6	References	70
4	APPENDIX	71

List of Tables

Table 1-1: GOLD COPD Severity Grade	9
Table 2-1: Participant Demographics	43
Table 4-1. Pulmonary Imaging-Derived Biomechanical Measurements.....	88
Table 4-2. Recent Pulmonary Imaging Studies of Biomechanics	93

List of Figures

Figure 1-1 Global Deaths Due to Chronic Respiratory Disease.....	1
Figure 1-2 Schematic of the Human Airway Tree.....	6
Figure 1-3: Small Airway Pathology in Asthma and COPD	9
Figure 1-4 Pulmonary Function Testing: Spirometry.....	10
Figure 1-5 Pulmonary Function Testing: Plethysmography.....	11
Figure 1-6 Frequency Dependence of the Forced Oscillation Technique	16
Figure 1-7 Computed Tomography of COPD and Asthma	19
Figure 1-8 ³ He Ventilation MRI of COPD and Asthma.....	23
Figure 1-9: Linear Single Compartment Model of the Lung.....	25
Figure 2-1: Pipeline for Co-Registration of MRI Ventilation Defects with Computational Airway Tree Model.....	42
Figure 2-2: VDP and FOT-measured Resistance and Reactance in Asthma, COPD and Ex- Smoker Subgroups.....	45
Figure 2-3: Relationships for VDP and FOT measurements	47
Figure 2-4: Differences in FEV ₁ , VDP and FOT Impedance Stratified by Disease Control..	49
Figure 2-5: Relationships between FOT-measured Resistance and MRI VDP with Quality of Life.....	51
Figure 2-6. Relationships for Model-predicted and FOT-measured Respiratory System Impedance.....	52
Figure 4-1. Respiratory System Mechanics and Function.....	86
Figure 4-2. Pulmonary Imaging Biomarkers of Lung Biomechanics.....	88

Figure 4-3. Mouse Lung Micro-CT	96
Figure 4-4 Synchrotron Radiation X-ray Micro-CT of Mouse Lung Microstructure Deformation.	98
Figure 4-5. Diffusion-Weighted ^3He and ^{129}Xe MRI Mean Linear Intercept and ADC Maps	100
Figure 4-6. Diffusion-weighted MRI Derived Regional Pressure-Volume Curves	102
Figure 4-7. Clinical CT Measurements of Pulmonary Structure and Function	103
Figure 4-8. Mapping the Distance between Healthy and Emphysematous Voxels	105
Figure 4-9. Static Breath-hold ^3He and ^{129}Xe Ventilation MRI.....	107
Figure 4-10. Ventilation MRI and CT of Obstructive Lung Disease	111
Figure 4-11. MR and CT Imaging of Lung Structure and Function.....	113

List of Appendices

Appendix A – Asthma Control Questionnaire.....	71
Appendix B – Asthma Quality of Life Questionnaire	73
Appendix C – St. George’s Respiratory Questionnaire	79
Appendix D – MRI and CT Lung Biomarkers: Towards an <i>In Vivo</i> Understanding of Lung Biomechanics	85
Appendix E – Permission for Reproduction of Scientific Articles.....	126
Appendix F – Health Science Research Ethics Board Approval Notices.....	128
Appendix G – Curriculum Vitae.....	131

List of Abbreviations

AATD	Alpha-1 Antitrypsin Deficiency
ACQ	Asthma Control Questionnaire
AQLQ	Asthma Quality of Life Questionnaire
BPD	Bronchopulmonary Dysplasia
COPD	Chronic Obstructive Pulmonary Disease
CT	Computed Tomography
DL _{CO}	Diffusing Capacity of the Lung for Carbon Monoxide
ES	Ex-Smoker
FEV ₁	Forced Expiratory Volume in 1 Second
FOT	Forced Oscillation Technique
FRC	Functional Residual Capacity
FVC	Forced Vital Capacity
¹ H	Proton
³ He	Helium-3
HU	Hounsfield Unit
IC	Inspiratory Capacity
MRI	Magnetic Resonance Imaging
mSv	Milisieverts
RA ₉₅₀	Relative Area Under -950 HU
R _{aw}	Airways Resistance
PFT	Pulmonary Function Test
Rb	Rubidium
R _{rs}	Respiratory System Resistance
RV	Residual Volume
SGRQ	St. George's Respiratory Questionnaire
TCV	Thoracic Cavity Volume
TLC	Total Lung Capacity
TV	Tidal Volume
UTE	Ultra-short Echo Time
VC	Vital Capacity
VDP	Ventilation Defect Percent
¹²⁹ Xe	Xenon-129
X _{rs}	Respiratory System Reactance
Z _{rs}	Respiratory System Impedance

CHAPTER 1

1 INTRODUCTION

Ventilation heterogeneity is a hallmark characteristic of obstructive lung diseases such as asthma and chronic obstructive pulmonary disease (COPD), and is related to airflow obstruction. In this thesis, the nature of ventilation heterogeneity is studied using measurements of biomechanical properties of the lung, pulmonary imaging and computational modeling of lung mechanics to better understand how these measures are related to patient outcomes.

1.1 Motivation and Rationale

Obstructive lung disease creates a tremendous global burden; chronic obstructive pulmonary disease (COPD) affects 175 million people worldwide and was responsible for 3.2 million deaths in 2015.¹ Asthma is the most prevalent chronic respiratory disease worldwide, affecting 358 million people, and was responsible for 0.4 million deaths in 2015.¹ Among all chronic respiratory diseases, obstructive lung disease is a leading cause of global death, as shown in Figure 1-1.

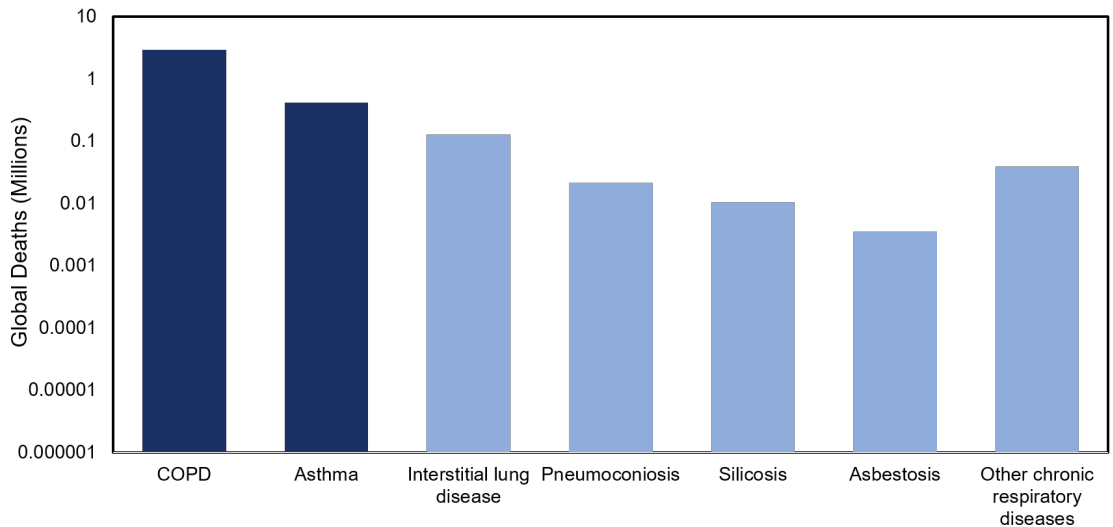


Figure 1-1 Global Deaths Due to Chronic Respiratory Disease

This graph shows the number of deaths globally from chronic lung disease in 2015 using a logarithmic scale. On the left, COPD (n=3.2 million) and asthma (n=0.4 million) are the leading causes of death among all chronic respiratory diseases. Adapted from GBD 2015 Chronic Respiratory Disease Collaborators, Lancet (2017).¹

Obstructive lung disease also presents a significant health care burden in Ontario and across Canada. In 2011, the total provincial healthcare costs of COPD and asthma were \$1.8 billion and \$3.9 billion respectively.² A significant portion of the health care costs from obstructive lung disease are related to exacerbations, or acute worsening of symptoms in asthma or in COPD patients. Exacerbations may lead to patients seeking emergency room care, or being admitted to the hospital. The health care cost of an exacerbation is variable, but hospitalization is known to contribute the most to exacerbation costs.³ As such, hospitalization is a very important metric to monitor when assessing management of COPD in the Canadian health care system. Across Canada, COPD was the leading cause of hospitalization (except for childbirth) in 2015 and admitted patients remained in hospital for over a week on average.⁴ A 2008 study found that the average cost of a hospital stay for a COPD exacerbation was nearly \$10 000 per patient, with the total cost of COPD hospitalizations estimated to be \$1.5 billion per year.⁵ Poorly controlled asthma also leads to high healthcare costs, in particular through emergency department (ED) visits. A recent survey showed that 93% of Canadians do not have their asthma under control,⁶ and asthma attacks were the cause of over 70,000 ED visits in 2015.⁷ These ED visits and admissions to hospital are large contributors to the economic burden of obstructive lung disease. This overwhelming economic and health care burden reflect limitations in the treatment and management of obstructive lung disease. In part, this is due to our limited understanding of the mechanisms leading to ventilation heterogeneity in these patients, and how these mechanisms are related to patient outcomes.

Obstructive lung disease is characterized by airflow obstruction that is clinically evaluated using measures of airflow taken at the mouth.⁸ Unfortunately, these airflow measurements are known to correlate weakly with patient outcomes⁹ in part because they are global measures of a heterogeneous disease, and in part because they are not sensitive to changes in the periphery of the lung. The forced oscillation technique (FOT) evaluates the biomechanical properties of the lung by applying a multi-frequency pressure wave at the mouth during passive breathing.¹⁰ This technique is easily and inexpensively applied in a clinical setting and can provide information about obstruction in the lung periphery,

making it a very promising tool to improve clinical evaluation and, hopefully, management of disease.

Pulmonary imaging tools are used clinically and in research to image lung structure and function in obstructive lung disease. Using inhaled hyperpolarized ^3He MRI, researchers capture spatial ventilation information and quantify ventilation abnormalities that are known to be related to disease severity^{11, 12} and control.¹³ However, the structural determinants of these abnormalities are not yet fully understood.¹⁴ Imaging measurements of ventilation can be combined with measurements using other techniques (such as FOT) to study structure-function relationships more deeply.

Computational models are used to study biomechanical properties of the lung and the relationships between lung structure and function.¹⁵⁻¹⁷ Modeling studies are advantageous in that they allow the researcher to specify the parameters of the system, and predict the function of the system based on these known parameters. Researchers are then able to study with high precision how the model responds to a known input. Computational modeling has been used to study the effects of the number, severity and spatial distribution of airway closure on respiratory system impedance. Recent studies have used functional imaging data to guide the spatial distribution of ventilation abnormalities, and studied how this is reflected by structural changes to the model.^{18, 19} If biomechanical measurements are acquired using FOT in these same patients, the measured impedance can be compared to model predictions. Unfortunately, only one small study to date has combined functional pulmonary imaging, FOT, and biomechanical modeling in asthma.²⁰ Accordingly, there is a need for larger studies that combine these three modalities to more deeply study structure-function relationships in obstructive lung disease.^{21, 22}

This thesis focuses on the application of FOT, pulmonary MRI and computational lung modeling in asthma and COPD. This chapter provides the background knowledge relevant to the original research presented in Chapter 2. It begins with an overview of the respiratory system's structure and function and the biomechanical processes behind normal respiration **(1.2)**, followed by the pathophysiology of obstructive lung disease **(1.3)**. The established clinical measurements of lung function are addressed next **(1.4)** followed by a discussion

of FOT as an emerging clinical tool (1.5) and current structural and functional pulmonary imaging techniques used in clinic and research (1.6). The final tool to be introduced is biomechanical modeling (1.7). Finally, the specific hypotheses and objectives of this thesis are introduced (1.8).

1.2 Lung Structure, Function, and Biomechanics

The respiratory system is a complex biomechanical system that serves primarily to deliver oxygenated gas to the bloodstream and to remove carbon dioxide. The system is composed of the oral and nasal cavities, the lungs (bronchi, bronchioles, alveolar ducts and alveoli), the diaphragm and the chest wall. The lungs themselves are composed of many soft tissue components including the airways, parenchymal tissue and vasculature.²³ These structures function together to bring oxygenated gas through the airways into the alveoli to participate in gas exchange and then expel the carbon-dioxide rich gas to the surroundings. This section will outline in detail the structures involved in this process, and how they function as part of this system.

1.2.1 The Conducting Airways

From the oral and nasal cavities, gas travels through a series of branching airways as it is carried into the lungs. The entire branching structure is shown in Figure 1-2. From the mouth gas first reaches the trachea, a large hollow tube with cartilage rings for structural support. The trachea branches to form the two main bronchi, which are also supported by cartilage and feed the left and right lungs. Once in the lungs, these main bronchi continue an asymmetrical dichotomous branching pattern. The bronchi, which transport gas throughout the lung, decrease in diameter as they branch while growing geometrically in number. After approximately four branching generations, these bronchi branch into bronchioles. Bronchioles are structurally different from bronchi in that they are no longer structurally supported by cartilage. Instead, these small airways are tethered to the surrounding parenchymal tissue for support. The airway walls of the bronchi are made of soft tissue, blood vessels and smooth muscle fibres which are wrapped circumferentially around the airway to control airway diameter.²³ Bronchioles continue the same branching pattern as the bronchi for approximately 16 branching generations. The airways from the

trachea to the terminal bronchioles are collectively called the conducting zone of the lung as their primary function is to conduct gas from the environment to the alveoli for gas exchange. In these airways, airflow is restricted by the airway diameter and is well described by Womersley flow as described in Section 1.7.2. It should be noted that the conducting airways are larger in diameter, but there are far fewer of them than small peripheral airways. As a result, the total cross-sectional diameter is smaller and the resistance to airflow is much larger in the conducting airways than in the peripheral airways. The terminal airway resistance is negligible in comparison, and therefore does not contribute to traditional measurements of airflow at the mouth which are discussed in Section 1.4.1.

1.2.2 The Peripheral Airways and Alveoli

The peripheral airways begin at the bronchioles and after approximately 16 branching generations, the terminal bronchioles branch into the respiratory bronchioles. This marks the start of the respiratory zone, so called because this is the generation at which alveoli are present and gas exchange starts to occur.²³ The respiratory zone makes up the final 7 generations of the airway tree. As shown in Figure 1-2, the respiratory bronchioles branch into the alveolar ducts, which are smaller in diameter and are surrounded by more alveoli. The ducts then branch into the terminal airways, called the alveolar sacs. The alveolar sacs are approximately 0.2mm in diameter, and are surrounded completely by alveoli to maximize the surface area available for gas exchange. The airways in the respiratory zone have a very small diameter, but there are many more of them than in earlier branching generations. As a result, they have a very large cross-sectional area and gas travels through them by diffusion rather than flow.

Alveoli are small sac structures, approximately 300µm in diameter.²³ They line the terminal airways in clusters, maximizing the surface area that is available for gas exchange. While these structures are very small, there are approximately 480 million alveoli in the average adult lung,²⁴ creating a very large functional surface area of approximately 85 square metres.²³ Alveoli do not have any supporting muscle tissue, but are also tethered to the surrounding parenchymal tissue for structural support. They are extremely thin (0.2-

0.3 μm)²³ in order to maximize diffusion of oxygen and carbon dioxide between the alveoli and the surrounding capillaries.

Due to the dichotomous branching structure of the airway tree, 50% of the total lung resistance originates from the large, central airways and only 10% of the resistance from the small airways (i.e., <2 mm in diameter). In passive breathing, the remaining 40% of the resistance derives from the mechanical properties of the lung tissue.²⁵ For this reason, the peripheral airways are referred to as the ‘quiet’²⁶ or ‘silent’²⁷ zone, referring to the fact that COPD is known to originate in the small airways and terminal airspaces²⁸ but these early stages are not reflected in clinical measurements such as spirometry. As a bulk airflow measurement, spirometry is largely sensitive to the central airways that contribute the most resistance and relatively insensitive to changes in the small airways.

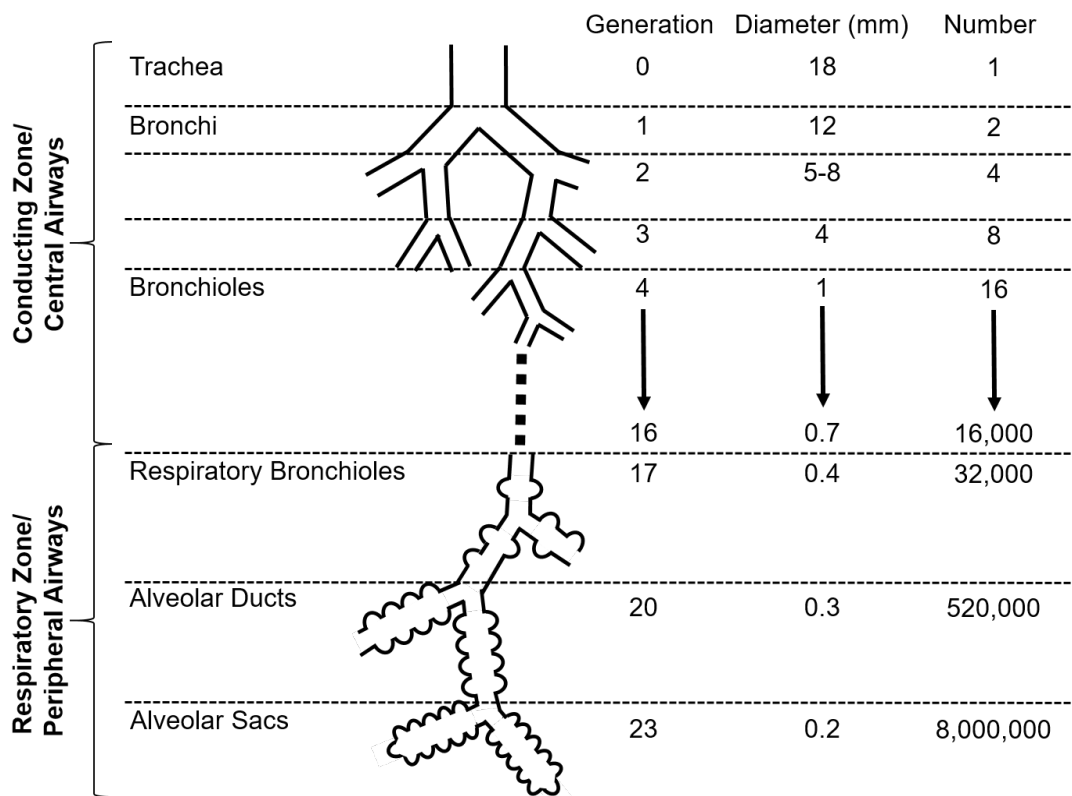


Figure 1-2 Schematic of the Human Airway Tree

The conducting airways are made up of the first 16 generations of branching airways, and are responsible for conducting gas to the alveoli for gas exchange. The final 7 branching generations make up the respiratory zone, and are lined with alveoli for gas exchange. Adapted from West, JB, *Respiratory Physiology: The Essentials*, Ninth Edition.²³ and Lumb, AB, *Nunn’s Applied Respiratory Physiology*.²⁹

1.2.3 Ventilation

Ventilation is the flow of gas into (or out of) the lungs, achieved by the biomechanical process of breathing. This complex process occurs by action of the intercostal muscles, abdominal muscles and the diaphragm. To inhale, these muscles all contract, bringing the diaphragm down and the ribs outward. This motion decreases the pressure in the thoracic cavity, causing gas to flow inward through the airways.²³ As previously mentioned, the motion of the gas is best described by flow in the conducting airways, and by diffusion in the respiratory bronchioles and alveolar ducts where the combined cross-sectional area is very large. Airflow mechanics in the airways will be discussed in detail in Section 1.7.2. Once the oxygenated gas reaches the alveoli, gas exchange occurs; oxygen diffuses into the capillaries through the thin membrane of the airway wall and carbon dioxide simultaneously diffuses out of the blood and into the alveoli. Expiration is a passive manoeuvre, during which the intercostal muscles, abdominal muscles and diaphragm relax. Recoil forces in the lung cause the diaphragm to rise and the ribs contract, causing the pressure in the thoracic cavity to increase and gas to flow back out of the lungs through the airways, carrying with it the carbon dioxide to be removed from the body.²³ It is important to note that ventilation and gas exchange are dependent on both the central and peripheral airways. If any obstruction causes resistance in the airways to increase, the same pressure differential will produce a lower rate of airflow, impeding the lung in performing its functional task.

1.3 Pathophysiology of Obstructive Lung Disease

Obstructive lung disease is characterized by persistent airflow limitation measured at the mouth. Importantly, the obstruction to airflow is not uniformly distributed throughout the lungs but rather, it is heterogeneous. Airflow obstruction can be caused by changes in the airway lumen, the airway wall or the peribronchial region, leading to the ventilation heterogeneity that is characteristic of obstructive lung disease. This thesis will focus on the two dominant forms of obstructive lung disease: asthma and COPD.

1.3.1 Asthma

Asthma is a chronic respiratory condition characterized by variable airflow limitation accompanied by shortness of breath, wheeze and a feeling of tightness in the chest;³⁰ these symptoms are usually reversible using an inhaled bronchodilator. Asthma can begin in childhood or adulthood, and affects many people throughout their adult lives. Airflow limitation in asthma is caused by narrowing of the airway lumen due to increased smooth muscle responsiveness, inflammation, and abnormal mucus production as illustrated in Figure 3.³¹ This narrowing has been observed in both the central and peripheral airways in histopathological studies.³² Airway inflammation is a multi-cellular process, but is characterized by eosinophils in asthma. The increased presence eosinophils in the airway walls promotes airway constriction, increasing the effect of smooth muscle constriction and decreasing the tethering forces of the parenchyma.³³ Increased smooth muscle mass in the airways is common in asthma and also contributes to thickening of the airway wall and narrowing of the lumen. Often the airway smooth muscle is hyperresponsive, meaning it excessively constricts in response to stimuli, causing severe airway narrowing and increased resistance to airflow. These cases of sudden acute airway obstruction are referred to as an asthma attack.

1.3.2 COPD

Chronic obstructive pulmonary disease (COPD) is characterized by chronic airflow obstruction that cannot be reversed using a bronchodilator. COPD develops over a patient's life as a result of exposure to cigarette smoke (the primary risk factor for COPD),³⁴ environmental irritants, or due to genetic conditions such as alpha-1 antitrypsin deficiency.³⁵ Exposure to these factors causes an inflammatory response in the small airways and alveoli that is associated with the destruction of alveolar tissue over time. This process leads to airflow limitations due to a loss of elastic recoil in the lung tissue,^{36, 37} small airway collapse due to loss of parenchymal tethering³¹ and inflammation in the small airways. Obstruction can also occur in the small airways as a result of excessive mucous production, as illustrated in Figure 3.

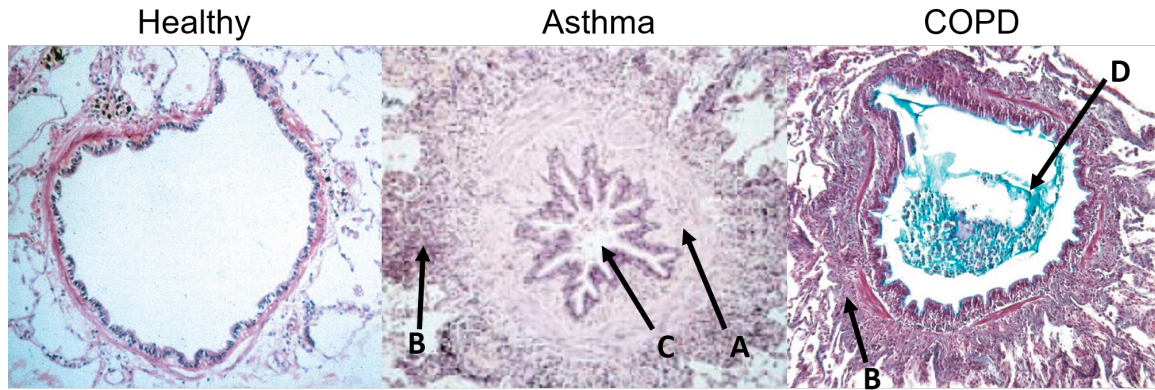


Figure 1-3: Small Airway Pathology in Asthma and COPD

Small airway changes from a healthy lung (left) to asthma (middle) and COPD (right). In asthma, thickening and contraction of the smooth muscle (A), as well as inflammation and thickening of the airway wall (B) contribute to airway narrowing (C). In COPD, there is inflammation and thickening of the airway wall (B), as well as an accumulation of excess mucus in the lumen (D). Adapted from Hogg JC, *Lancet* (2004)³⁸ and Saetta M *et al.* *Eur Respir J* (2001).³³

The severity of airflow obstruction as measured by spirometry (described in detail in Section 1.4.1) has been standardized and is used to classify COPD subjects into four severity grades³⁹ as shown in Table 1-1.

Table 1-1: GOLD COPD Severity Grade

If $FEV_1/FVC < 70\%$:		
GOLD I	Mild	$FEV_1 > 80\%_{pred}$
GOLD II	Moderate	$50\% \leq FEV_1 < 80\%_{pred}$
GOLD III	Severe	$30\% \leq FEV_1 < 50\%_{pred}$
GOLD IV	Very Severe	$FEV_1 < 30\%_{pred}$

FEV_1 : forced expiratory volume in 1 second; FVC: forced vital capacity

1.4 Clinical Measurements of Lung Function

Clinically, there are several tests used to evaluate a patient's lung function for diagnosis or monitoring of obstructive lung disease. Physicians primarily rely on pulmonary function tests (PFTs) to evaluate lung function in the clinic. These tests involve a variety of breathing manoeuvres and measurements made at the mouth that provide information about

how the lungs are functioning as a whole. This section introduces spirometry, plethysmography, diffusing capacity of the lung for carbon monoxide and clinical questionnaires used to measure disease control and quality of life. Measurements of volume and airflow are often presented as a percent of the predicted value ($\%_{\text{pred}}$) based on the patient's age, sex, height, and ethnicity.⁴⁰

1.4.1 Spirometry

Spirometry can be performed using a handheld spirometer like the one shown on the left in Figure 1-4. To perform spirometry, the patient wears nose plugs and begins by breathing normally into the mouthpiece. After approximately 4 normal breaths, the patient is asked to fully inhale until they reach total lung capacity. Then, they sharply and forcefully exhale using maximum effort, and continue to exhale until they cannot expel any more air.⁸ Gas volume and flow are measured using the spirometer throughout this test, and a representative volume-time curve is shown on the right in Figure 1-4. Two measurements are derived from this manoeuver: the forced expiratory volume in 1 second (FEV_1), which is the maximum volume of gas that can be expired in the first second of expiration; and the forced vital capacity (FVC), which is the total volume of gas that the patient can expire from full inspiration.⁸

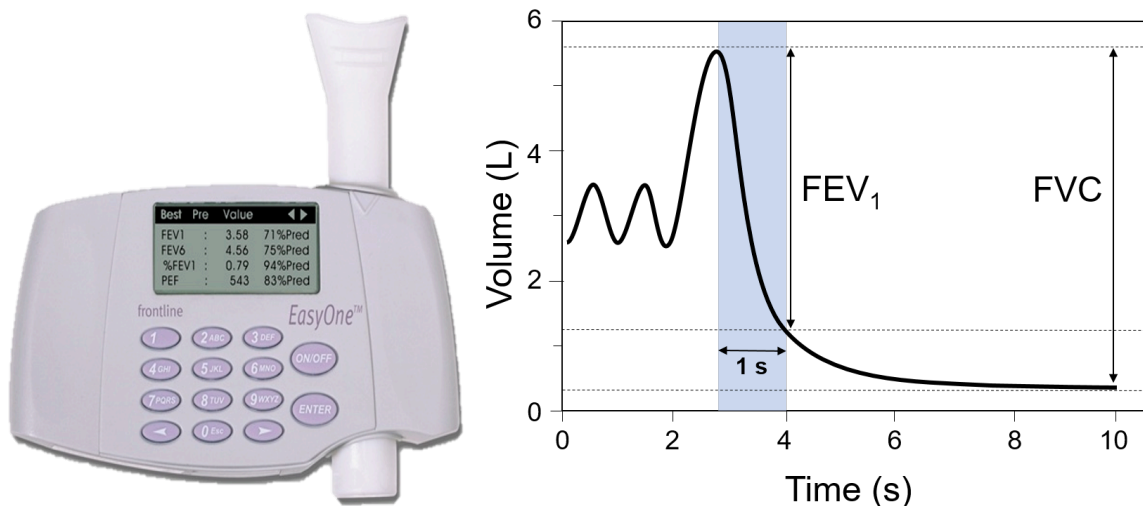


Figure 1-4 Pulmonary Function Testing: Spirometry

Above is a handheld spirometer used to conduct spirometry (left) and the resulting volume-time curve that is used to determine FEV_1 and FVC (right).

1.4.2 Plethysmography

Plethysmography is a technique used to measure lung volumes using Boyle's law.⁴¹ In a seated position inside a sealed chamber, the patient is asked to perform a series of breathing manoeuvres including tidal breathing, full inspiration, and full expiration. Pressure is measured in the chamber throughout this test, while the volume of the sealed chamber is constant. The lung volumes are calculated from these measurements using Boyle's law. The volume-time curve from this test and the measured lung volumes are illustrated in Figure 1-5. The volumes of interest that are calculated from this test are: functional residual capacity (FRC), inspiratory capacity (IC), tidal volume (TV), residual volume (RV), vital capacity (VC) and total lung capacity (TLC).⁴¹ FRC is the remaining volume in the lungs after a normal exhalation, IC is the maximum volume of gas that can be inhaled from FRC, TV is the volume of gas inhaled/exhaled during tidal breathing, RV is the volume of gas remaining in the lungs after maximum exhalation, VC is the volume of gas between total inspiration and total expiration and TLC is the maximum volume of the lungs at full inspiration.⁴¹

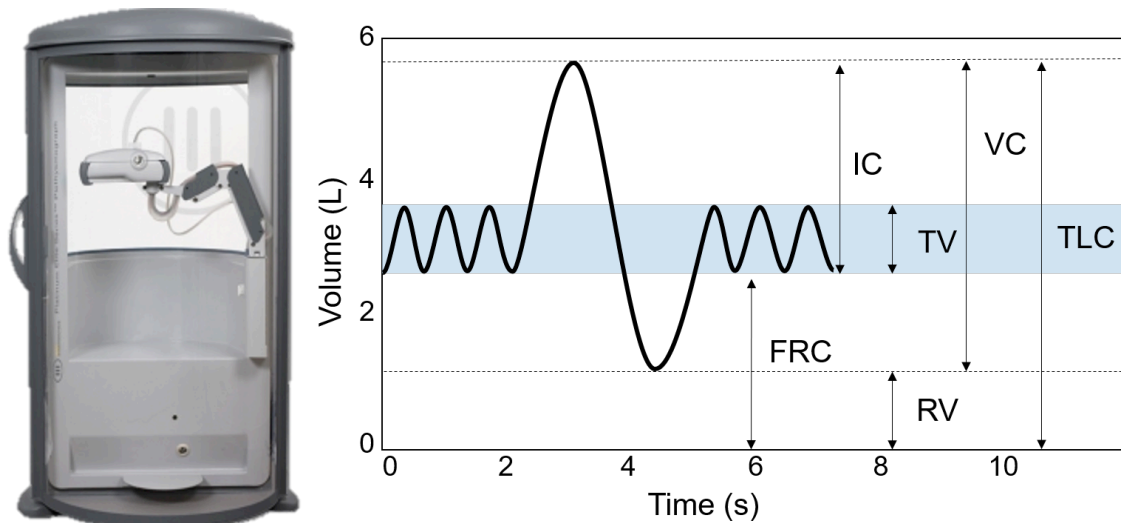


Figure 1-5 Pulmonary Function Testing: Plethysmography

Above is a whole body plethysmograph (left) and a sample volume-time curve used to determine lung volumes (right).

1.4.3 Diffusing Capacity of the Lung

The diffusing capacity of the lung for carbon monoxide (DL_{CO}) is used to evaluate pulmonary function for patients with emphysema.⁴² The test is used to determine the extent to which the destruction of alveolar tissue has reduced the capacity for oxygen to diffuse into the bloodstream. To perform this test, the patient exhales to RV and inhales a specialized test gas containing a low concentration of CO (0.3%) to TLC. The patient then holds their breath for 8 seconds, allowing the CO to diffuse into the bloodstream, and exhales through the mouthpiece. The concentration of CO in the exhaled gas is measured, and compared to the known concentration in the inhaled gas to determine how much diffused into the blood.⁴²

1.4.4 Disease Control and Quality of Life

Asthma control is measured using the Asthma Control Questionnaire (ACQ),⁴³ and quality of life is measured using the Asthma Quality of Life Questionnaire (AQLQ).⁴⁴ The ACQ is designed to collect information about how patients perceive their symptoms, how their symptoms limit their activities and how often they rely on a bronchodilator. It is designed to determine if a patient is achieving the primary goal of asthma treatment- control of the disease. The AQLQ asks more specific questions regarding symptoms and how a patient feels about them. It evaluates how specific symptoms may affect the activities in the patient's day to day life in order to quantify patient health-related quality of life.

In COPD, quality of life is measured using the St. George's Respiratory Questionnaire (SGRQ).⁴⁵ This single questionnaire collects information about patient symptoms, activity, and impacts on daily life. From the complete questionnaire, scores are calculated for each component, as well as an overall score. The ACQ, AQLQ and SGRQ were developed as sensitive standardized methods to quantify quality of life for patients with asthma or COPD for use in scientific studies or clinical care.

1.4.5 Obstructive Lung Disease

The tests described above are all sensitive to the pathology of obstructive lung disease described in Section 1.3. Spirometry measurements such as FEV_1 and FVC are reduced in

obstructive lung disease due to airway obstruction and early airway closure in expiration. This leads to an increase in RV and TLC due to premature airway closure and, in COPD, loss of elastic recoil. COPD patients also have decreased DL_{CO} as a result of alveolar destruction.

1.5 Emerging Clinical Measurements of Lung Function

1.5.1 Mechanical Properties of the Lung

As previously described, the respiratory system functions through the mechanical expansion and contraction of the thoracic cavity which causes oscillations in the pressure inside, resulting in flow through the airways, or ventilation. In order to better understand the process of ventilation, one must understand the relationships between oscillations of pressure and airflow in the lung.

The respiratory system can be modeled as a linear dynamic system, which means that it is described by linear differential equations and it evolves in time. This is explained in greater detail in Section 1.7. Pressure (P) and flow (the time-derivative of volume, \dot{V}) are related by a quantity called respiratory system impedance (Z_{rs}).⁴⁶ Impedance is a complex value, as it describes the relationship for both amplitude and phase between P and \dot{V} as shown in the linear differential equation below (Equation 1.1).

$$P(f) = Z_{rs}(f)\dot{V}(f) \quad (1.1)$$

The real and imaginary components of impedance are called the respiratory system resistance (R_{rs}) and reactance (X_{rs}), respectively, as expressed in Equation 1.2.

$$Z_{rs}(f) = R_{rs}(f) + iX_{rs}(f) \quad (1.2)$$

R_{rs} and X_{rs} are intrinsic properties of the system that affect how the system responds to input. R_{rs} is related to airway lumen calibre; as airways narrow their resistance to airflow increases.⁴⁶ This can occur in obstructive lung disease as a result of inflammation, smooth muscle constriction, or excessive mucus production as explained in Section 1.3. X_{rs} is related to elastic properties of the tissue, although the exact property being measured is

dependent on the frequency at which the measurement is made. At low frequencies, X_{rs} has a negative value and reflects elastic reactance. At the resonant frequency, where X_{rs} is equal to zero, ($f_{res} < 10\text{Hz}$ for a healthy adult) the elastic and inertial forces are equal and opposite, and pressure and airflow are perfectly in phase. For $f > f_{res}$, X_{rs} is positive and reflects the inertial reactance of the tissue.^{10, 47} Inflammatory processes that occur in both asthma and COPD can decrease the elasticity of lung tissue, and this change is measured by X_{rs} .

In obstructive lung disease, both resistance and reactance of the respiratory system are increased. Resistance increases as a result of airway obstruction, and the frequency dependence of resistance increases with heterogeneous obstruction. Reactance is increased due to inflammation in the airways and surrounding tissue, which decreases tissue elasticity. In order to measure these changes in the mechanical properties of the lung in obstructive lung disease, one must measure the pressure and flow of gas in the lungs at some known frequency. One way to do this is to apply a pressure wave (at one or many frequencies) at the mouth, and measure pressure and airflow in response to this input. This method is known as the forced oscillation technique (FOT).

1.5.2 The Forced Oscillation Technique

The application of pressure oscillations to probe the mechanical properties of the lung originated with Dubois *et al.* over sixty years ago.⁴⁸ Since this study, forced oscillations have been used widely in research, and clinical technology has been developed for the use of FOT. Typically for this technique, a multi-frequency pressure waveform is applied at the mouth. In this thesis, I will focus on the use of frequencies from 5Hz to 37Hz. In Figure 1-6, a commercialized FOT device is shown that operates in this frequency range (Tremoflow, Thorasys, Montreal CA). To acquire a measurement, the patient supports the soft tissue of their cheeks and chin with their hands to minimize the contribution of the upper airways. The patient breathes normally into the mouthpiece while a multi-frequency pressure oscillation is applied by the device for approximately 10 seconds. The FOT device measures the pressure and airflow in response to this stimulation to calculate R_{rs} and X_{rs} at each frequency.

Previous studies have investigated the frequency dependence of this signal and found that low-frequency oscillations probe the entire airway tree, while the higher frequency oscillations are damped out in the mid-range airways and are therefore not able to probe the small airways.^{47, 49} Based on these studies, specific frequencies have been identified for clinically relevant measurements; 5Hz is a low frequency known to probe the entire airway tree (including the small airways) and 19Hz is a high frequency oscillation that is known to probe the large airways, and is dampened out before reaching the small airways. This means that FOT can be used to measure the impedance related to the small airways in particular as shown in Equation 1.3, an important feature not present in many other PFTs.

$$R_{small} = R_{rs}(5 - 19Hz) = R_{rs}(5Hz) - R_{rs}(19Hz) \quad (1.3)$$

As described in Equation 1.3, the frequency dependence of the FOT impedance signal can be used to identify the region in which resistance is elevated, in the central or peripheral airways as illustrated in Figure 1-6. FOT has been used extensively to study various forms of lung disease including both obstructive and restrictive diseases, and while it is not able to distinguish between obstructive and restrictive disease,¹⁰ it is able to determine severity within obstructive lung disease.^{50, 51}

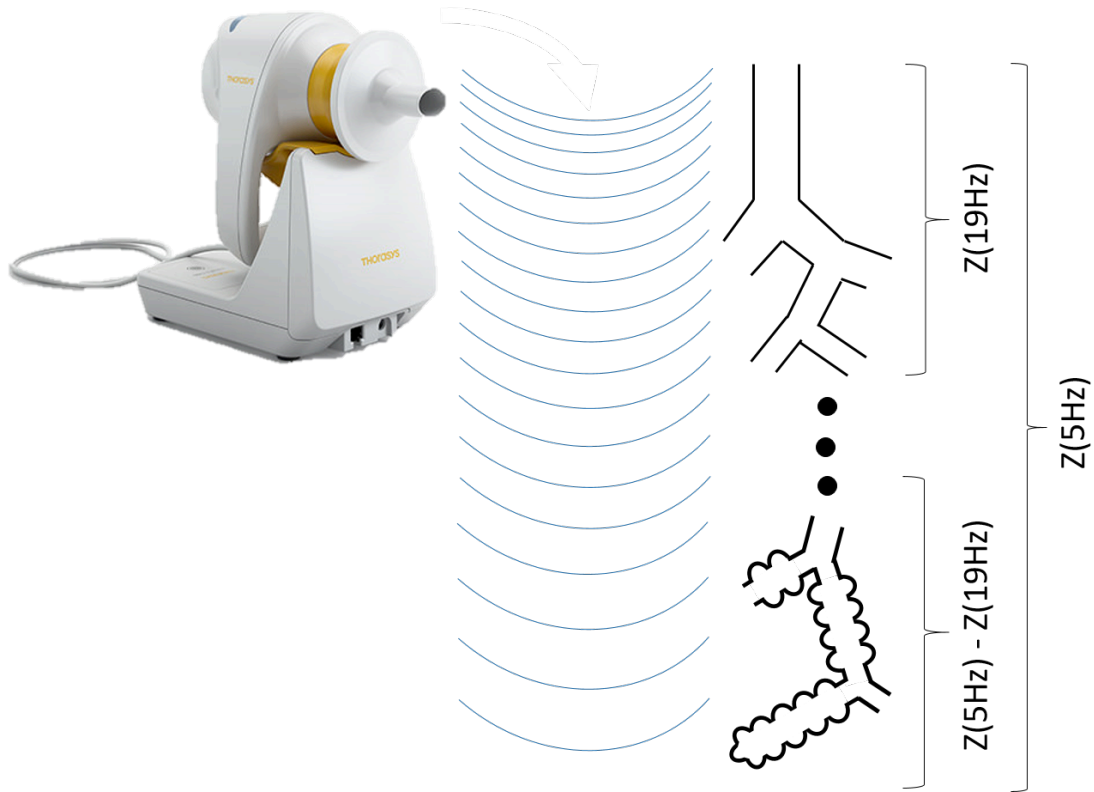


Figure 1-6 Frequency Dependence of the Forced Oscillation Technique

A multi-frequency pressure wave is produced and travels through the airways during passive breathing. The low-frequency component (5Hz) is able to travel through the entire airway tree, while the high-frequency component (19Hz) is damped out before reaching the peripheral airways.

1.6 Imaging Measurements of Lung Structure and Function

While PFTs provide measurements of lung function that are easily integrated into clinical workflows, they are limited by their global nature. As discussed in Section 1.2.2, global measures such as spirometry are not sensitive to changes in the small airways because they contribute little to the overall resistance of the respiratory system. While FOT is sensitive to the differences between central and peripheral airways, it is still not able to provide specific spatial information. Pulmonary imaging has been developed to provide structural and functional information with high spatial and temporal resolution, providing a wealth of additional information about the regions of the lung that are affected by disease. Pulmonary imaging is also used in a variety of ways to study lung biomechanics, as is discussed in depth in Appendix D. The anatomical and functional imaging methods discussed in this thesis include planar x-ray, computed tomography (CT), single photon

emission computed tomography (SPECT), positron emission tomography (PET) and magnetic resonance imaging (MRI).

1.6.1 Structural and Anatomical Imaging

Anatomical imaging is used to generate high-resolution structural images of the respiratory system in order to identify anatomical changes that occur in lung disease. These changes may include changes to the airway structure, or changes to the density of the parenchymal tissue. These changes are primarily measured using planar or CT x-ray imaging, but can also be measured using MRI.

X-ray Imaging

Planar x-ray imaging is the earliest developed and most common type of imaging acquired in lung disease. X-rays were discovered by Wilhelm Röntgen in 1895, when he famously captured an x-ray image of his wife's hand. It is still widely used for chest and lung imaging because it is inexpensive, and requires a low radiation dose to acquire (0.01 mSv).⁵² To generate these images, a cone-shaped beam of x-rays is directed at the patient's chest. Some of these x-rays will be absorbed by the body, and some will travel through the body and reach a detector on the other side which absorbs and measures them. The number of absorbed (or attenuated) x-rays is dependent on the electron density of the tissue. For example, bones have high density and appear bright in an x-ray image, while gas inside the lungs has very low density and appears very dark in an x-ray image. X-ray images can be used to detect changes in the shape of the lungs (indicative of gas trapping or emphysema)⁵³ or structural changes to the airways. In severe emphysema, the decreased density of the parenchymal tissue is also visible as a darker region in the image.⁵⁴ Planar x-ray imaging is limited because it is a 2D projection of all the structures in the thoracic cavity, making it difficult to localize abnormalities. This limitation was addressed by the development of 3-dimensional x-ray computed tomography (CT) imaging.

Computed Tomography

CT imaging was developed in the 1970s to generate 3-dimensional medical images. The 3D volume is computed from many x-ray images collected at different angles around the

patient. The patient is positioned supine on the CT scanner bed, and passes through a donut-shaped scanner containing an x-ray source and a detector array positioned opposite to it. The source and detector rotate around the patient, collecting multiple planar x-ray images. Using computational reconstruction techniques including filtered back projection and iterative reconstruction, these images can be reconstructed into a 3-dimensional volume image.⁵⁵ Each voxel in the image is a measurement of the tissue density normalized to the density of water using Hounsfield units (HU)⁵⁶ as shown below in Equation 1.4.

$$\text{Hounsfield Unit} = \left(\frac{\mu_{\text{tissue}} - \mu_{\text{water}}}{\mu_{\text{water}}} \right) 1000 [HU] \quad (1.4)$$

Using CT imaging, much higher resolution and contrast images can be acquired than with planar x-ray alone. CT can be used to visualize and measure various structural components of the lungs, and the structural changes that occur in lung disease. Some of these structural features are shown in Figure 1-7. For example, the voxel-wise density measured in the lung parenchyma can be used to identify healthy tissue and emphysematous tissue in COPD. The value of -950 HU has been established to identify the threshold below which tissue has been subjected to destruction and is considered emphysematous (in an inspiration image).⁵⁷ Using simple threshold methods, emphysematous tissue can be easily defined in an inspiration CT image in COPD. This is quantified using the relative area of the density histogram below -950 HU (RA₉₅₀). Similarly, the -856 HU has been used as a threshold to identify trapped gas in an expiration image in either asthma or COPD and quantify it by the relative area below the density histogram below -856 HU (RA₈₅₆).⁵⁸ Emphysema, or airspace enlargement, are shown in representative CT images in Figure 1-7.

Using specialized software (Pulmonary Workstation V.2.0. VIDA Diagnostics, Coralville, Iowa, USA) the airway tree can be segmented from a CT image, up to the 2mm airways. Representative airway trees for COPD and asthma are shown in Figure 1-7. Using the segmented airway tree, the airway lumen and the airway wall thickness can be measured and compared to measurements derived from a healthy lung to determine the extent of airway narrowing. For example, a recent study shown that there is increased heterogeneity in airway tone in asthma as compared to healthy subjects.⁵⁹

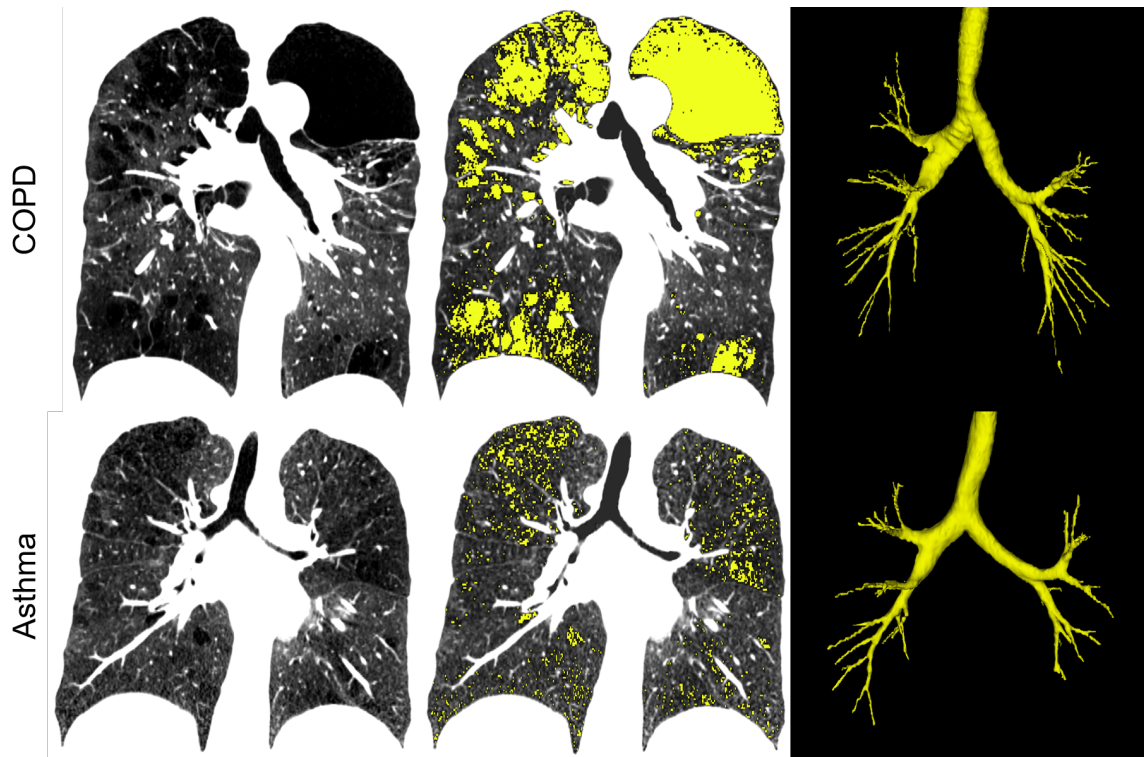


Figure 1-7 Computed Tomography of COPD and Asthma

Above are computed tomography (CT) images for COPD (top) and Asthma (bottom) with RA₉₅₀ maps shown in yellow in the center and 3D renderings of the airway tree on the right.

The radiation dose from a thoracic CT scan is approximately 7mSv, or approximately 2-3 years of background radiation exposure.⁶⁰ Recently, advancements in imaging technology have led to the development of low-dose and ultra-low dose acquisition procedures so that patients may one day have access to CT imaging with much lower radiation exposure. However, these techniques have not yet been clinically implemented and concerns remain about repeated CT imaging for patients with lung disease, especially for longitudinal monitoring. In response to these concerns, there has been recent interest in advanced MRI acquisition methods to acquire structural images of the lung using MRI.

Ultra-short Echo Time MRI

Very low signal intensity is measured in the lung parenchyma with traditional MR methods in part because of the many air-tissue interfaces, which cause the transverse signal to decay very quickly (0.4-0.9ms).^{61, 62} In order to overcome this, the echo time (TE, the time between the RF excitation pulse and data acquisition) must be extremely short to acquire

signal from the parenchymal tissue before it decays.^{63, 64} Due to recent technological developments, TE of 0.03ms is now achievable and due to advanced image sampling and reconstruction techniques, UTE images of the entire lung volume can be acquired in a single breath-hold with minimal motion artifacts.⁶⁵ UTE MR signal intensity is correlated with tissue density in COPD⁶⁵ and asthma,⁶⁶ and may be related to structural changes such as emphysema.

1.6.2 Functional Imaging

The primary function of the lung is ventilation; the delivery of oxygenated gas to the alveoli throughout the lung and the removal of carbon dioxide.²³ In order to generate functional images of the lung, one must be able to image the distribution of inhaled gas. In the last three decades, several techniques have been developed to acquire functional images of the lung using both contrast-enhanced and non-contrast enhanced methods.

Non-Contrast Enhanced Functional Imaging

Indirect measurements of lung function can be gathered from the changes in tissue density or tissue deformation measured using structural imaging. This can be done by acquiring structural CT or MR images at multiple lung volumes, including full inspiration and full expiration. Using deformable registration techniques, these images can be co-registered and by using the deformation field,⁶⁷ or the voxel-wise changes in tissue density,⁶⁸ the voxel-wise change in gas volume can be calculated as a surrogate measure of ventilation.⁶⁹ Using this technique, researchers are also able to use the deformation of the lung tissue to study its biomechanical properties. This technique is the earliest application of medical imaging to study breathing and lung mechanics^{70, 71} and is discussed in further detail in Appendix D.

Another non-contrast enhanced method for functional imaging is Fourier Decomposition (FD) MRI. This technique, which has been developed over the past decade, is implemented by acquiring a time series of ¹H MR images during tidal breathing. These images are non-rigidly co-registered, and represented as a voxel-wise time series of signal intensity values. The Fourier Transform is applied to each time series, and by measuring the amplitude of

the Fourier signal at the breathing frequency, one obtains the amplitude of the change in tissue density due to breathing.⁷² Similar to multi-volume CT methods, this method provides a surrogate measure of ventilation but does not subject patients to any ionizing radiation exposure. This has been applied in COPD⁷³ and asthma⁷⁴ and is correlated with hyperpolarized gas MRI ventilation, which will be described in Section 1.6.3.

Contrast-Enhanced Functional Imaging

Ventilation can also be directly imaged using inhaled contrast agents. This technique has been applied using many modalities, including MRI and nuclear imaging techniques such as single photon emission computed tomography (SPECT) and positron emission tomography (PET). In SPECT, patients inhale a radioactive tracer gas that emits a high energy photon (gamma ray) when it decays. The emitted photons are collected at multiple angles around the patient and used to reconstruct the spatial distribution of the gas; this has been applied to study ventilation in obstructive lung disease.⁷⁵⁻⁷⁸ In PET, the tracer produces two simultaneous photons travelling antiparallel to each other that can also be used to reconstruct the spatial distribution of the inhaled tracer.^{17, 79} These methods are limited by the patient exposure to ionizing radiation, low spatial resolution and dependence on a cyclotron for isotope production. This renders them inappropriate for some applications in obstructive lung disease, such as longitudinal monitoring.

1.6.3 Inhaled Noble Gas Magnetic Resonance Imaging

MRI is a promising technique for imaging lung function as it does not involve any exposure to ionizing radiation, and is therefore suitable for longitudinal studies. However, MR imaging techniques are limited by the low proton density and many tissue-air interfaces in the lung that lead to extremely low MR signal in the parenchyma. Inhaled noble gas MRI addresses this limitation by directly imaging the gas that is inhaled by the patient, rather than imaging the lung tissue. To acquire these images, the patient inhales a known volume of hyperpolarized noble gas (approximately 5mL/kg body weight) and holds their breath for approximately 10-16 seconds while the image of the gas distribution is acquired. These images are co-registered to anatomical MR images in order to identify the regions of the

patient's lungs that are ventilated and, more importantly, the regions that are poorly ventilated.

Hyperpolarization

Hyperpolarized noble gas imaging is currently performed using one of two gases, helium-3 (^3He) and xenon-129 (^{129}Xe). The first hyperpolarized gas image of the lung was generated in 1994 using ^{129}Xe ,⁸⁰ and was shortly followed by images using ^3He .⁸¹ ^3He was initially preferred for imaging due to the high signal-to-noise ratio that could be achieved. However, due to the limited supply and increasing price of ^3He ,⁸² there has been renewed interest in ^{129}Xe for ventilation imaging in the future.

An optical spin-exchange system is used to achieve hyperpolarization of a noble gas. A circularly polarized laser at the wavelength corresponding to the electronic orbital transition energy of rubidium (Rb) is used to excite electrons of vaporized Rb (or another alkali metal). The excited Rb vapor is contained in an optical cell that is also filled with $^3\text{He}/^{129}\text{Xe}$. The Rb and $^3\text{He}/^{129}\text{Xe}$ atoms collide and by a process called the spin-spin interaction, angular momentum is transferred into the $^3\text{He}/^{129}\text{Xe}$ atom. This increases the nuclear polarization of the unpaired nuclear proton. The optical cell is maintained in a constant magnetic field so the polarized atoms will decay much more slowly to their ground state. As collisions continue to occur, up to 45% of the gas can be polarized; at this point it is considered hyperpolarized. This hyperpolarized gas has four orders of magnitude greater polarization than at thermal equilibrium (thermal polarization in a 3.0 Tesla magnetic field $\approx 10^{-5}$).^{83, 84}

Ventilation Imaging

For the acquisition of ventilation images, the patient inhales a 1.0L volume of gas (approximately 25% hyperpolarized noble gas, 75% ultra-high purity nitrogen gas) while lying supine, and holds their breath for approximately 10-16 seconds as the image is acquired.⁸⁵ The inhaled gas travels to all ventilated regions of the lung within this single breath hold, so in a healthy subject the ventilation is uniformly distributed throughout the lungs. However, in poorly ventilated regions of the lung there are dark voids in the

ventilation image because very little hyperpolarized gas was able to enter.^{85, 86} These regions are called ventilation defects, and are shown in Figure 1-8 below.

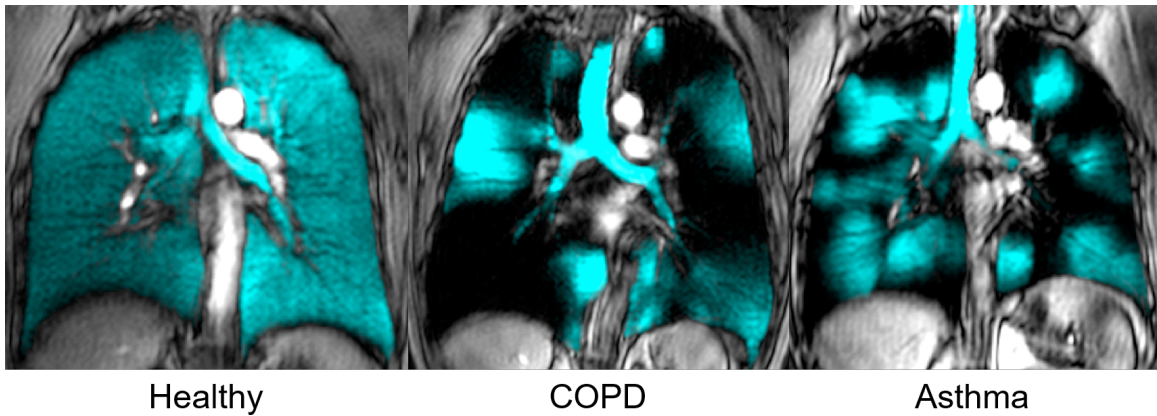


Figure 1-8 ³He Ventilation MRI of COPD and Asthma

Ventilation MRI of a healthy volunteer, a subject with COPD and an asthmatic subject. Hyperpolarized ³He MRI gas distribution (in cyan) is co-registered to ¹H MRI of the thorax (in grey-scale). Dark regions in the image indicate ventilation defects.

As shown by the ventilation defects in Figure 1-8, the distribution of hyperpolarized gas is heterogeneous in patients with obstructive lung disease. In order to quantify these defects, the ventilation images are segmented and co-registered with the anatomical proton image. A k-means clustering algorithm is used to bin the ventilation into five clusters⁸⁷ such that the lowest ventilation cluster corresponds to the background signal intensity, and is used to identify ventilation defects. In order to quantify the defects in the whole lung, the ventilation defect volume (VDV) is normalized to the thoracic cavity volume (TCV); this measurement is called the ventilation defect percent (VDP) and is shown in Equation 1.5 below.

$$VDP = \left(\frac{VDV}{TCV} \right) \times 100\% \quad (1.5)$$

This measurement has been used to quantify ventilation heterogeneity in a variety of lung diseases, including asthma¹⁴ and COPD.⁸⁸ The structural determinants of ventilation defects and their clinical consequences are still not fully understood,¹⁴ and studies of these are ongoing. In asthma, recent work has shown that ventilation defects are related asthma control,¹³ and are spatially related to remodeled airways.¹⁴ In COPD, defects have been

shown to be related to exacerbations,⁸⁹ and represent a mixed airways disease-emphysema phenotype.⁹⁰ Hyperpolarized gas MRI has also been used to show treatment response in obstructive lung disease.^{91, 92} Together, these studies strongly suggest that ventilation heterogeneity measured by MRI is related to disease of the airways and airspaces. In order to gain a deeper understanding of the small-scale structural changes associated with MRI ventilation defects, multi-modality studies are needed to probe ventilation heterogeneity and changes to the small airways, such as combining FOT measurements of small-airways resistance and MRI.

1.7 Biomechanical Modeling of the Lung

“A mathematical model is a set of equations that serve both as a precise statement of our assumptions about how the lung works mechanically and as a means of exploring the consequences of those assumptions.” Bates 2009.⁴⁶

As detailed in the previous sections, we can acquire a variety of functional and structural measurements that reflect changes to the lung tissue occurring in obstructive lung disease. However, because the functional unit of the lung is so small ($\approx 300\mu\text{m}$),²³ current techniques lack the spatial resolution to image and study them directly. Therefore, the relationships between structural and functional changes occurring in the small airways and alveoli are unclear. Biomechanical modeling of the lung is used to probe these relationships, and can be divided into two categories, inverse modeling and forward modeling.

1.7.1 Inverse Modeling

Inverse modeling refers to the process of constructing a model of a system from measurements of inputs and outputs of the system. In the case of the lungs, this refers to using measurements of respiratory system pressure and airflow (function) to model the mechanical properties of the lung tissue (structure). Due to the limited number of distinct functional measurements available, inverse models are simplified models that specify only a few parameters of the system's structure. However, a good inverse model is able to effectively describe the overall behaviour of the system. The simplest model of the lungs is the linear single compartment model. While many higher-order models have been

developed, the linear single compartment model provides a surprisingly robust model of lung mechanics. Rather than two lungs composed of millions of airways and alveoli, this model is composed of a single elastic compartment supplied by a single conduit as shown in Figure 1-9. The compartment has some variable pressure (P) and volume (V), and there is some flow of gas (\dot{V}) resulting from a pressure differential across the conduit (ΔP). These variables are dependent on the elastic properties of the compartment (E), and the resistance of the conduit (R).

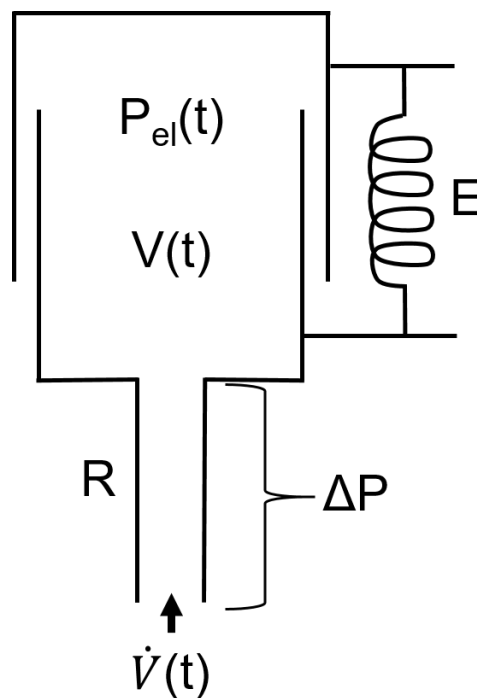


Figure 1-9: Linear Single Compartment Model of the Lung

The mechanical properties of the lung can be estimated by a single elastic compartment with elastance E , supplied by a tube with resistance R . P_{el} is the pressure in the elastic compartment, and ΔP is the pressure difference across the tube. V is the volume of gas in the compartment, and \dot{V} is the airflow into the tube. Adapted from Bates *et al.* 2009.⁴⁶

A linear system is one in which the dependent variable varies linearly with the independent variable when all other parameters are held constant; in this case the two variables (pressure and volume) are related through a linear differential equation by a quantity called impedance. This impedance is complex, and is composed of resistance and reactance (which is related to elastance, as shown in Equation 1.7 below) as discussed in Section 1.5.

In deriving the relationship between pressure and volume, we assume that when elastance (E) is constant, P_{el} and V vary linearly (ie. $P_{el} = EV$). Similarly, we assume that when resistance is constant, the relationship between ΔP and \dot{V} is linear (ie $\Delta P = R\dot{V}$). ΔP and P_{el} must be combined in order to calculate pressure for the entire system (Equation 1.6).

$$P_{tp}(t) = EV(t) + R\dot{V}(t) + P_0(t) \quad (1.6)$$

Where P_0 is the offset pressure, to account for the fact that the transpulmonary pressure (P_{tp}) is non-zero when V and \dot{V} are zero due to the pressure of the pleural space.⁹³ This equation is sometimes referred to as ‘the equation of motion of the lung’, as it is the fundamental equation describing the relationship between pressure and volume in the linear single-compartment model of the lung.⁴⁶ While this is not an exact description of the behaviour of the lung, it forms a good approximation that is used widely in studies of lung mechanics, including in this thesis. To show this, we apply the Fourier Transform to Equation 1.6, giving Equation 1.7.

$$P(f) = \left(R - \frac{iE}{2\pi f} \right) \dot{V}(f) \quad (1.7)$$

The relationship between reactance and elastance is given in Equation 1.8.

$$X_{rs}(f) = \frac{iE(f)}{2\pi f} \quad (1.8)$$

Using Equations 1.1, 1.7, and 1.8 we recover the equation for respiratory system impedance defined in Equation 1.2 that used in FOT to calculate R_{rs} and X_{rs} .

1.7.2 Forward Modeling

Forward modeling, otherwise known as simulation, involves devising a model with set parameters, and using this model to predict the output of the system. In other words, this approach requires making a set of assumptions about the parameters of the system (structure), and using these parameters to predict the system’s behaviour (function). In mechanical modeling of the lungs, computational airway tree models with many branching

generations and alveolar compartments are used to predict the pressure or airflow response to a known stimulus.⁹⁴ These models often also account for the mechanical properties of the upper airways and the chest wall. In most studies, airflow is described by Womersley flow⁹⁵ as shown in Equation 1.7.

$$Z_a(f) = \frac{i2f\rho_{air}l_a}{r_a^2} \left[1 - \frac{2J_1(\alpha_a\sqrt{-i})}{\alpha_a\sqrt{-i}J_0(\alpha_a\sqrt{-i})} \right]^{-1} \quad (1.9)$$

Where i is the unit imaginary number, f is the oscillation frequency in Hz, ρ_{air} is the density of air (1.16 kg/m³), l_a is the length and r_a is the radius of the airway, J_0 and J_1 are the complex Bessel functions of order 0 and 1 respectively and α_a is the Womersley number for the airway given by Equation 1.8:

$$\alpha_a = r_a \sqrt{\frac{2\pi\rho_{air}f}{\mu_{air}}} \quad (1.10)$$

Where μ_{air} is the dynamic viscosity of humid air at 37 degrees C (1.85 x 10⁻⁵ Pa.s). Elastic properties of the parenchymal tissue are also accounted for in many modeling studies. Using these properties of elasticity and airflow, as well as many other parameters including chest wall compliance and upper airway shunt,⁹⁶ the impedance of the computational system can be estimated.

1.7.3 Pulmonary Imaging and Biomechanical Modeling

Forward models have been well developed and widely used to study lung mechanics in the past two decades. Anatomically accurate computational models with up to 26 branching airway generations⁹⁴ are used to study lung mechanics under a variety of conditions. There has recently been increasing interest in incorporating spatial functional information from pulmonary imaging into computational modeling in order to more deeply understand the relationships between ventilation defects observed in obstructive lung disease and structural changes in the lung. By incorporating imaging functional data into modeling studies, researchers can evaluate the effects of various known distributions of mechanical

changes throughout the lung in order to probe these relationships. This has previously been applied in asthma, in an effort to understand the distribution of large and small airway closures that are involved in generating ventilation defects.^{18, 97} The combination of functional imaging and computational modeling presents many opportunities to explore more deeply the relationships between structure and function in obstructive lung disease.

1.8 Thesis Objectives and Hypotheses

In this thesis, I assessed MRI-measured ventilation defect percent, respiratory system impedance measured by the forced oscillation technique (FOT), patient quality of life and model-predicted respiratory system impedance in 100 obstructive lung disease patients. My objective was to evaluate the relationships between FOT-measured impedance and MRI-measured ventilation heterogeneity, as well as clinical measurements of patient quality of life. I also compared FOT-measured impedance and the values predicted using patient-specific airway tree models. I hypothesized that FOT-measured respiratory system impedance would be related to MRI ventilation heterogeneity and patient quality of life in asthma and COPD. Additionally, I hypothesized that measured and predicted impedance would be significantly correlated in all subjects.

In Chapter 3, an overview and summary of the important findings and conclusions of Chapter 2 is provided. The study specific and general limitations of this study will be discussed and some potential solutions. The thesis concludes with an outline of future studies that can build on the work presented in this thesis.

1.9 References

- (1) Global, regional, and national deaths, prevalence, disability-adjusted life years, and years lived with disability for chronic obstructive pulmonary disease and asthma, 1990-2015: a systematic analysis for the Global Burden of Disease Study 2015. (2017).
- (2) Ontario Lung Association. Your Lungs, Your Life: Insights and Solutions to Lung Health in Ontario. (2011).
- (3) Toy, E.L., Gallagher, K.F., Stanley, E.L., Swensen, A.R. & Duh, M.S. The economic impact of exacerbations of chronic obstructive pulmonary disease and exacerbation definition: a review. *COPD* **7**, 214-28 (2010).
- (4) Canadian Institute for Health Information. Inpatient Hospitalizations, Surgeries, Newborns and Childbirth Indicators, 2015-2016. (2017).
- (5) Mittmann, N. et al. The cost of moderate and severe COPD exacerbations to the Canadian healthcare system. *Respir Med* **102**, 413-21 (2008).
- (6) The Lung Association. Asthma Control in Canada Survey. (2016). www.lung.ca/ (Retrieved November 2016).
- (7) Asthma Canada. Asthma Facts and Statistics, FAQs. (2017). www.asthma.ca (accessed November 2017).
- (8) Miller, M.R. et al. Standardisation of spirometry. *Eur Respir J* **26**, 319-38 (2005).
- (9) Coxson, H.O., Leipsic, J., Parraga, G. & Sin, D.D. Using pulmonary imaging to move chronic obstructive pulmonary disease beyond FEV1. *Am J Respir Crit Care Med* **190**, 135-44 (2014).
- (10) Oostveen, E. et al. The forced oscillation technique in clinical practice: methodology, recommendations and future developments. *Eur Respir J* **22**, 1026-41 (2003).
- (11) de Lange, E.E. et al. Evaluation of asthma with hyperpolarized helium-3 MRI: correlation with clinical severity and spirometry. *Chest* **130**, 1055-62 (2006).
- (12) Kirby, M. et al. COPD: Do Imaging Measurements of Emphysema and Airway Disease Explain Symptoms and Exercise Capacity? *Radiology* **277**, 872-80 (2015).
- (13) Svenningsen, S., Nair, P., Guo, F., McCormack, D.G. & Parraga, G. Is ventilation heterogeneity related to asthma control? *Eur Respir J* **48**, 370-9 (2016).
- (14) Svenningsen, S. et al. What are ventilation defects in asthma? *Thorax* **69**, 63-71 (2014).

- (15) Tgavalekos, N.T., Venegas, J.G., Suki, B. & Lutchen, K.R. Relation between structure, function, and imaging in a three-dimensional model of the lung. *Ann Biomed Eng* **31**, 363-73 (2003).
- (16) Bhatawadekar, S.A., Leary, D. & Maksym, G.N. Modelling resistance and reactance with heterogeneous airway narrowing in mild to severe asthma. *Can J Physiol Pharmacol* **93**, 207-14 (2015).
- (17) Venegas, J.G. et al. Self-organized patchiness in asthma as a prelude to catastrophic shifts. *Nature* **434**, 777-82 (2005).
- (18) Leary, D. et al. Hyperpolarized ³He magnetic resonance imaging ventilation defects in asthma: relationship to airway mechanics. *Physiol Rep* **4**, e12761 (2016).
- (19) Tgavalekos, N.T. et al. Relationship between airway narrowing, patchy ventilation and lung mechanics in asthmatics. *Eur Respir J* **29**, 1174-81 (2007).
- (20) Farrow, C.E. et al. Peripheral Ventilation Heterogeneity Determines the Extent of Bronchoconstriction in Asthma. *J Appl Physiol (1985)*, jap 00640 2016 (2017).
- (21) Kaczka, D.W., Cao, K., Christensen, G.E., Bates, J.H. & Simon, B.A. Analysis of regional mechanics in canine lung injury using forced oscillations and 3D image registration. *Ann Biomed Eng* **39**, 1112-24 (2011).
- (22) Thien, F. Measuring and imaging small airways dysfunction in asthma. *Asia Pac Allergy* **3**, 224-30 (2013).
- (23) West, J.B. *Respiratory Physiology: The Essentials* (Lippincott Williams & Wilkins, 2012).
- (24) Ochs, M. et al. The number of alveoli in the human lung. *Am J Respir Crit Care Med* **169**, 120-4 (2004).
- (25) Kaczka, D.W., Ingenito, E.P., Suki, B. & Lutchen, K.R. Partitioning airway and lung tissue resistances in humans: effects of bronchoconstriction. *J Appl Physiol (1985)* **82**, 1531-41 (1997).
- (26) Mead, J. The Lung's "Quiet Zone". *N Engl J Med* **282**, 1318-9 (1970).
- (27) Woolcock, A.J., Vincent, N.J. & Macklem, P.T. Frequency dependence of compliance as a test for obstruction in the small airways. *J Clin Invest* **48**, 1097-106 (1969).
- (28) McDonough, J.E. et al. Small-airway obstruction and emphysema in chronic obstructive pulmonary disease. *N Engl J Med* **365**, 1567-75 (2011).
- (29) Lumb, A.B. *Nunn's Applied Respiratory Physiology* (Elsevier Health Sciences, 2016).

- (30) Global Strategy for Asthma Management and Prevention (GINA). 2017 GINA Report, Global Strategy for Asthma Management and Prevention. (2017). <http://www.ginasthma.org> (accessed November 2017).
- (31) West, J.B. Pulmonary Pathophysiology: The Essentials (Lippincott Williams & Wilkins, 2012).
- (32) Hamid, Q. et al. Inflammation of small airways in asthma. *J Allergy and Clin Immunol* **100**, 44-51 (1997).
- (33) Saetta, M. & Turato, G. Airway pathology in asthma. *Eur Respir J Suppl* **34**, 18s-23s (2001).
- (34) US Department of Health and Human Services. The health consequences of smoking: a report of the Surgeon General. (2004). Atlanta, GA: US Department of Health and Human Services, Centers for Disease Control and Prevention, National Center for Chronic Disease Prevention and Health Promotion, Office on Smoking and Health.
- (35) Laurell, C.-B. & Eriksson, S. The electrophoretic α 1-globulin pattern of serum in α 1-antitrypsin deficiency. *Scand J Clin Lab Invest* **15**, 132-140 (1963).
- (36) Mead, J., Turner, J.M., Macklem, P.T. & Little, J.B. Significance of the relationship between lung recoil and maximum expiratory flow. *J Appl Physiol* **22**, 95-108 (1967).
- (37) Butler, J., Caro, C.G., Alcalá, R. & Dubois, A.B. Physiological factors affecting airway resistance in normal subjects and in patients with obstructive respiratory disease. *J Clin Invest* **39**, 584-91 (1960).
- (38) Hogg, J.C. Pathophysiology of airflow limitation in chronic obstructive pulmonary disease. *Lancet* **364**, 709-21 (2004).
- (39) Vestbo, J. et al. Global strategy for the diagnosis, management, and prevention of chronic obstructive pulmonary disease: GOLD executive summary. *Am J Respir Crit Care Med* **187**, 347-65 (2013).
- (40) Clayton, N. Lung function made easy: assessing lung size. *Chron Respir Dis* **4**, 151-7 (2007).
- (41) Wanger, J. et al. Standardisation of the measurement of lung volumes. *Eur Respir J* **26**, 511-22 (2005).
- (42) Macintyre, N. et al. Standardisation of the single-breath determination of carbon monoxide uptake in the lung. *Eur Respir J* **26**, 720-35 (2005).

- (43) Juniper, E.F., O'Byrne, P.M., Guyatt, G.H., Ferrie, P.J. & King, D.R. Development and validation of a questionnaire to measure asthma control. *Eur Respir J* **14**, 902-7 (1999).
- (44) Juniper, E.F., Buist, A.S., Cox, F.M., Ferrie, P.J. & King, D.R. Validation of a standardized version of the Asthma Quality of Life Questionnaire. *Chest* **115**, 1265-70 (1999).
- (45) Jones, P.W., Quirk, F.H., Baveystock, C.M. & Littlejohns, P. A self-complete measure of health status for chronic airflow limitation. The St. George's Respiratory Questionnaire. *Am Rev Respir Dis* **145**, 1321-7 (1992).
- (46) Bates, J.H. Lung Mechanics: An Inverse Modeling Approach (Cambridge University Press, 2009).
- (47) Goldman, M.D. Clinical application of forced oscillation. *Pulm Pharmacol Ther* **14**, 341-50 (2001).
- (48) Dubois, A.B., Brody, A.W., Lewis, D.H. & Burgess, B.F., Jr. Oscillation mechanics of lungs and chest in man. *J Appl Physiol* **8**, 587-94 (1956).
- (49) Brashier, B. & Salvi, S. Measuring lung function using sound waves: role of the forced oscillation technique and impulse oscillometry system. *Breathe (Sheff)* **11**, 57-65 (2015).
- (50) Di Mango, A.M., Lopes, A.J., Jansen, J.M. & Melo, P.L. Changes in respiratory mechanics with increasing degrees of airway obstruction in COPD: detection by forced oscillation technique. *Respir Med* **100**, 399-410 (2006).
- (51) Cavalcanti, J.V., Lopes, A.J., Jansen, J.M. & Melo, P.L. Detection of changes in respiratory mechanics due to increasing degrees of airway obstruction in asthma by the forced oscillation technique. *Respir Med* **100**, 2207-19 (2006).
- (52) Brenner, D.J. & Hall, E.J. Computed tomography--an increasing source of radiation exposure. *N Engl J Med* **357**, 2277-84 (2007).
- (53) Rebuck, A.S. Radiological aspects of severe asthma. *Australas Radiol* **14**, 264-8 (1970).
- (54) Thurlbeck, W.M. & Simon, G. Radiographic appearance of the chest in emphysema. *AJR Am J Roentgenol* **130**, 429-40 (1978).
- (55) Goldman, L.W. Principles of CT and CT technology. *J Nucl Med Technol* **35**, 115-28; quiz 129-30 (2007).
- (56) Hounsfield, G.N. Computerized transverse axial scanning (tomography): Part 1. Description of system. *Br J Radiol* **46**, 1016-1022 (1973).

- (57) Hayhurst, M.D. et al. Diagnosis of pulmonary emphysema by computerised tomography. *Lancet* **2**, 320-2 (1984).
- (58) Zach, J.A. et al. Quantitative computed tomography of the lungs and airways in healthy nonsmoking adults. *Invest Radiol* **47**, 596-602 (2012).
- (59) Brown, R.H. & Toghiani, A. Measurement of intraindividual airway tone heterogeneity and its importance in asthma. *J Appl Physiol (1985)* **121**, 223-32 (2016).
- (60) Mettler, F.A., Jr., Huda, W., Yoshizumi, T.T. & Mahesh, M. Effective doses in radiology and diagnostic nuclear medicine: a catalog. *Radiology* **248**, 254-63 (2008).
- (61) Ohno, Y. et al. T2* measurements of 3-T MRI with ultrashort TEs: capabilities of pulmonary function assessment and clinical stage classification in smokers. *AJR Am J Roentgenol* **197**, W279-85 (2011).
- (62) Ohno, Y. et al. Pulmonary MR imaging with ultra-short TEs: utility for disease severity assessment of connective tissue disease patients. *Eur J Radiol* **82**, 1359-65 (2013).
- (63) Bergin, C., Pauly, J. & Macovski, A. Lung parenchyma: projection reconstruction MR imaging. *Radiology* **179**, 777-781 (1991).
- (64) Gatehouse, P.D. & Bydder, G.M. Magnetic resonance imaging of short T2 components in tissue. *Clin Radiol* **58**, 1-19 (2003).
- (65) Ma, W. et al. Ultra-short echo-time pulmonary MRI: evaluation and reproducibility in COPD subjects with and without bronchiectasis. *J Magn Reson Imaging* **41**, 1465-74 (2015).
- (66) Sheikh, K. et al. Ultrashort echo time MRI biomarkers of asthma. *J Magn Reson Imaging* **45**, 1204-1215 (2017).
- (67) Reinhardt, J.M. et al. Registration-based estimates of local lung tissue expansion compared to xenon CT measures of specific ventilation. *Med Image Anal* **12**, 752-63 (2008).
- (68) Guerrero, T. et al. Dynamic ventilation imaging from four-dimensional computed tomography. *Phys Med Biol* **51**, 777 (2006).
- (69) Fuld, M. et al. CT-measured regional specific volume change reflects regional ventilation in supine sheep. *J Appl Physiol (1985)* **104**, 1177-84 (2008).
- (70) Hubmayr, R.D., Rodarte, J.R., Walters, B.J. & Tonelli, F. Regional ventilation during spontaneous breathing and mechanical ventilation in dogs. *J Appl Physiol (1985)* **63**, 2467-2475 (1987).

- (71) Wilson, T. et al. Geometry and respiratory displacement of human ribs. *J Appl Physiol (1985)* **62**, 1872-1877 (1987).
- (72) Bauman, G. et al. Non-contrast-enhanced perfusion and ventilation assessment of the human lung by means of fourier decomposition in proton MRI. *Magn Reson Med* **62**, 656-664 (2009).
- (73) Capaldi, D.P. et al. Free-breathing pulmonary ¹H and Hyperpolarized ³He MRI: comparison in COPD and bronchiectasis. *Acad Radiol* **22**, 320-9 (2015).
- (74) Capaldi, D.P.I. et al. Free-breathing Functional Pulmonary MRI: Response to Bronchodilator and Bronchoprovocation in Severe Asthma. *Acad Radiol* (2017).
- (75) Stavngaard, T. et al. Hyperpolarized ³He MRI and ⁸¹mKr SPECT in chronic obstructive pulmonary disease. *Eur J Nucl Med Mol Imaging* **32**, 448-57 (2005).
- (76) King, G.G., Eberl, S., Salome, C.M., Meikle, S.R. & Woolcock, A.J. Airway closure measured by a technegas bolus and SPECT. *Am J Respir Crit Care Med* **155**, 682-8 (1997).
- (77) Norberg, P. et al. Quantitative lung SPECT applied on simulated early COPD and humans with advanced COPD. *EJNMMI Res* **3**, 28 (2013).
- (78) Suga, K., Kawakami, Y., Yamashita, T., Zaki, M. & Matsunaga, N. Characterization of ¹³³Xe gas washout in pulmonary emphysema with dynamic ¹³³Xe SPECT functional images. *Nucl Med Commun* **27**, 71-80 (2006).
- (79) Senda, M., Murata, K., Itoh, H., Yonekura, Y. & Torizuka, K. Quantitative evaluation of regional pulmonary ventilation using PET and nitrogen-13 gas. *J Nucl Med* **27**, 268-73 (1986).
- (80) Albert, M.S. et al. Biological magnetic resonance imaging using laser-polarized ¹²⁹Xe. *Nature* **370**, 199-201 (1994).
- (81) Ebert, M. et al. Nuclear magnetic resonance imaging with hyperpolarised helium-3. *Lancet* **347**, 1297-9 (1996).
- (82) Shea, D.A. & Morgan, D. (Congressional Research Service, Library of Congress, 2010).
- (83) Saam, B.T. Magnetic resonance imaging with laser-polarized noble gases. *Nat Med* **2**, 358-9 (1996).
- (84) Moller, H.E. et al. MRI of the lungs using hyperpolarized noble gases. *Magn Reson Med* **47**, 1029-51 (2002).

- (85) Parraga, G. et al. Hyperpolarized ^3He ventilation defects and apparent diffusion coefficients in chronic obstructive pulmonary disease: preliminary results at 3.0 Tesla. *Invest Radiol* **42**, 384-91 (2007).
- (86) Altes, T.A. et al. Hyperpolarized ^3He MR lung ventilation imaging in asthmatics: preliminary findings. *J Magn Reson Imaging* **13**, 378-84 (2001).
- (87) Kirby, M. et al. Hyperpolarized ^3He magnetic resonance functional imaging semiautomated segmentation. *Acad Radiol* **19**, 141-52 (2012).
- (88) Kirby, M. et al. Chronic obstructive pulmonary disease: longitudinal hyperpolarized (^3He) MR imaging. *Radiology* **256**, 280-9 (2010).
- (89) Kirby, M., Kanhere, N., Etemad-Rezai, R., McCormack, D.G. & Parraga, G. Hyperpolarized helium-3 magnetic resonance imaging of chronic obstructive pulmonary disease exacerbation. *J Magn Reson Imaging* **37**, 1223-7 (2013).
- (90) Capaldi, D.P. et al. Pulmonary Imaging Biomarkers of Gas Trapping and Emphysema in COPD: (^3He) MR Imaging and CT Parametric Response Maps. *Radiology* **279**, 597-608 (2016).
- (91) Kirby, M. et al. Chronic obstructive pulmonary disease: quantification of bronchodilator effects by using hyperpolarized (^3He) MR imaging. *Radiology* **261**, 283-92 (2011).
- (92) Svenningsen, S. et al. Hyperpolarized (^3He) and (^{129}Xe) MRI: differences in asthma before bronchodilation. *J Magn Reson Imaging* **38**, 1521-30 (2013).
- (93) Bates, J.H. & Lutchen, K.R. The interface between measurement and modeling of peripheral lung mechanics. *Respir Physiol Neurobiol* **148**, 153-64 (2005).
- (94) Tawhai, M.H. et al. CT-based geometry analysis and finite element models of the human and ovine bronchial tree. *J Appl Physiol (1985)* **97**, 2310-21 (2004).
- (95) Kaczka, D.W., Massa, C.B. & Simon, B.A. Reliability of estimating stochastic lung tissue heterogeneity from pulmonary impedance spectra: a forward-inverse modeling study. *Ann Biomed Eng* **35**, 1722-38 (2007).
- (96) Cauberghs, M. & Van de Woestijne, K.P. Mechanical properties of the upper airway. *J Appl Physiol Respir Environ Exerc Physiol* **55**, 335-42 (1983).
- (97) Campana, L. et al. Probing airway conditions governing ventilation defects in asthma via hyperpolarized MRI image functional modeling. *J Appl Physiol (1985)* **106**, 1293-300 (2009).

CHAPTER 2

2 OSCILLOMETRY AND PULMONARY MRI OF VENTILATION HETEROGENEITY IN OBSTRUCTIVE LUNG DISEASE: RELATIONSHIP TO QUALITY OF LIFE AND DISEASE CONTROL

To better understand the relationships between FOT-measured respiratory system impedance, MRI ventilation defects and patient quality of life, we evaluated 100 patients with obstructive lung disease using ^3He MRI, FOT, and quality of life and control questionnaires.

The contents of this chapter were submitted to the Journal of Applied Physiology. HM Young, F Guo, RL Eddy, GN Maksym, G Parraga. Oscillometry and Pulmonary MRI of Ventilation Heterogeneity in Obstructive Lung Disease: Relationship to Quality of Life and Disease Control. J Appl Physiol (Submitted November 15 2017).

2.1 Introduction

Ventilation heterogeneity is a hallmark characteristic of obstructive lung diseases such as asthma¹⁻⁴ and chronic obstructive pulmonary disease (COPD)^{5,6} and is related to disease symptoms and control.^{3,6-8} Ventilation heterogeneity can be measured using a variety of techniques including multiple breath gas washout methods⁹⁻¹¹ and pulmonary imaging.¹²⁻¹⁶ Despite decades of research that focused on the quantification and development of our understanding of causes and clinical implications of ventilation abnormalities, many patients with obstructive lung disease and ventilation heterogeneity still have poor disease control and quality of life.¹⁷⁻²⁰ This may be due in part, to the fact that the complex structural and biomechanical changes underlying ventilation heterogeneity are still not fully understood,²¹⁻²³ including those contributed by airway abnormalities.

The forced oscillation technique (FOT), first developed over 50 years ago,²⁴ non-invasively probes the mechanical properties of the respiratory system (respiratory system impedance, Z_{rs}) during quiet breathing by applying multi-frequency pressure oscillations at the mouth. The measured impedance reflects both resistance (R_{rs}) and reactance (X_{rs}) and is acquired at multiple frequencies to ascertain the frequency dependence of R_{rs} , which is believed to be related to small airway dysfunction.²⁵ FOT has been extensively used to study patients

with COPD²⁶⁻²⁸ and asthma²⁷⁻³¹ including the measurement of responses to bronchoconstriction in asthma³⁰ and to bronchodilation.^{27, 28, 31} Previous studies have shown that both R_{rs} and X_{rs} are sensitive to heterogeneous airway narrowing in asthma^{32, 33} but the exact location of this airway narrowing could not be identified. On the other hand, hyperpolarized ^3He MRI ventilation imaging has been used to identify the spatial location of ventilation abnormalities (or heterogeneity) in patients with asthma^{16, 21, 34-36} and COPD.³⁷⁻⁴⁰ MRI ventilation defects reflect the severity of airflow obstruction^{34, 41} and respond to provocation (in asthma)^{15, 36, 42} and treatment.^{16, 43-45} In addition, MRI-derived ventilation heterogeneity was recently shown to be uniquely predictive of asthma control¹² and COPD exacerbations⁴⁶.

Computational airway modelling has also been used to study the relationship between airway caliber and ventilation heterogeneity. Using an anatomical computational airway tree model,⁴⁷ the caliber of the airway lumen can be manipulated to study the effects on respiratory impedance or ventilation distribution. In some of these studies, the results suggested that airway narrowing must occur throughout the entire airway tree and in a heterogeneous fashion in order to replicate the respiratory impedance observed in asthma.^{25, 48, 49} In particular, modeling studies that incorporated ventilation data derived from positron emission tomography (PET) in asthmatics showed that airway narrowing near ventilation defects was not sufficient to replicate the impedance measured in participants.^{25, 48} Moreover, narrowing of the small airways was required to simulate impedance values observed in patients, as narrowing of large airways alone was not sufficient.⁴⁹ Other modelling studies showed that ventilation abnormalities were positively correlated with increased R_{rs} ⁵⁰ and that a large proportion of the small airways (over 75% in severe asthma) had to be narrowed in order for the model-predicted resistance and reactance to agree with measured values.⁵¹ A follow-up study used functional information derived from hyperpolarized ^3He MRI in a model whereby airways that were spatially related to ventilation defects were narrowed to generate patient-specific predictions of impedance.⁵² Numerous studies have probed structure-function relationships in asthma using biomechanical models informed by ^3He MRI,^{49, 52} PET^{25, 48} and single photon emission computed tomography (SPECT),¹⁴ but few have compared impedance predictions

to experimental FOT measurements in patients. Some studies have acquired impedance measurements for incorporation in models^{48, 49, 53} and a single study in a small group of asthmatic patients combined image functional modelling for comparison with experimentally-measured impedance.¹⁴

There is a clear need for multi-scale studies that combine functional lung imaging, computational airway models and experimental oscillometry measurements to provide a deeper understanding of the relationships between structure and function in obstructive lung disease. Ultimately, this should lead to an understanding of how disease control and quality of life can be improved in patients.⁵⁴⁻⁵⁷ Therefore, the objective of this work was to evaluate the relationships between ventilation heterogeneity measured using hyperpolarized ³He MRI and FOT, and to ascertain how these measures are related to disease control and quality of life in obstructive lung disease. Our second objective was to use ventilation MRI to modify a computational airway tree model to generate patient-specific predictions of respiratory impedance, and compare these predictions to FOT-measured impedance. We hypothesized that MRI ventilation defect percent (VDP) would be significantly related to FOT-measured respiratory impedance in patients with asthma and ex-smokers, and that both measurements would be related to quality of life and disease control in these patients.

2.2 Materials and Methods

2.2.1 Study Design

All participants provided written informed consent to study protocols (NCT# NCT02351141, NCT02263794, NCT02279329) approved by the local research ethics board. Participants between ages 18 to 70 years with a current diagnosis of asthma, and patients between ages 50 to 90 years with a history of smoking were recruited from a tertiary care center and evaluated using spirometry, plethysmography, FOT and pulmonary MRI in a single visit. Ex-smokers with COPD were identified using the Global initiative for chronic Obstructive Lung Disease (GOLD) criteria.⁵⁸ Disease control was evaluated in asthmatics using the Asthma Control Questionnaire (ACQ⁵⁹ with permission) and in ex-

smokers by monitoring exacerbation events requiring hospitalization. The number of exacerbations requiring hospitalization was determined using patient hospital records during the 2.5 year period following the visit to the research center. Patient quality of life was evaluated using the Asthma Quality of Life Questionnaire (AQLQ⁶⁰ with permission) for asthma, and the St. George's Respiratory Questionnaire (SGRQ⁶¹ with permission) for ex-smokers. For participants with asthma, all imaging and pulmonary function tests (PFTs) were acquired at baseline and within 1.5 hours after administration of four 100µg doses of Novo-Salbutamol HFA (Teva Novopharm Ltd., Toronto, Canada) using a metered dose inhaler with an AeroChamber Plus spacer (Trudell Medical International; London, Canada). In this work, only baseline measurements were investigated. For ex-smokers, all data were acquired within 1.5 hours after administration of four 100µg doses of salbutamol as described for asthmatic patients. Spirometry and body plethysmography were performed according to the American Thoracic Society (ATS) guidelines⁶² using a whole-body system (MedGraphics Corporation, Saint Paul USA). FOT measurements were acquired using the TremoFlo C-100 Airwave Oscillometry System (Thorasys, Montreal CA).

2.2.2 Image Acquisition and Analysis

MRI was performed on a whole body 3T system (MR750 Discovery, GEHC, Milwaukee, WI) with broadband imaging capability. ³He MRI was acquired using a single-channel, rigid elliptical transmit/receive chest coil (RAPID Biomedical GmbH, Wuerzburg, Germany). The ³He gas was polarized to 30-40% polarization using a spin-exchange optical polarizer (Polarean Inc, Durham, NC). Subjects were positioned supine in the scanner with their arms raised above their head and inhaled a 1L gas mixture of ³He/N₂ (25% ³He by volume) from functional residual capacity (FRC). Image acquisition was performed under breath-hold conditions.³⁷ The hyperpolarized ³He MR images were analyzed using custom software as previously described.⁶³ Briefly, a single user (HMY) placed seeds on the ¹H and ³He MR images to label the lung and the surrounding tissue and image segmentation was completed using a convex optimization technique. ³He ventilation defects were identified using a k-means clustering approach,⁶⁴ and ventilation defect percent (VDP) was calculated as the total ventilation defect volume normalized to

the thoracic cavity volume. The ventilation cluster map for each subject was then non-rigidly registered to the computational airway tree as previously described.⁵²

2.2.3 Computational Modeling

We adapted a three-dimensional airway tree consisting of 64,895 airways (M. Tawhai, U. Auckland), to generate a computational airway tree model. A full description of the model was previously provided.⁴⁷ To summarize, the airway tree was derived from a thoracic x-ray computed tomography (CT) image including up to the eighth-generation airways and the remaining generations were constructed using a volume filling algorithm that preserved the anatomical branching geometry.⁴⁷

Airways located within two voxels (6.25mm) of an MRI ventilation defect or distal to a ventilation defect were labelled as related to the defect. These airways were identified using custom software designed in MATLAB and narrowed to 10% of their initial diameter, effectively increasing their resistance by a factor of 10^4 according to Poiseuille's law.⁵² Airways larger than the 14th generation in the airway tree were excluded to ensure that we evaluated only small airways < 2mm in diameter. We evaluated the impact of small airway constriction, which has been shown to play a critical role in increased airway impedance and ventilation defects.⁴⁹ Figure 2-1 shows a schematic outlining MR image processing steps, and the integration of MRI data into the computational model to generate patient-specific predictions. Airway impedance predictions were generated as previously described from these individually modified airway trees.^{51, 52} First, the airway lengths and diameters were reduced to 80% of their original TLC volume. The flow in the non-terminal airways was described using Womersley flow⁶⁵ using the following equation:

$$Z_a(f) = \frac{i2f\rho_{air}l_a}{r_a^2} \left[1 - \frac{2J_1(\alpha_a\sqrt{-i})}{\alpha_a\sqrt{-i}J_0(\alpha_a\sqrt{-i})} \right]^{-1} \quad (2.1)$$

Where i is the unit imaginary number, f is the oscillation frequency in Hz, ρ_{air} is the density of air (1.16 kg/m^3), l_a is the length and r_a is the radius of the airway, J_0 and J_1 are the complex Bessel functions of order 0 and 1 respectively and α_a is the Womersley number for the airway given by:

$$\alpha_a = r_a \sqrt{\frac{2\pi\rho_{air}f}{\mu_{air}}} \quad (2.2)$$

Where μ_{air} is the dynamic viscosity of humid air at 37 degrees C (1.85×10^{-5} Pa.s).

To model the compliance of the lung parenchyma, each terminal airway was modeled as an alveolar compartment with a known elastance. Then, the impedance of a terminal airway is given by:

$$Z_t = Z_a - i \frac{Et}{\omega} \quad (2.3)$$

Where E is the elastance of the terminal airway unit, set to 53 cmH₂O/L as was done previously.⁵² The resistance of the upper airways and the chest wall were each assigned a value of 0.5 cmH₂O·s/L,⁶⁶⁻⁶⁸ and the elastance of the chest wall as assigned a value of 10.6 cmH₂O·s/L.⁶⁹ Finally, the effects of upper airway shunt were included using previously published values.⁷⁰ These values were added to the lung resistance and reactance to calculate the final values for R_{rs} and X_{rs} .

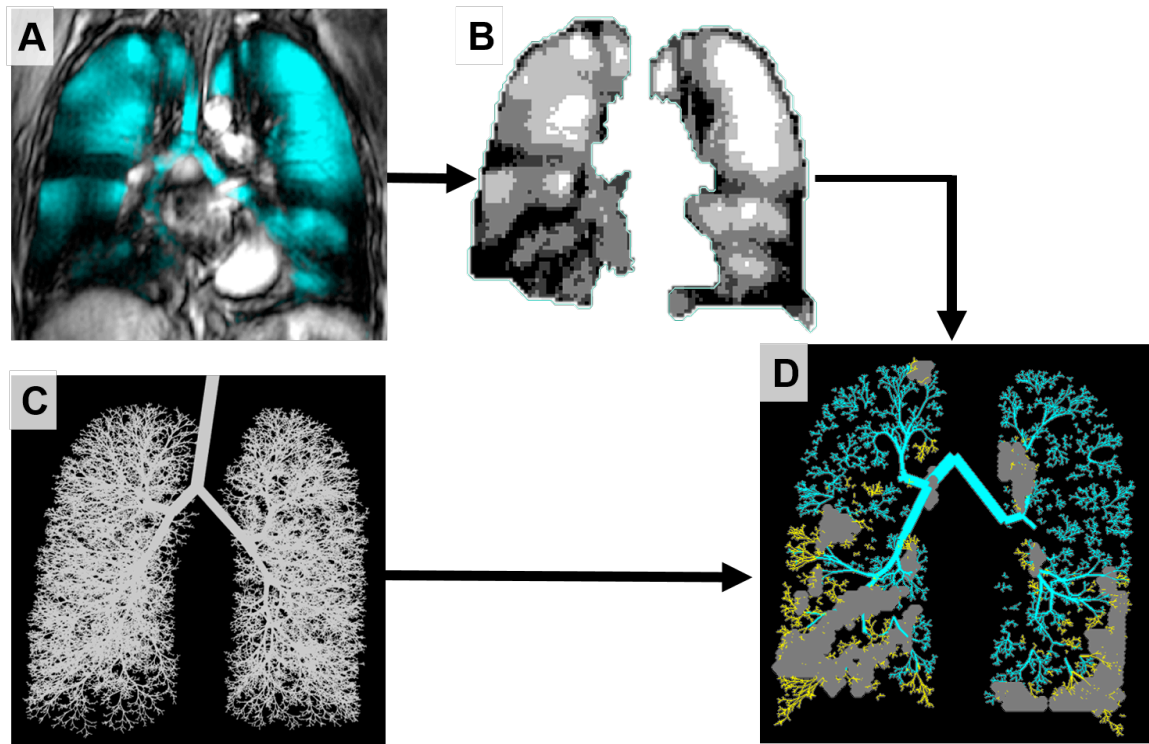


Figure 2-1: Pipeline for Co-Registration of MRI Ventilation Defects with Computational Airway Tree Model.

(A) Hyperpolarized ^3He MRI shown in cyan co-registered with anatomical ^1H MRI in greyscale. (B) The thoracic cavity, including the lungs, was automatically segmented using a manually-seeded algorithm and ventilation defects identified, shown in black. (C) An asymmetric branching computational airway tree model used to calculate respiratory system impedance. (D) The ventilation defect map was co-registered to the airway tree model. The small airways that were within or distal to a ventilation defect were identified, and narrowed to 10% of their original diameter. Ventilation defects are in grey and the airways related to defects are in yellow.

2.2.4 Statistics

The Shapiro-Wilk test was used to test data normality and non-parametric tests were used when the data were not normally distributed. Independent samples t tests and Mann-Whitney U tests were used to evaluate differences between asthma and COPD patients. Levene's test for equality of variances was used to test if the variance in the data was equal between two groups and when the variance was not equal, Welch's correction was applied to independent samples t tests. The Holm-Bonferroni correction was used to adjust for multiple comparisons. Univariate relationships were evaluated using Spearman correlations (ρ) because the data were not normally distributed. Significant relationships

identified using Spearman correlation were evaluated using linear regression. Results were considered statistically significant when the probability of making a Type I error was less than 5% ($p < 0.05$). All statistical tests were performed using SPSS 24.0 (IBM).

2.3 Results

2.3.1 Participant Demographics

As shown in Table 2-1, 100 participants were evaluated including 50 subjects with asthma (17 mild-moderate and 33 severe), and 50 ex-smokers. Within the ex-smoker group, 28 subjects had COPD (12 mild (GOLD I), 11 moderate (GOLD II) and 5 severe (GOLD III)). The ex-smokers were significantly older than the asthma subjects ($p < 0.001$). FEV₁ was significantly higher in the ex-smokers as compared to the asthmatic ($p < 0.001$) and the COPD subjects ($p < 0.001$), and plethysmography-measured airways resistance (R_{aw}) was significantly greater in the asthma group as compared to the COPD group ($p < 0.001$) and the ex-smokers ($p < 0.001$).

Table 2-1: Participant Demographics

Mean (\pm SD)	All (n=100)	Asthma (n=50)	COPD (n=28)	Ex- Smokers (n=22)	Asthma - COPD (p)	Asthma - Ex- Smokers (p)	COPD - Ex- Smokers (p)
Male n	54	21	19	14	-	-	-
Age years	61 (16)	49 (12)	75 (8)	70 (10)	<0.001	<0.001	0.2
BMI kg·m ⁻²	28 (4)	28 (4)	26 (4)	30 (4)	0.5	0.03	0.003
FEV ₁ % _{pred}	78 (26)	70 (23)	74 (25)	102 (20)	1.0	<0.001	<0.001
FVC % _{pred}	89 (20)	83 (20)	94 (19)	95 (20)	0.06	0.1	1.0
FEV ₁ /FVC %	65 (15)	64 (15)	56 (10)	80 (15)	0.02	<0.001	<0.001
TLC % _{pred}	102 (15)	103 (15)	107 (16)	95 (13)	0.8	0.1	0.02
RV/TLC %	43 (9)	41 (9)	47 (9)	40 (8)	0.04	1.0	0.04
DL _{CO} % _{pred}	-	-	60 (21)	83 (15)	-	-	<0.001
R_{aw} % _{pred}	127 (80)	171 (83)	95 (43)	65 (25)	<0.001	<0.001	0.6

Sig Dif: significance of difference between groups determined with a one-way ANOVA with Bonferroni post-hoc test. SD: standard deviation; %_{pred}: percent of predicted value; BMI: body mass index; FEV₁: forced expiratory volume in one second; FVC: forced vital capacity; TLC: total lung capacity; RV: residual volume; DL_{CO}: diffusing capacity of the lung for carbon monoxide; R_{aw} : airways resistance.

As shown in Figure 2-2, subjects with COPD had significantly higher VDP than ex-smokers ($p < 0.001$) and asthmatic subjects ($p < 0.001$), but there was not a significant difference in VDP between asthmatics and ex-smokers ($p = 0.4$). FOT-measured reactance

(X_{rs} 5Hz) was significantly more negative in asthma as compared to COPD subjects ($p = 0.04$) and ex-smokers ($p = 0.02$) and FOT-measured R_{rs} 5Hz and R_{rs} 5-19Hz, related to the obstruction of all airways and of the small airways respectively, were significantly greater in asthma as compared to COPD (R_{rs} 5Hz: $p < 0.001$, R_{rs} 5-19Hz: $p < 0.001$) and ex-smokers (R_{rs} 5Hz: $p < 0.001$, R_{rs} 5-19Hz: $p < 0.001$). There was no significant difference in FOT-measured R_{re} (R_{rs} 5Hz: $p = 1.0$, R_{rs} 5-19Hz: $p = 0.8$) or X_{rs} ($p = 1.0$) between ex-smokers and COPD patients.

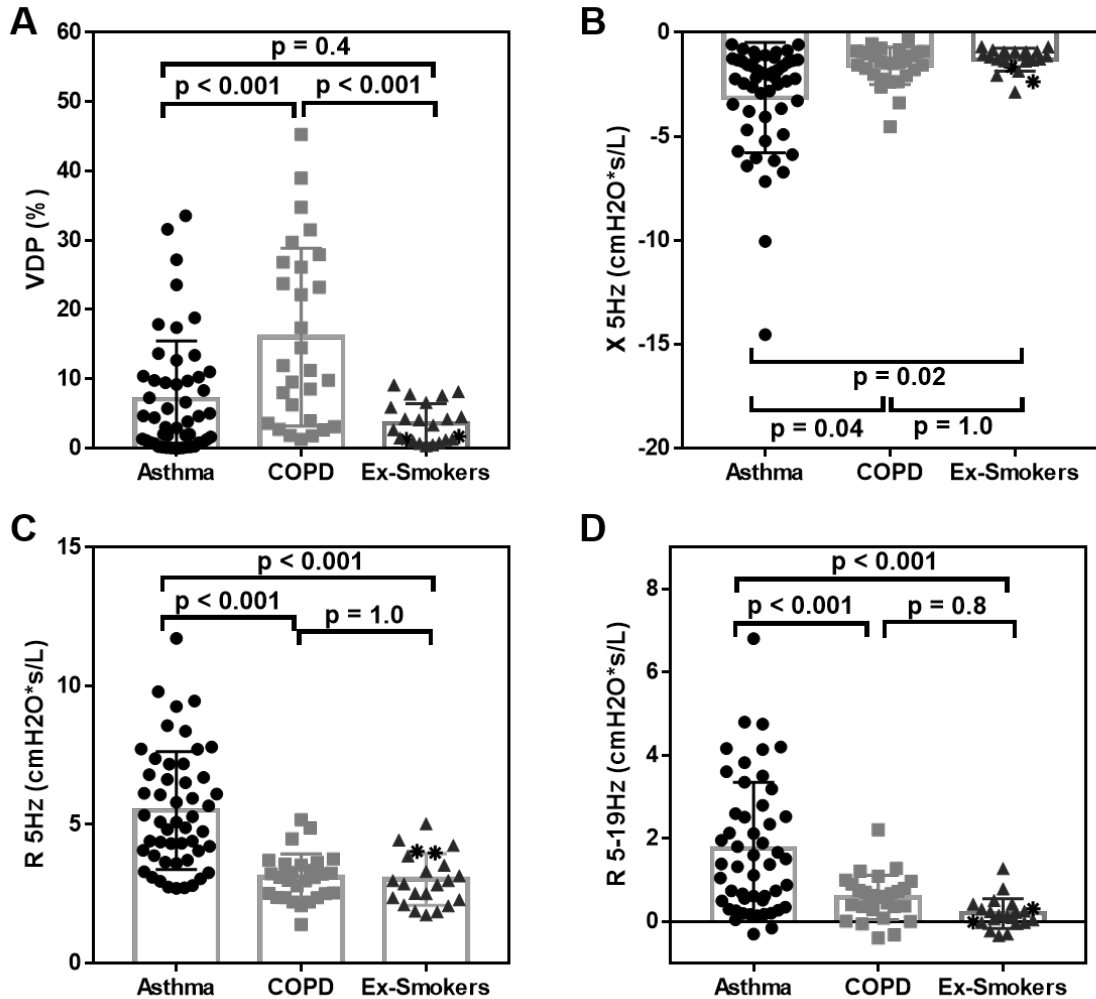


Figure 2-2: VDP and FOT-measured Resistance and Reactance in Asthma, COPD and Ex-Smoker Subgroups.

(A) VDP for asthma and COPD ($p < 0.001$) and COPD and ex-smoker ($p < 0.001$) subgroups were significantly different, but VDP was not different between asthmatic and ex-smoker groups ($p = 0.4$). (B) FOT-measured X_{rs} 5Hz was significantly greater in the asthmatic as compared to the COPD subgroup ($p = 0.04$) and the ex-smoker group ($p = 0.02$). X_{rs} was not different between COPD and ex-smoker subgroups ($p = 1.0$). (C) FOT-measured R_{rs} 5Hz was significantly greater in the asthmatic as compared to the COPD ($p < 0.001$) and ex-smoker ($p < 0.001$) subgroups, but it was not different between COPD and ex-smoker subgroups ($p = 1.0$). (D) FOT-measured R_{rs} 5-19Hz was significantly greater in the asthmatic as compared to the COPD ($p < 0.001$) and ex-smoker ($p < 0.001$) subgroups, but was not different between COPD and ex-smokers ($p = 0.8$).

* The two non-COPD ex-smokers who experienced exacerbations are indicated by the symbol (□) ES4: FEV1=102%_{pred}, FVC= 97%_{pred}, FEV1/FVC=80%, R_{rs} 5Hz=4.0 cmH₂O*s/L, X_{rs} 5Hz=-1.7cmH₂O*s/L, R_{rs} 5-19Hz=0.0cmH₂O*s/L, VDP=2%. ES14: FEV1=81%_{pred}, FVC=70%_{pred}, FEV1/FVC=88%, R_{rs} 5Hz=4.0cmH₂O*s/L, X_{rs} 5Hz=-2.4cmH₂O*s/L, R_{rs} 5-19Hz= 0.3cmH₂O*s/L, VDP=1%.

2.3.2 FOT and ³He MRI VDP Relationships

As shown in Figure 2-3, MRI VDP was significantly correlated with FOT-measured respiratory system resistance (R_{rs} 5Hz: $\rho = 0.3$, $p = 0.02$) and reactance (X_{rs} 5Hz: $\rho = -0.5$, $p < .001$) in asthmatics, while these measurements were not correlated in COPD patients (R_{rs} 5Hz: $\rho = -0.04$, $p = 0.8$; X_{rs} 5Hz: $\rho = -0.2$, $p = 0.4$) or ex-smokers (R_{rs} 5Hz: $\rho = -0.3$, $p = 0.2$; X_{rs} 5Hz: $\rho = 0.3$, $p = 0.2$). In both asthmatics ($\rho = 0.5$, $p < 0.001$) and COPD patients ($\rho = 0.5$, $p = 0.01$), small airways resistance (R_{rs} 5-19Hz) was significantly correlated with VDP, but these measurements were not correlated in ex-smokers ($\rho = -0.2$, $p = 0.4$).

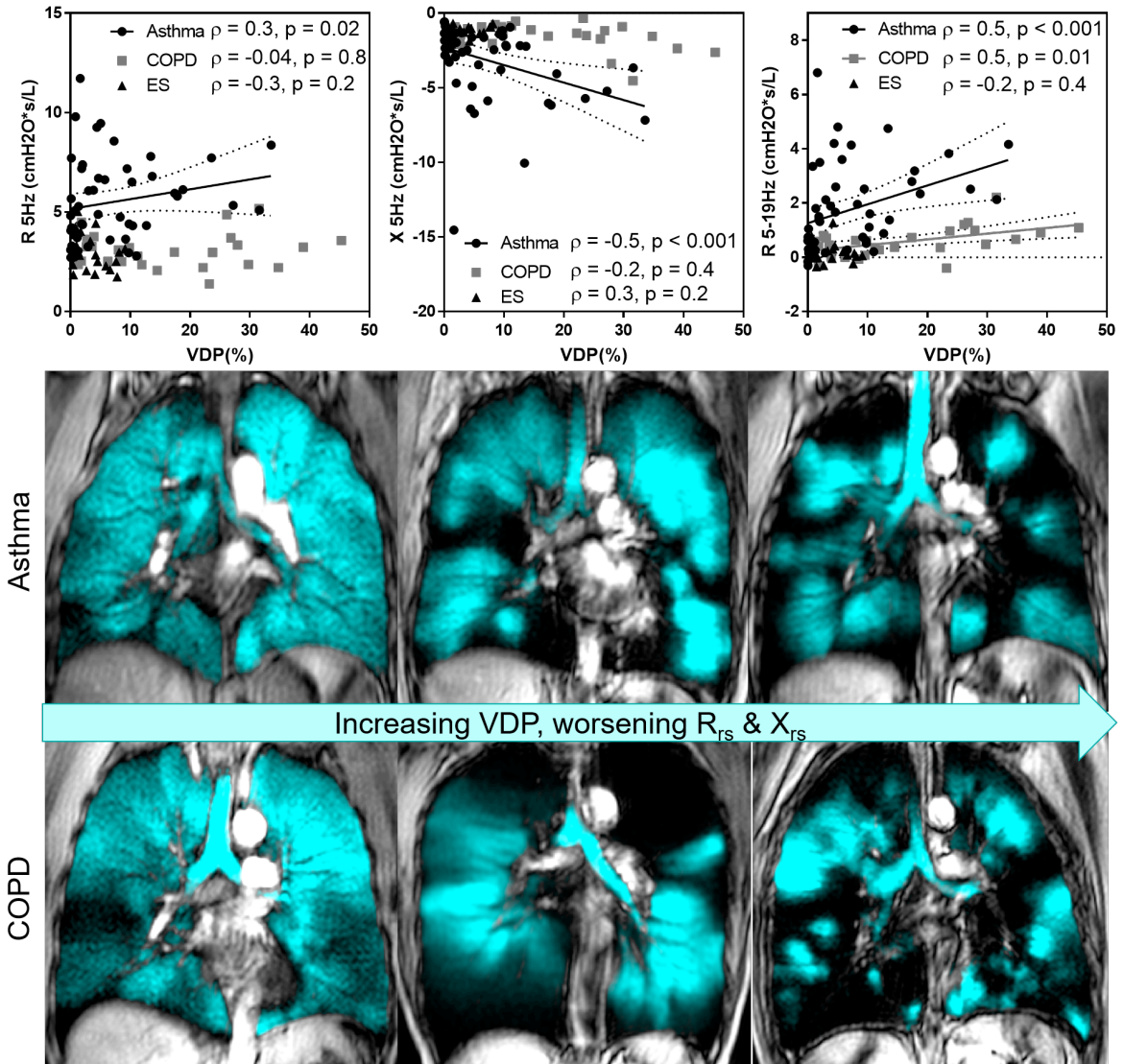


Figure 2-3: Relationships for VDP and FOT measurements

Top: FOT-measured R_{rs} 5Hz was significantly correlated with VDP in asthmatics (slope = 0.05 ± 0.03 , $\rho = 0.3$, $p = 0.02$) but not in COPD patients ($\rho = -0.04$, $p = 0.8$) or ex-smokers ($\rho = -0.3$, $p = 0.2$). FOT-measured X_{rs} 5Hz was significantly correlated with VDP in asthmatics (slope = -0.12 ± 0.04 , $\rho = -0.5$, $p < 0.001$) but not in COPD patients ($\rho = -0.2$, $p = 0.4$) or ex-smokers ($\rho = 0.3$, $p = 0.2$). FOT-measured R_{rs} 5-19Hz was significantly correlated with VDP in both asthmatic (slope = 0.07 ± 0.02 , $\rho = 0.5$, $p < 0.001$) and COPD patients (slope = 0.02 ± 0.007 , $\rho = 0.5$, $p = 0.01$) but not in ex-smokers ($\rho = -0.2$, $p = 0.4$). Centre: Three representative asthmatic subjects with worsening VDP and FOT-measured impedance from left to right. Bottom: Three representative COPD subjects with worsening VDP and FOT-measured impedance from left to right.

2.3.3 Relationships with Disease Control and Quality of Life Scores

All participants with asthma were stratified using the ACQ (well controlled = $ACQ \leq 2$, poorly controlled = $ACQ > 2$) as previously described.¹² Ex-smokers (including subjects with and without COPD) were classified based on the presence of an exacerbation requiring hospitalization within 2.5 years, such that patients who had been hospitalized at least once due to COPD or pneumonia were classified as poorly controlled. Nine out of fifty ex-smokers were poorly controlled, including 7 COPD patients and 2 subjects from the non-COPD group. As shown in Figure 2-4, FEV_1 was significantly different in poorly-controlled asthmatic patients ($p = 0.04$) but not ex-smokers ($p = 0.08$). Plethysmography-measured R_{aw} was significantly greater in poorly-controlled asthma ($p = 0.03$) and ex-smokers ($p = 0.04$), while VDP was significantly greater in patients with poorly-controlled asthma ($p = 0.03$) but not in ex-smokers with exacerbations ($p = 0.1$). In poorly-controlled asthmatics, FOT-measured respiratory system reactance (X_{rs} 5Hz, $p = 0.03$) and resistance of all airways (R_{rs} 5Hz, $p = 0.01$) and the small airways resistance (R_{rs} 5-19Hz, $p = 0.006$) were significantly different than in well-controlled asthmatics. None of the FOT measures of airway impedance (X_{rs} 5Hz, $p = 0.2$; R_{rs} 5Hz, $p = 0.6$; R_{rs} 5-19Hz, $p = 0.3$) were significantly different in ex-smokers with exacerbations.

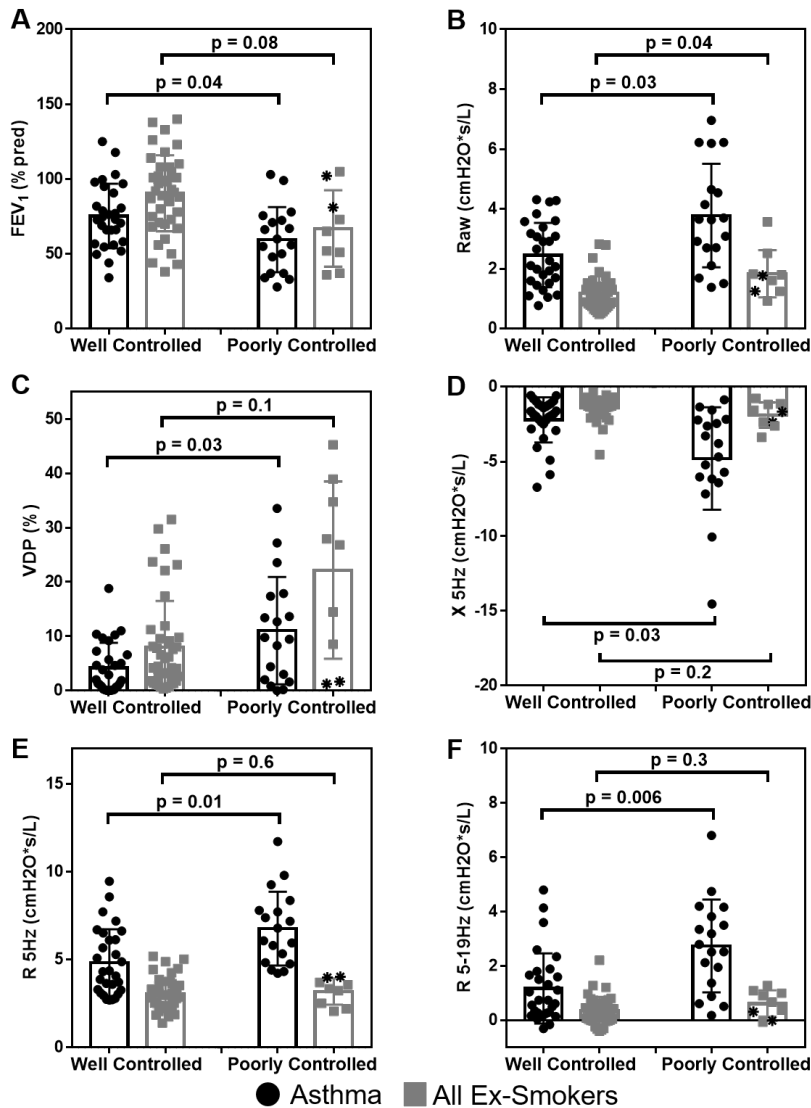


Figure 2-4: Differences in FEV₁, VDP and FOT Impedance Stratified by Disease Control.

Subjects were stratified based on disease control using the asthma control questionnaire (ACQ) for asthmatics or the presence of at least a single exacerbation requiring hospitalization in ex-smokers (including those with and without COPD). (A) FEV₁ was significantly different in asthma patients with poor control ($p = 0.04$) but not in ex-smokers ($p = 0.08$). (B) Plethysmography-measured R_{aw} was significantly decreased in poorly-controlled asthmatic patients ($p = 0.03$) and ex-smokers ($p = 0.04$). (C) VDP was significantly increased in poorly-controlled asthmatics ($p = 0.03$) but not in ex-smokers experiencing an exacerbation ($p = 0.1$). (D) FOT-measured X_{rs} 5Hz was significantly different in poorly-controlled asthmatics ($p = 0.03$) but not in ex-smokers experiencing an exacerbation ($p = 0.2$). (E) FOT-measured R_{rs} 5Hz was significantly increased in poorly-controlled asthmatics ($p = 0.01$) but not in ex-smokers ($p = 0.6$). (F) FOT-measured R_{rs} 5-19Hz was significantly different in poorly-controlled asthmatics ($p = 0.006$) but not in ex-smokers ($p = 0.3$). * The two non-COPD ex-smokers who experienced exacerbations are indicated by the symbol (□)

In asthmatics, as shown in Figure 2-5, AQLQ score was correlated only with FOT-measured small airways resistance (R_{rs} 5-19Hz; $\rho = -0.3$, $p = 0.04$) and VDP ($\rho = -0.3$, $p = 0.04$) and not with any other measurement acquired. Quality of life in COPD patients measured using the SGRQ score was significantly correlated with FEV₁ ($\rho = -0.5$, $p = 0.006$), R_{aw} ($\rho = 0.4$, $p = 0.03$), FOT-measured resistance of the small airways R_{rs} 5-19Hz ($\rho = 0.4$, $p = 0.04$) and VDP ($\rho = 0.6$, $p = 0.003$). SGRQ scores were not significantly related to FOT-measured resistance R_{rs} 5Hz ($\rho = 0.1$, $p = 0.5$) or reactance, X_{rs} 5Hz ($\rho = -0.2$, $p = 0.3$). In the non-COPD ex-smoker group, SGRQ scores were only significantly related to plethysmography-measured R_{aw} ($\rho = 0.5$, $p = 0.01$).

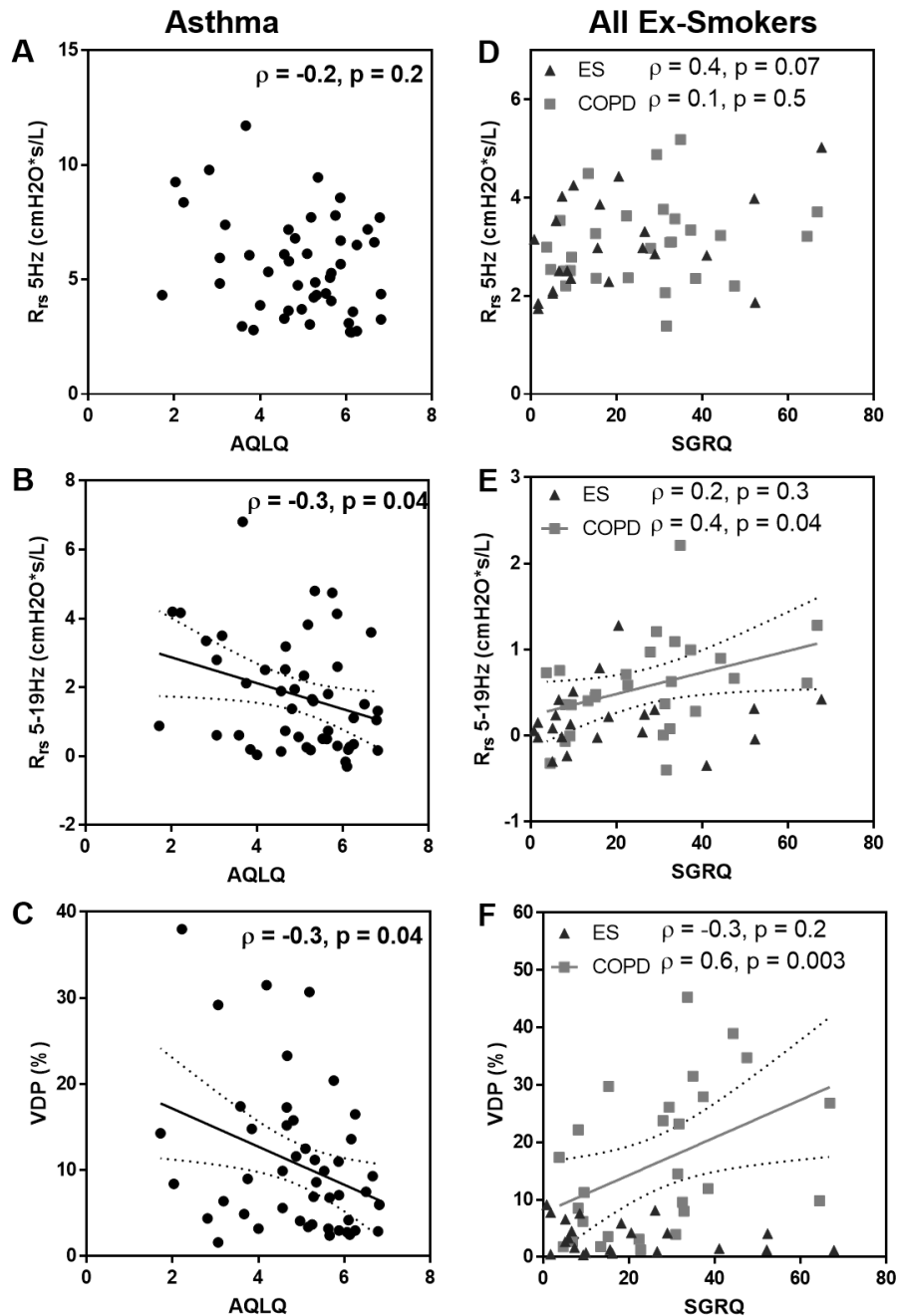


Figure 2-5: Relationships between FOT-measured Resistance and MRI VDP with Quality of Life.

Quality of life was measured using the Asthma Quality of Life Questionnaire (AQLQ) and the St. George's Respiratory Questionnaire (SGRQ). In asthmatics, AQLQ relationships with (A) FOT-measured R_{rs} 5Hz ($\rho = -0.2, p = 0.2$), (B) FOT-measured R_{rs} 5-19Hz (slope = -0.4 ± 0.2 , $\rho = -0.3, p = 0.04$), and (C) MRI-measured VDP (slope = -2.2 ± 0.9 , $\rho = -0.3, p = 0.04$). In COPD patients and ex-smokers, SGRQ relationships with (D) FOT-measured R_{rs} 5Hz (COPD: $\rho = 0.1, p = 0.5$; ES: $\rho = 0.4, p = 0.07$), (E) FOT-measured R_{rs} 5-19Hz (COPD: slope = 0.01 ± 0.006 , $\rho = 0.4, p = 0.04$; ES: $\rho = 0.2, p = 0.3$), and (F) MRI-measured VDP (COPD: slope = 0.3 ± 0.1 , $\rho = 0.6, p = 0.003$; ES: $\rho = -0.3, p = 0.2$).

2.3.4 Experimental and Model Impedance Measurements

As shown in Figure 2-6, FOT-measured resistance of all airways (R_{rs} 5Hz_{meas}) was not significantly related to model-predicted resistance (R_{rs} 5Hz_{pred}) in asthmatics ($\rho = 0.2$, $p = 0.2$) nor in ex-smokers ($\rho = -0.3$, $p = 0.2$) and COPD patients ($\rho = 0.001$, $p = 1.0$). However, FOT-measured respiratory system reactance (X_{rs} 5Hz_{meas}) was significantly related to model-predicted reactance (X_{rs} 5Hz_{pred}) in asthmatics (slope = 1.4 ± 0.6 , $\rho = 0.5$, $p = 0.001$) but not in COPD patients ($\rho = 0.2$, $p = 0.4$) or ex-smokers ($\rho = -0.3$, $p = 0.2$). In contrast, FOT-measured small airway resistance (R_{rs} 5-19Hz_{meas}) was significantly correlated with model-predictions (R_{rs} 5-19Hz_{pred}) in COPD patients (slope = 2.6 ± 0.7 , $\rho = 0.5$, $p = 0.004$) but not in ex-smokers ($\rho = -0.1$, $p = 0.6$) or asthmatics ($\rho = 0.2$, $p = 0.1$).

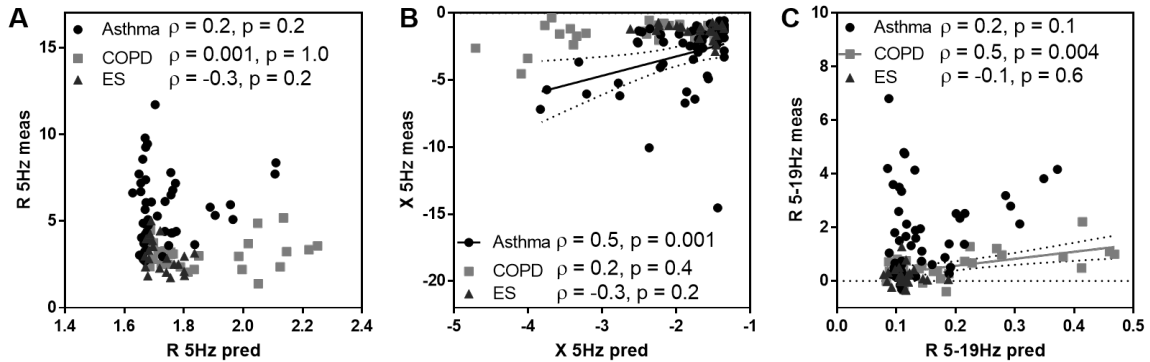


Figure 2-6. Relationships for Model-predicted and FOT-measured Respiratory System Impedance.

(A) FOT-measured R_{rs} 5Hz_{meas} was not significantly related to model-predicted R_{rs} 5Hz_{pred} in asthma ($\rho = 0.2$, $p = 0.2$), COPD patients ($\rho = 0.001$, $p = 1.0$) or ex-smokers ($\rho = -0.3$, $p = 0.2$). (B) FOT-measured X_{rs} 5Hz_{meas} was significantly related to model-predicted X_{rs} 5Hz_{pred} in asthmatic patients (slope = 1.4 ± 0.6 , $\rho = 0.5$, $p = 0.001$) but not in COPD patients ($\rho = 0.2$, $p = 0.4$) or ex-smokers ($\rho = -0.3$, $p = 0.2$). (C) FOT-measured R_{rs} 5-19Hz_{meas} was significantly correlated with model-predicted R_{rs} 5-19Hz_{pred} in COPD (slope = 2.6 ± 0.7 , $\rho = 0.5$, $p = 0.004$) but not in asthmatics ($\rho = 0.2$, $p = 0.1$) or ex-smokers ($\rho = -0.1$, $p = 0.6$).

2.4 Discussion

In ex-smokers and patients with asthma, ^3He MRI ventilation heterogeneity and oscillometry measurements were evaluated as was their relationship with one another, with quality of life scores and with disease control/exacerbations. We also generated respiratory

impedance predictions using an airway tree model modified based on patient-specific MRI ventilation maps and evaluated model-based and experimental impedance measurements. We made a number of important observations including: 1) in asthmatics, MRI VDP was related to FOT-measured X_{rs} 5Hz, R_{rs} 5Hz and R_{rs} 5-19Hz, but in COPD patients, only VDP and R_{rs} 5-19Hz were related and in ex-smokers MRI VDP was not related to FOT-measured impedance, 2) VDP and FOT-measured X_{rs} and R_{rs} were independently correlated with AQLQ (in asthmatics) and SGRQ (in COPD patients) but were not correlated with SGRQ in ex-smokers without COPD, 3) FOT-measured impedance and MRI VDP were independently related to disease control in asthmatic patients but not in ex-smokers or COPD patients, and finally, 4) in patients with asthma, measured and predicted respiratory impedance (X_{rs} 5Hz) were significantly correlated, whereas in patients with COPD, only measured and predicted small airways resistance (R_{rs} 5-19Hz) were related.

2.4.1 FOT and ^3He MRI Ventilation Heterogeneity

First, we observed that FOT-measured R_{rs} and X_{rs} were correlated with MRI VDP, providing direct evidence that the biomechanical properties of the respiratory system are related to ventilation heterogeneity in both asthma and COPD patients. In particular, in asthmatics, R_{rs} , X_{rs} and R_{rs} 5-19Hz were all related to VDP, but in COPD, only R_{rs} 5-19Hz was related. This suggests that there are differences in the etiology of ventilation defects in asthmatic and COPD patients, and that in the COPD patients studied here, VDP was dominated by small airway resistance. Interestingly, non-COPD ex-smokers had similar small airway resistance to the subjects with COPD, but had significantly lower VDP. This suggests that similar biomechanical changes are present in ex-smokers, but they are not severe enough to cause ventilation defects. These findings certainly support the ongoing conversation about the important role of small airways disease in COPD patients⁷¹ and provide new impetus for the development of small airway treatments of COPD. Previously described computational modelling⁴⁹ and ventilation heterogeneity studies⁷² have focused on asthma but to our knowledge, our observations in COPD patients are novel. A recent SPECT study¹⁴ evaluated the impact of bronchoconstriction in asthmatics and suggested that respiratory impedance may be too complex to be directly evaluated using ventilation

imaging. However, here we showed that MRI ventilation abnormalities may be explained by oscillometry measurements and surprisingly, MRI ventilation abnormalities measured during a static breath-hold may be explained by impedance measurements made during tidal breathing.

2.4.2 FOT, Disease Control and Quality of Life

Second, we observed that FOT-measured small airways resistance and VDP were related to quality of life scores in patients with asthma and COPD, but not in ex-smokers. This is important because for FEV₁, which is the most commonly used measurement of obstructive lung disease, relationships with important outcomes like quality of life are generally weak to insignificant.⁷³⁻⁷⁵ As patient-centered care becomes a priority in clinical settings, the ability to relate physiological measurements to patient quality of life is increasingly important. This has motivated the development of tools that are more sensitive to these important patient outcomes so that they may be predicted in individual patients. Our results suggest that FOT and MRI provide clinically-useful measurements, for this purpose, in asthmatics and COPD patients.

Perhaps more importantly for clinical decision makers, while we observed that plethysmography-measured R_{aw} was significantly worse in asthmatics, ex-smokers and COPD patients with poorly controlled disease, FOT-measured R_{rs} and X_{rs} as well as VDP were all significantly worse in poorly-controlled asthmatics. While we did not observe significant relationships in COPD patients or ex-smokers, some of these relationships were certainly trending towards significance and this result may stem from the small number of exacerbations in these patients – which was used as a surrogate endpoint for disease control. It is understood that R_{aw} and R_{rs} are significantly correlated, although these correlations are not always strong.⁷⁶ A power analysis assuming unequal sample size using hospitalizations as a conservative measure of disease control revealed that 104 ex-smokers (including COPD patients) would be required for R_{rs} 5-19Hz as a predictor of hospitalizations, while only 40 patients would be needed for R_{aw}. Larger studies to investigate the power of both FOT and MRI to predict and prevent COPD hospitalization

will be important because COPD exacerbations comprises a very large health utilization burden in Canada^{77, 78} and around the world.^{79, 80}

2.4.3 Measured Impedance and Image Functional Modeling

Finally, we generated impedance predictions using an airway tree model adapted using ventilation MRI measurements. We were not surprised to find that the experimental and model-predicted values of R_{rs} 5Hz were not significantly correlated, because it is likely that some airway narrowing may not directly lead to ventilation defects in patients. We also observed that FOT-measured and model-predicted reactance (X_{rs}) were significantly related in asthmatics, which was in agreement with previous findings.^{32, 51, 81} Finally, the measured and predicted resistance reflecting the small airways (R_{rs} 5-19Hz) were significantly correlated in COPD patients, but not asthmatics and this is consistent with our understanding of the dominant role of small airways disease in COPD.⁷¹ It is important to note that while there were moderately strong correlations between the measured and predicted impedance values, the predicted values were significantly smaller (based on the slopes of the linear regression). This was expected because previous work⁵¹ showed that up to 75% of the small airways need to be constricted to achieve model and experimental measurement agreement. Impedance predictions were systematically underestimated⁵¹ when only airways within a defect were considered, supporting previous demonstrations⁴⁸ that showed constriction of airways beyond those proximal to ventilation defects is required to simulate impedance measurements in asthmatics.

2.4.4 Limitations

We acknowledge and recognize a number of study limitations, including the fact that we considered ventilation defects only and not regions of decreased or partial ventilation. Based on previous modeling studies⁴⁸ and MRI evidence of patchy ventilation sometimes observed in asthmatics and ex-smokers, it would be relevant to consider hyper-intense ventilation regions as well as hypo-intense regions that are not captured by VDP. We note as well that the airway tree⁴⁷ used in the modelling studies was not patient-specific, nor were the impedance values of the upper airway and chest wall. However, we expect these

factors to contribute much less to R_{rs} and X_{rs} than the changes occurring within the lung itself in obstructive lung disease. Despite these limitations, we observed significant correlations between measured and model-predicted impedance for the small airways which is important for further model development. Another limitation of this work is the use of hospitalizations as a surrogate measure of disease control in ex-smokers. While hospitalizations have the highest impact on patients and the health-care system,⁷⁷ only nine of fifty ex-smokers studied here experienced an exacerbation which certainly diminished statistical power. A retrospective power analysis showed that 104 ex-smokers would be required to determine the role of FOT impedance measurements as predictors of COPD hospitalizations; larger studies will be needed to explore these relationships. Finally, while we observed significant relationships between FOT measurements of resistance and reactance with MRI VDP and patient quality of life, these relationships were of moderate to weak strength. This means that there are other variables that have not yet been fully accounted for, and further work must be done to fully understand how respiratory impedance and ventilation heterogeneity are related to patient outcomes.

2.4.5 Conclusions

In conclusion, we made oscillometry and MRI measurements in ex-smokers and patients with asthma and directly compared these measurements with disease control and patient quality of life scores. We observed significant relationships for FOT-measured impedance and VDP with quality of life, providing strong evidence that airway resistance and reactance are reflective of MRI ventilation defects, and importantly they both explain quality of life in patients. We also used MRI ventilation defects to generate patient-specific computational airway model predictions of respiratory system impedance and, for the first time, compared these predictions with experimental measurements. Taken together, these results provide strong motivation for multiscale studies that explore how small airways disease and ventilation abnormalities may explain and help improve disease control and quality of life in patients.

2.5 References

- (1) Downie, S.R. et al. Ventilation heterogeneity is a major determinant of airway hyperresponsiveness in asthma, independent of airway inflammation. *Thorax* **62**, 684-9 (2007).
- (2) Macleod, K.A. et al. Ventilation heterogeneity in children with well controlled asthma with normal spirometry indicates residual airways disease. *Thorax* **64**, 33-7 (2009).
- (3) Farah, C.S. et al. Ventilation heterogeneity predicts asthma control in adults following inhaled corticosteroid dose titration. *J Allergy Clin Immunol* **130**, 61-8 (2012).
- (4) Verbanck, S., Schuermans, D., Paiva, M. & Vincken, W. Nonreversible conductive airway ventilation heterogeneity in mild asthma. *J Appl Physiol (1985)* **94**, 1380-6 (2003).
- (5) Verbanck, S., Schuermans, D., Meysman, M., Paiva, M. & Vincken, W. Noninvasive assessment of airway alterations in smokers: the small airways revisited. *Am J Respir Crit Care Med* **170**, 414-9 (2004).
- (6) Boeck, L. et al. Single-Breath Washout Tests to Assess Small Airway Disease in COPD. *Chest* **150**, 1091-1100 (2016).
- (7) Bourdin, A. et al. Nitrogen washout slope in poorly controlled asthma. *Allergy* **61**, 85-9 (2006).
- (8) Thompson, B.R. et al. Peripheral lung function in patients with stable and unstable asthma. *J Allergy Clin Immunol* **131**, 1322-8 (2013).
- (9) Becklake, M.R. A new index of the intrapulmonary mixture of inspired air. *Thorax* **7**, 111-6 (1952).
- (10) Robinson, P.D. et al. Consensus statement for inert gas washout measurement using multiple- and single- breath tests. *Eur Respir J* **41**, 507-22 (2013).
- (11) Robinson, P.D., Goldman, M.D. & Gustafsson, P.M. Inert gas washout: theoretical background and clinical utility in respiratory disease. *Respiration* **78**, 339-55 (2009).
- (12) Svenningsen, S., Nair, P., Guo, F., McCormack, D.G. & Parraga, G. Is ventilation heterogeneity related to asthma control? *Eur Respir J* **48**, 370-9 (2016).
- (13) Venegas, J.G. et al. Self-organized patchiness in asthma as a prelude to catastrophic shifts. *Nature* **434**, 777-82 (2005).

- (14) Farrow, C.E. et al. Peripheral Ventilation Heterogeneity Determines the Extent of Bronchoconstriction in Asthma. *J Appl Physiol* (1985), jap 00640 2016 (2017).
- (15) Tzeng, Y.S., Lutchen, K. & Albert, M. The difference in ventilation heterogeneity between asthmatic and healthy subjects quantified using hyperpolarized ³He MRI. *J Appl Physiol* (1985) **106**, 813-22 (2009).
- (16) Altes, T.A. et al. Hyperpolarized ³He MR lung ventilation imaging in asthmatics: preliminary findings. *J Magn Reson Imaging* **13**, 378-84 (2001).
- (17) Canadian Institute for Health Information. Inpatient Hospitalizations, Surgeries, Newborns and Childbirth Indicators, 2015-2016. (2017).
- (18) The Lung Association. Asthma Control in Canada Survey. (2016). www.lung.ca/ (Retrieved November 2016).
- (19) Asthma Canada. Asthma Facts and Statistics, FAQs. (2017). www.asthma.ca (accessed November 2017).
- (20) Ontario Lung Association. Your Lungs, Your Life: Insights and Solutions to Lung Health in Ontario. (2011).
- (21) Svenningsen, S. et al. What are ventilation defects in asthma? *Thorax* **69**, 63-71 (2014).
- (22) DeBoer, E.M., Spielberg, D.R. & Brody, A.S. Clinical potential for imaging in patients with asthma and other lung disorders. *J Allergy Clin Immunol* **139**, 21-28 (2017).
- (23) Altes, T.A. et al. Clinical correlates of lung ventilation defects in asthmatic children. *J Allergy Clin Immunol* **137**, 789-96 e7 (2016).
- (24) Dubois, A.B., Brody, A.W., Lewis, D.H. & Burgess, B.F., Jr. Oscillation mechanics of lungs and chest in man. *J Appl Physiol* **8**, 587-94 (1956).
- (25) Tgavalekos, N.T., Venegas, J.G., Suki, B. & Lutchen, K.R. Relation between structure, function, and imaging in a three-dimensional model of the lung. *Ann Biomed Eng* **31**, 363-73 (2003).
- (26) Di Mango, A.M., Lopes, A.J., Jansen, J.M. & Melo, P.L. Changes in respiratory mechanics with increasing degrees of airway obstruction in COPD: detection by forced oscillation technique. *Respir Med* **100**, 399-410 (2006).
- (27) Van Noord, J.A., Smeets, J., Clement, J., Van de Woestijne, K.P. & Demedts, M. Assessment of reversibility of airflow obstruction. *Am J Respir Crit Care Med* **150**, 551-4 (1994).

- (28) Zerah, F., Lorino, A.M., Lorino, H., Harf, A. & Macquin-Mavier, I. Forced oscillation technique vs spirometry to assess bronchodilatation in patients with asthma and COPD. *Chest* **108**, 41-7 (1995).
- (29) Cavalcanti, J.V., Lopes, A.J., Jansen, J.M. & Melo, P.L. Detection of changes in respiratory mechanics due to increasing degrees of airway obstruction in asthma by the forced oscillation technique. *Respir Med* **100**, 2207-19 (2006).
- (30) Duiverman, E.J., Neijens, H.J., Van der Snee-van Smaalen, M. & Kerrebijn, K.F. Comparison of forced oscillometry and forced expirations for measuring dose-related responses to inhaled methacholine in asthmatic children. *Bull Eur Physiopathol Respir* **22**, 433-6 (1986).
- (31) Delacourt, C. et al. Use of the forced oscillation technique to assess airway obstruction and reversibility in children. *Am J Respir Crit Care Med* **161**, 730-6 (2000).
- (32) Lutchen, K.R. & Gillis, H. Relationship between heterogeneous changes in airway morphometry and lung resistance and elastance. *J Appl Physiol (1985)* **83**, 1192-201 (1997).
- (33) Kaczka, D.W., Ingenito, E.P., Israel, E. & Lutchen, K.R. Airway and lung tissue mechanics in asthma. Effects of albuterol. *Am J Respir Crit Care Med* **159**, 169-78 (1999).
- (34) de Lange, E.E. et al. Evaluation of asthma with hyperpolarized helium-3 MRI: correlation with clinical severity and spirometry. *Chest* **130**, 1055-62 (2006).
- (35) de Lange, E.E. et al. Changes in regional airflow obstruction over time in the lungs of patients with asthma: evaluation with ³He MR imaging. *Radiology* **250**, 567-75 (2009).
- (36) Samee, S. et al. Imaging the lungs in asthmatic patients by using hyperpolarized helium-3 magnetic resonance: assessment of response to methacholine and exercise challenge. *J Allergy Clin Immunol* **111**, 1205-11 (2003).
- (37) Parraga, G. et al. Hyperpolarized ³He ventilation defects and apparent diffusion coefficients in chronic obstructive pulmonary disease: preliminary results at 3.0 Tesla. *Invest Radiol* **42**, 384-91 (2007).
- (38) Mathew, L. et al. Hyperpolarized ³He magnetic resonance imaging: preliminary evaluation of phenotyping potential in chronic obstructive pulmonary disease. *Eur J Radiol* **79**, 140-146 (2011).
- (39) Kauczor, H.U. et al. Imaging of the lungs using ³He MRI: preliminary clinical experience in 18 patients with and without lung disease. *J Magn Reson Imaging* **7**, 538-43 (1997).

- (40) Kirby, M. et al. Hyperpolarized ^3He and ^{129}Xe MR imaging in healthy volunteers and patients with chronic obstructive pulmonary disease. *Radiology* **265**, 600-10 (2012).
- (41) Kirby, M. et al. COPD: Do Imaging Measurements of Emphysema and Airway Disease Explain Symptoms and Exercise Capacity? *Radiology* **277**, 872-80 (2015).
- (42) Costella, S. et al. Regional pulmonary response to a methacholine challenge using hyperpolarized (^3He) magnetic resonance imaging. *Respirology* **17**, 1237-46 (2012).
- (43) Svenningsen, S. et al. Hyperpolarized (^3He) and (^{129}Xe) MRI: differences in asthma before bronchodilation. *J Magn Reson Imaging* **38**, 1521-30 (2013).
- (44) Kirby, M. et al. Chronic obstructive pulmonary disease: quantification of bronchodilator effects by using hyperpolarized (^3He) MR imaging. *Radiology* **261**, 283-92 (2011).
- (45) Kirby, M., Heydarian, M., Wheatley, A., McCormack, D.G. & Parraga, G. Evaluating bronchodilator effects in chronic obstructive pulmonary disease using diffusion-weighted hyperpolarized helium-3 magnetic resonance imaging. *J Appl Physiol (1985)* **112**, 651-7 (2012).
- (46) Kirby, M., Kanhere, N., Etemad-Rezai, R., McCormack, D.G. & Parraga, G. Hyperpolarized helium-3 magnetic resonance imaging of chronic obstructive pulmonary disease exacerbation. *J Magn Reson Imaging* **37**, 1223-7 (2013).
- (47) Tawhai, M.H. et al. CT-based geometry analysis and finite element models of the human and ovine bronchial tree. *J Appl Physiol (1985)* **97**, 2310-21 (2004).
- (48) Tgavalekos, N.T. et al. Relationship between airway narrowing, patchy ventilation and lung mechanics in asthmatics. *Eur Respir J* **29**, 1174-81 (2007).
- (49) Campana, L. et al. Probing airway conditions governing ventilation defects in asthma via hyperpolarized MRI image functional modeling. *J Appl Physiol (1985)* **106**, 1293-300 (2009).
- (50) Leary, D., Bhatawadekar, S.A., Parraga, G. & Maksym, G.N. Modeling stochastic and spatial heterogeneity in a human airway tree to determine variation in respiratory system resistance. *J Appl Physiol (1985)* **112**, 167-75 (2012).
- (51) Bhatawadekar, S.A., Leary, D. & Maksym, G.N. Modelling resistance and reactance with heterogeneous airway narrowing in mild to severe asthma. *Can J Physiol Pharmacol* **93**, 207-14 (2015).
- (52) Leary, D. et al. Hyperpolarized ^3He magnetic resonance imaging ventilation defects in asthma: relationship to airway mechanics. *Physiol Rep* **4**, e12761 (2016).

- (53) Tgavalekos, N.T. et al. Identifying airways responsible for heterogeneous ventilation and mechanical dysfunction in asthma: an image functional modeling approach. *J Appl Physiol* (1985) **99**, 2388-97 (2005).
- (54) Kaczka, D.W., Lutchen, K.R. & Hantos, Z. Emergent behavior of regional heterogeneity in the lung and its effects on respiratory impedance. *J Appl Physiol* (1985) **110**, 1473-81 (2011).
- (55) Bhatawadekar, S.A., Hernandez, P. & Maksym, G.N. Oscillatory Mechanics in Asthma: Emphasis on Airway Variability and Heterogeneity. *Crit Rev Biomed Eng* **43**, 97-130 (2015).
- (56) Thien, F. Measuring and imaging small airways dysfunction in asthma. *Asia Pac Allergy* **3**, 224-30 (2013).
- (57) Bates, J.H. & Lutchen, K.R. The interface between measurement and modeling of peripheral lung mechanics. *Respir Physiol Neurobiol* **148**, 153-64 (2005).
- (58) Vestbo, J. et al. Global strategy for the diagnosis, management, and prevention of chronic obstructive pulmonary disease: GOLD executive summary. *Am J Respir Crit Care Med* **187**, 347-65 (2013).
- (59) Juniper, E.F., O'Byrne, P.M., Guyatt, G.H., Ferrie, P.J. & King, D.R. Development and validation of a questionnaire to measure asthma control. *Eur Respir J* **14**, 902-7 (1999).
- (60) Juniper, E.F., Buist, A.S., Cox, F.M., Ferrie, P.J. & King, D.R. Validation of a standardized version of the Asthma Quality of Life Questionnaire. *Chest* **115**, 1265-70 (1999).
- (61) Jones, P.W., Quirk, F.H., Baveystock, C.M. & Littlejohns, P. A self-complete measure of health status for chronic airflow limitation. The St. George's Respiratory Questionnaire. *Am Rev Respir Dis* **145**, 1321-7 (1992).
- (62) Miller, M.R. et al. Standardisation of spirometry. *Eur Respir J* **26**, 319-38 (2005).
- (63) Guo, F. et al. Globally optimal co-segmentation of three-dimensional pulmonary (1)H and hyperpolarized (3)He MRI with spatial consistence prior. *Med Image Anal* **23**, 43-55 (2015).
- (64) Kirby, M. et al. Hyperpolarized 3He magnetic resonance functional imaging semiautomated segmentation. *Acad Radiol* **19**, 141-52 (2012).
- (65) Kaczka, D.W., Massa, C.B. & Simon, B.A. Reliability of estimating stochastic lung tissue heterogeneity from pulmonary impedance spectra: a forward-inverse modeling study. *Ann Biomed Eng* **35**, 1722-38 (2007).

- (66) Nagels, J., Landser, F.J., van der Linden, L., Clement, J. & Van de Woestijne, K.P. Mechanical properties of lungs and chest wall during spontaneous breathing. *J Appl Physiol Respir Environ Exerc Physiol* **49**, 408-16 (1980).
- (67) Barnas, G.M., Yoshino, K., Loring, S.H. & Mead, J. Impedance and relative displacements of relaxed chest wall up to 4 Hz. *J Appl Physiol (1985)* **62**, 71-81 (1987).
- (68) Barnas, G.M. et al. Chest wall impedance partitioned into rib cage and diaphragm-abdominal pathways. *J Appl Physiol (1985)* **66**, 350-9 (1989).
- (69) Barnas, G.M. et al. Total and local impedances of the chest wall up to 10 Hz. *J Appl Physiol (1985)* **68**, 1409-14 (1990).
- (70) Cauberghs, M. & Van de Woestijne, K.P. Mechanical properties of the upper airway. *J Appl Physiol Respir Environ Exerc Physiol* **55**, 335-42 (1983).
- (71) Hogg, J.C. et al. The nature of small-airway obstruction in chronic obstructive pulmonary disease. *N Engl J Med* **350**, 2645-53 (2004).
- (72) Downie, S.R. et al. Effect of methacholine on peripheral lung mechanics and ventilation heterogeneity in asthma. *J Appl Physiol (1985)* **114**, 770-7 (2013).
- (73) Woodruff, P.G. et al. Clinical Significance of Symptoms in Smokers with Preserved Pulmonary Function. *N Engl J Med* **374**, 1811-21 (2016).
- (74) Alcaide, A.B. et al. Clinical Features of Smokers With Radiological Emphysema But Without Airway Limitation. *Chest* **151**, 358-365 (2017).
- (75) Teeter, J.G. & Bleecker, E.R. Relationship between airway obstruction and respiratory symptoms in adult asthmatics. *Chest* **113**, 272-7 (1998).
- (76) Hellinckx, J., Cauberghs, M., De Boeck, K. & Demedts, M. Evaluation of impulse oscillation system: comparison with forced oscillation technique and body plethysmography. *Eur Respir J* **18**, 564-70 (2001).
- (77) Toy, E.L., Gallagher, K.F., Stanley, E.L., Swensen, A.R. & Duh, M.S. The economic impact of exacerbations of chronic obstructive pulmonary disease and exacerbation definition: a review. *COPD* **7**, 214-28 (2010).
- (78) Gershon, A.S., Guan, J., Victor, J.C., Goldstein, R. & To, T. Quantifying health services use for chronic obstructive pulmonary disease. *Am J Respir Crit Care Med* **187**, 596-601 (2013).
- (79) Foster, T.S. et al. Assessment of the economic burden of COPD in the U.S.: a review and synthesis of the literature. *COPD* **3**, 211-8 (2006).

- (80) Oostenbrink, J.B. & Rutten-van Molken, M.P. Resource use and risk factors in high-cost exacerbations of COPD. *Respir Med* **98**, 883-91 (2004).
- (81) Thorpe, C.W. & Bates, J.H. Effect of stochastic heterogeneity on lung impedance during acute bronchoconstriction: a model analysis. *J Appl Physiol (1985)* **82**, 1616-25 (1997).

CHAPTER 3

3 CONCLUSIONS AND FUTURE DIRECTIONS

3.1 Overview and Research Questions

Obstructive lung disease represents a huge health care burden in Ontario¹ and worldwide,² reflecting the need for a better understanding of the mechanisms of disease and how they can be treated. While obstructive lung disease is known to be spatially heterogeneous and to involve small airway dysfunction, the structure-function relationships related to ventilation defects are not fully understood. The objective of this thesis was to apply the forced oscillation technique (FOT), hyperpolarized ³He magnetic resonance imaging (MRI), and computational airway tree modelling to study obstructive lung disease. The specific research questions were: 1) How are structural and mechanical changes measured by FOT related to MRI ventilation defects? 2) How do these measures of ventilation heterogeneity relate to disease control and patient quality of life in obstructive lung disease?

3.2 Summary and Conclusions

In this thesis, I evaluated 100 subjects (50 asthma, 28 COPD, 22 ex-smokers) using quality of life questionnaires, FOT, and hyperpolarized ³He MRI. I sought to measure the relationships between respiratory system impedance, MRI ventilation heterogeneity, and patient quality of life. I also developed upon previous work using MRI ventilation defects to modify a computational airway tree model to generate patient-specific predictions of airway impedance and compared them to FOT-measured impedance in all 100 patients.³ FOT-measured small airways resistance was significantly correlated with VDP in both asthma ($\rho=0.5$, $p<0.001$) and COPD ($\rho=0.5$, $p=0.01$) but not in ex-smokers ($\rho=-0.2$, $p=0.4$), and only in asthma was respiratory system impedance (X_{rs} 5Hz: $\rho=-0.5$, $p<0.001$; R_{rs} 5Hz: $\rho=0.3$, $p=0.02$; R_{rs} 5-19Hz: $\rho=0.5$, $p<0.001$) related to VDP. FOT-measured small airways resistance (COPD: $\rho=0.4$, $p=0.04$; asthma: $\rho=-0.3$, $p=0.04$) and MRI-measured VDP (COPD: $\rho=0.6$, $p=0.003$; asthma: $\rho=-0.3$, $p=0.04$) were the only metrics that were significantly related to patient quality of life in these two groups. In ex-smokers without

COPD, only plethysmography-measured R_{aw} was significantly related to quality of life ($\rho=0.5$, $p=0.01$). Asthmatic patients with poor asthma control had significantly increased respiratory system impedance (R_{rs} 5Hz, $p=0.01$; X_{rs} 5Hz, $p=0.03$), and increased small airways resistance (R_{rs} 5-19Hz $p=0.006$). Predicted reactance (X_{rs} 5Hz) was correlated with FOT-measured reactance in asthma ($\rho=0.5$, $p=0.001$), and predicted resistance reflecting small airways dysfunction (R_{rs} 5-19Hz) was correlated with measured values in COPD ($\rho=0.5$, $p=0.004$). Predicted and FOT-measured resistance and reactance were not correlated in ex-smokers without COPD (R_{rs} 5Hz $\rho=-0.3$, $p=0.2$; X_{rs} 5Hz $\rho=-0.3$, $p=0.2$; R_{rs} 5-19Hz $\rho=-0.1$, $p=0.6$). This study provided strong evidence that heterogeneous small airway obstruction is related to ventilation defects, and importantly, both are related to quality of life in obstructive lung disease.

3.3 Limitations

In this section the most significant limitations from Chapter 2 will be discussed. It should be noted that these limitations are also presented in the Discussion section of Chapter 2.

In Chapter 2 I evaluated 100 patients with obstructive lung disease with severity ranging from mild to severe using hyperpolarized ^3He MRI and FOT to study the relationships between structure and function in obstructive lung disease. However, I did not evaluate any COPD patients with GOLD stage IV (very severe) disease and only 5 patients with GOLD stage III (severe) disease. This study could therefore be improved by the inclusion of more patients in these severe and very severe categories, in order to study the changes in structure and function together as disease worsens.

It should be noted that while there were moderately strong correlations between the FOT-measured and model-predicted impedance values, the predicted values were consistently less than those measured by FOT. This is consistent with previous work⁴ using the same computational model (scaled so that the predicted impedance with no constriction corresponded with measured impedance in healthy volunteers). The authors showed that up to 75% of the small airways had to be constricted in asthma in order for the predicted impedance values to correspond with FOT measurements, suggesting that when only airways within a defect are considered, impedance is systematically underestimated in this

model. This supports another previous study⁵ suggesting that constriction of airways outside ventilation defects is necessary to generate accurate impedance predictions in asthma. Therefore, a limitation of the present work is that I implemented a binary approach where airways either remained at 100% of their original diameter, or were reduced to 10% of their original diameter. In reality, there is likely a distribution of narrowed airways throughout the lung, with the most severe narrowing occurring in ventilation defects. Future work will expand on this model by using MRI ventilation data to incorporate moderate airway narrowing outside ventilation defects as explained in Section 3.4.3.

The airway tree modelling calculations are also subject to several limitations. First, while the model was modified to reflect the unique distribution of ventilation defects for each patient, this model did not exactly represent each patient's airway tree geometry. Rather, it was generated from a representative healthy female subject⁶ and modified to reflect some of the functional changes measured in these subjects. I also used representative values for the impedance of the upper airway and chest wall for all impedance predictions, so the variation of these parameters between patients was not accounted for. However, these factors are expected to contribute much less to R_{rs} and X_{rs} than the changes occurring within the lung in obstructive lung disease. Despite these limitations, I demonstrated significant correlations between FOT-measured and model-predicted impedance from small airway obstruction in ventilation defects alone. This emphasizes the importance of small airway dysfunction in ventilation defects and in respiratory system impedance.

3.4 Future Directions

3.4.1 FOT Biomarkers in Severe Asthmatics Undergoing Bronchial Thermoplasty

While small airway dysfunction is hypothesized to play an important role in asthmatic ventilation heterogeneity, constriction of larger airways is also known to occur, especially in severe asthma. Bronchial thermoplasty (BT) is an invasive treatment that targets the smooth muscle in these larger airways to prevent constriction, with the goal of improving symptoms and disease control.⁷ This treatment has shown promise for improving pulmonary function in early studies,^{8,9} but there is debate over how widely applicable this

may be as it does not treat the small airways directly. FOT is sensitive to obstruction in the central and peripheral airways independently, and can be easily integrated into clinical workflows.

As part of a study that is currently underway, we have collected FOT impedance measurements and ventilation MRI in several severe asthmatics who are candidates for BT before and after treatment. By comparing the FOT, MRI, and other functional data before and after BT, we may be able to better understand how ablation of smooth muscle in the large and mid-sized airways affects breathing mechanics and airflow through the rest of the lung. This will provide a more complete understanding of the effects of BT on the lung beyond the specific ablated airways, and how these changes affect lung function and patient quality of life.

3.4.2 FOT Biomarkers and Higher-Order Image Features in ^3He MRI

In this thesis, ^3He MRI was used to quantify ventilation heterogeneity by calculating the VDP. This was done by sorting the signal intensities into one of five clusters, and mapping the lowest-intensity cluster within the lung.¹⁰ However, there is a wealth of other ventilation information available in ^3He MR images beyond this validated biomarker. By investigating other intensity-based metrics and other spatial features available in each image, we may be able to account for other aspects of ventilation heterogeneity that may be reflected by oscillometry.

For example, higher-order metrics have previously been proposed to evaluate heterogeneity in obstructive lung disease.¹¹ While the clinical meaning of these metrics may not yet be fully understood, the combination of MRI heterogeneity analysis and FOT measurements of impedance may yield new insights into the clinical relevance of these higher-order ventilation measurements.

In addition, pulmonary imaging may be able to differentiate between heterogeneous ventilation patterns related to the obstruction of small airways alone and obstruction with large airway involvement. This may be possible using functional information derived from MRI, and structural information derived from CT. Using high-resolution CT imaging,

airway trees can be resolved and segmented until the airways are approximately 2mm in diameter (the typical threshold for identifying the ‘small airways’). Using deformable co-registration techniques, ventilation maps may be co-registered to the patient’s airway tree and ventilation abnormalities may be classified as related to a large airway, or only in the small airways. This classification can then be compared to FOT measurements related to central and peripheral airway narrowing for validation. The ability to identify which defects are related to large or small airway dysfunction is important in the development of novel treatments for asthma.

3.4.3 Image Functional Modeling Incorporating all MRI Ventilation

One of the limitations of this thesis, as discussed in Section 3.3, is the fact that when the computational airway tree was modified using patient ventilation MRI data, only airways that were within or distal to a ventilation defect were narrowed. Using this method, airways within regions of the lung that are otherwise abnormally ventilated are not taken into account. This may have been part of the reason that, while there was moderately strong correlation between measured and predicted impedance, predicted impedance was consistently lower than impedance measured by MRI. However, it has been suggested in other modeling studies that in order to replicate experimental FOT measurements of impedance, moderate narrowing of many or all airways in the tree is necessary.^{4, 5} In my MRI analysis ³He MRI ventilation data was grouped into five clusters using a k-means approach, meaning that other levels of increased or decreased ventilation have been quantified, but not yet incorporated into the model. By scaling the diameter of each airway in a manner that corresponds to the ventilation measured in that region, we may be able to produce more accurate patient-specific predictions of impedance.

3.5 Significance and Impact

Obstructive lung disease affects hundreds of millions of people globally, and is responsible for millions of deaths each year.² Despite the prevalence and impact of this disease and decades of ongoing research, we are still developing our understanding of how obstructive lung disease affects structure and function, and how these changes are related to quality of life and exacerbations for these patients. Many patients do not have well-controlled disease

with currently available therapies. Hyperpolarized ^3He MRI has advanced our understanding of the spatially heterogeneous nature of these diseases, but the structural changes related to the ventilation heterogeneity we observe are still not fully understood. In order to advance our understanding of structure-function relationships in asthma and COPD, there is a need for multi-modality studies that incorporate more structural and functional measurements.

In this thesis I evaluated 100 patients with obstructive lung disease using hyperpolarized ^3He MRI, FOT, and quality of life questionnaires. I showed significant relationships between FOT-measured impedance and quality of life, as well as with MRI VDP. This study provided strong evidence that heterogeneous small airway obstruction is implicated in ventilation defects observed with MRI, and importantly, is related to quality of life in obstructive lung disease. I also used MRI ventilation defects to generate patient-specific computational model predictions of airway impedance and, for the first time, showed that predictions of reactance in asthma and resistance in COPD were significantly related to FOT-measured impedance. These results provide strong support for the broader clinical implementation of FOT for evaluating obstructive pulmonary disease. FOT is a clinically applicable method that I have shown to be significantly related to patient quality of life and to asthma control. Wider use of this technology may help to improve disease control, reducing the burden of obstructive lung disease on patients and on the Canadian health care system.

3.6 References

- (1) Ontario Lung Association. Your Lungs, Your Life: Insights and Solutions to Lung Health in Ontario. (2011).
- (2) Global, regional, and national deaths, prevalence, disability-adjusted life years, and years lived with disability for chronic obstructive pulmonary disease and asthma, 1990-2015: a systematic analysis for the Global Burden of Disease Study 2015. (2017).
- (3) Leary, D. et al. Hyperpolarized ^3He magnetic resonance imaging ventilation defects in asthma: relationship to airway mechanics. *Physiol Rep* **4**, e12761 (2016).
- (4) Bhatawadekar, S.A., Leary, D. & Maksym, G.N. Modelling resistance and reactance with heterogeneous airway narrowing in mild to severe asthma. *Can J Physiol Pharmacol* **93**, 207-14 (2015).
- (5) Tgavalekos, N.T. et al. Relationship between airway narrowing, patchy ventilation and lung mechanics in asthmatics. *Eur Respir J* **29**, 1174-81 (2007).
- (6) Tawhai, M.H. et al. CT-based geometry analysis and finite element models of the human and ovine bronchial tree. *J Appl Physiol (1985)* **97**, 2310-21 (2004).
- (7) Cox, P.G., Miller, J., Mitzner, W. & Leff, A.R. Radiofrequency ablation of airway smooth muscle for sustained treatment of asthma: preliminary investigations. *Eur Respir J* **24**, 659-63 (2004).
- (8) Pavord, I.D. et al. Safety and efficacy of bronchial thermoplasty in symptomatic, severe asthma. *Am J Respir Crit Care Med* **176**, 1185-91 (2007).
- (9) Cox, G. et al. Asthma control during the year after bronchial thermoplasty. *N Engl J Med* **356**, 1327-37 (2007).
- (10) Kirby, M. et al. Hyperpolarized ^3He magnetic resonance functional imaging semiautomated segmentation. *Acad Radiol* **19**, 141-52 (2012).
- (11) Zha, N. et al. Second-order Texture Measurements of (^3He) Ventilation MRI: Proof-of-concept Evaluation of Asthma Bronchodilator Response. *Acad Radiol* **23**, 176-85 (2016).

4 APPENDIX

Appendix A – Asthma Control Questionnaire

Name: _____
Subject Number: _____
Visit Date: _____

Asthma Control Questionnaire

ASTHMA CONTROL QUESTIONNAIRE

Please answer Questions 1–6.

Circle the number of the response that best describes how you have been during the past week.

1. On average, during the past week, how often were you woken by your asthma during the night?
 - 0 Never
 - 1 Hardly ever
 - 2 A few times
 - 3 Several times
 - 4 Many times
 - 5 A great many times
 - 6 Unable to sleep because of asthma

2. On average, during the past week, how bad were your asthma symptoms when you woke up in the morning?
 - 0 No symptoms
 - 1 Very mild symptoms
 - 2 Mild symptoms
 - 3 Moderate symptoms
 - 4 Quite severe symptoms
 - 5 Severe symptoms
 - 6 Very severe symptoms

3. In general, during the past week, how limited were you in your activities because of your asthma?
 - 0 Not limited at all
 - 1 Very slightly limited
 - 2 Slightly limited
 - 3 Moderately limited
 - 4 Very limited
 - 5 Extremely limited
 - 6 Totally limited

Name: _____

Subject Number: _____

Visit Date: _____

4. In general, during the past week, how much shortness of breath did you experience because of your asthma?
- 0 None
 - 1 A very little
 - 2 A little
 - 3 A moderate amount
 - 4 Quite a lot
 - 5 A great deal
 - 6 A very great deal
5. In general, during the past week, how much of the time did you wheeze?
- 0 Not at all
 - 1 Hardly any of the time
 - 2 A little of the time
 - 3 A moderate amount of the time
 - 4 A lot of the time
 - 5 Most of the time
 - 6 All the time
6. On average, during the past week, how many puffs of short-acting bronchodilator (e.g., Ventolin) have you used each day?
- 0 None
 - 1 1–2 puffs most days
 - 2 3–4 puffs most days
 - 3 5–8 puffs most days
 - 4 9–12 puffs most days
 - 5 13–16 puffs most days
 - 6 More than 16 puffs most days
7. To be completed by a member of the clinic staff, FEV1 prebronchodilator:
- 0 > 95% predicted
 - 1 95–90%
 - 2 89–80%
 - 3 79–70%
 - 4 69–60%

The Asthma Control Questionnaire is copyrighted. It may not be changed, translated, or sold (paper or software) without the permission of Elizabeth Juniper.

Appendix B – Asthma Quality of Life Questionnaire

Name: _____

Subject Number: _____

Visit Date: _____

ASTHMA QUALITY OF LIFE QUESTIONNAIRE WITH STANDARDISED ACTIVITIES (AQLQ(S))

SELF-ADMINISTERED

© 1998
QOL TECHNOLOGIES LTD.

For further information:

Elizabeth Juniper, MCSP, MSc
Professor
20 Marcuse Fields
Bosham, West Sussex
PO18 8NA, England
Telephone: +44 1243 572124
Fax: +44 1243 573680
E-mail: juniper@qoltech.co.uk
Web: <http://www.qoltech.co.uk>

Development and validation
supported by
GLAXO WELLCOME, INC

© The Asthma Quality of Life Questionnaire with Standardised Activities (AQLQ(S)) is copyrighted and all rights are reserved. No part of this questionnaire may be sold, modified or reproduced in any form without the express permission of Elizabeth Juniper on behalf of QOL Technologies Limited

APRIL 2008

Modified September 2010
AQLQ(S)-SA North American English Version

ASTHMA QUALITY OF LIFE QUESTIONNAIRE (S)

Name: _____
 Subject Number: _____
 Visit Date: _____

SELF-ADMINISTERED

Please complete all questions by circling the number that best describes how you have been during the last 2 weeks as a result of your asthma.

HOW LIMITED HAVE YOU BEEN DURING THE LAST 2 WEEKS IN THESE ACTIVITIES AS A RESULT OF YOUR ASTHMA?

	Totally Limited	Extremely Limited	Very Limited	Moderate Limitation	Some Limitation	A Little Limitation	Not at all Limited
1. STRENUOUS ACTIVITIES (such as hurrying, exercising, running up stairs, sports)	1	2	3	4	5	6	7
2. MODERATE ACTIVITIES (such as walking, housework, gardening, shopping, climbing stairs)	1	2	3	4	5	6	7
3. SOCIAL ACTIVITIES (such as talking, playing with pets/children, visiting friends/relatives)	1	2	3	4	5	6	7
4. WORK-RELATED ACTIVITIES (tasks you have to do at work*)	1	2	3	4	5	6	7
*If you are not employed or self-employed, these should be tasks you have to do most days.							
5. SLEEPING	1	2	3	4	5	6	7

HOW MUCH DISCOMFORT OR DISTRESS HAVE YOU FELT DURING THE LAST 2 WEEKS?

	A Very Great Deal	A Great Deal	A Good Deal	Moderate Amount	Some	Very Little	None
6. How much discomfort or distress have you felt over the last 2 weeks as a result of CHEST TIGHTNESS?	1	2	3	4	5	6	7

ASTHMA QUALITY OF LIFE QUESTIONNAIRE (S)

Name: _____

Subject Number: _____

Visit Date: _____

SELF-ADMINISTERED

Page 2 of 5

IN GENERAL, HOW MUCH OF THE TIME DURING THE LAST 2 WEEKS DID YOU:

	All of the Time	Most of the Time	A Good Bit of the Time	Some of the Time	A Little of the Time	Hardly Any of the Time	None of the Time
7. Feel CONCERNED ABOUT HAVING ASTHMA?	1	2	3	4	5	6	7
8. Feel SHORT OF BREATH as a result of your asthma?	1	2	3	4	5	6	7
9. Experience asthma symptoms as a RESULT OF BEING EXPOSED TO CIGARETTE SMOKE?	1	2	3	4	5	6	7
10. Experience a WHEEZE in your chest?	1	2	3	4	5	6	7
11. Feel you had to AVOID A SITUATION OR ENVIRONMENT BECAUSE OF CIGARETTE SMOKE?	1	2	3	4	5	6	7

HOW MUCH DISCOMFORT OR DISTRESS HAVE YOU FELT DURING THE LAST 2 WEEKS?

	A Very Great Deal	A Great Deal	A Good Deal	Moderate Amount	Some	Very Little	None
12. How much discomfort or distress have you felt over the last 2 weeks as a result of COUGHING?	1	2	3	4	5	6	7

IN GENERAL, HOW MUCH OF THE TIME DURING THE LAST 2 WEEKS DID YOU:

	All of the Time	Most of the Time	A Good Bit of the Time	Some of the Time	A Little of the Time	Hardly Any of the Time	None of the Time
13. Feel FRUSTRATED as a result of your asthma?	1	2	3	4	5	6	7
14. Experience a feeling of CHEST HEAVINESS?	1	2	3	4	5	6	7

ASTHMA QUALITY OF LIFE QUESTIONNAIRE (S)

Name: _____

Subject Number: _____

Visit Date: _____

SELF-ADMINISTERED

Page 3 of 5

IN GENERAL, HOW MUCH OF THE TIME DURING THE LAST 2 WEEKS DID YOU:

	All of the Time	Most of the Time	A Good Bit of the Time	Some of the Time	A Little of the Time	Hardly Any of the Time	None of the Time
15. Feel CONCERNED ABOUT THE NEED TO USE MEDICATION for your asthma?	1	2	3	4	5	6	7
16. Feel the need to CLEAR YOUR THROAT?	1	2	3	4	5	6	7
17. Experience asthma symptoms as a RESULT OF BEING EXPOSED TO DUST?	1	2	3	4	5	6	7
18. Experience DIFFICULTY BREATHING OUT as a result of your asthma?	1	2	3	4	5	6	7
19. Feel you had to AVOID A SITUATION OR ENVIRONMENT BECAUSE OF DUST?	1	2	3	4	5	6	7
20. WAKE UP IN THE MORNING WITH ASTHMA SYMPTOMS?	1	2	3	4	5	6	7
21. Feel AFRAID OF NOT HAVING YOUR ASTHMA MEDICATION AVAILABLE?	1	2	3	4	5	6	7
22. Feel bothered by HEAVY BREATHING?	1	2	3	4	5	6	7
23. Experience asthma symptoms as a RESULT OF THE WEATHER OR AIR POLLUTION OUTSIDE?	1	2	3	4	5	6	7
24. Were you WOKEN AT NIGHT by your asthma?	1	2	3	4	5	6	7
25. AVOID OR LIMIT GOING OUTSIDE BECAUSE OF THE WEATHER OR AIR POLLUTION?	1	2	3	4	5	6	7

ASTHMA QUALITY OF LIFE QUESTIONNAIRE (S)

Name: _____

Subject Number: _____

Visit Date: _____

SELF-ADMINISTERED

Page 4 of 5

IN GENERAL, HOW MUCH OF THE TIME DURING THE LAST 2 WEEKS DID YOU:

	All of the Time	Most of the Time	A Good Bit of the Time	Some of the Time	A Little of the Time	Hardly Any of the Time	None of the Time
26. Experience asthma symptoms as a RESULT OF BEING EXPOSED TO STRONG SMELLS OR PERFUME?	1	2	3	4	5	6	7
27. Feel AFRAID OF GETTING OUT OF BREATH?	1	2	3	4	5	6	7
28. Feel you had to AVOID A SITUATION OR ENVIRONMENT BECAUSE OF STRONG SMELLS OR PERFUME?	1	2	3	4	5	6	7
29. Has your asthma INTERFERED WITH GETTING A GOOD NIGHT'S SLEEP?	1	2	3	4	5	6	7
30. Have a feeling of FIGHTING FOR AIR?	1	2	3	4	5	6	7

HOW LIMITED HAVE YOU BEEN DURING THE LAST 2 WEEKS?

	Severely Limited Most Not Done	Very Limited	Moderately Limited Several Not Done	Slightly Limited	Very Slightly Limited Very Few Not Done	Hardly Limited At All	Not Limited Have Done All Activities
31. Think of the OVERALL RANGE OF ACTIVITIES that you would have liked to have done during the last 2 weeks. How much has your range of activities been limited by your asthma?	1	2	3	4	5	6	7

ASTHMA QUALITY OF LIFE QUESTIONNAIRE (S)

Name: _____

Subject Number: _____

Visit Date: _____

SELF-ADMINISTERED

Page 5 of 5

HOW LIMITED HAVE YOU BEEN DURING THE LAST 2 WEEKS?

	Totally Limited	Extremely Limited	Very Limited	Moderate Limitation	Some Limitation	A Little Limitation	Not at all Limited
32. Overall, among ALL THE ACTIVITIES that you have done during the last 2 weeks, how limited have you been by your asthma?	1	2	3	4	5	6	7

DOMAIN CODE:

Symptoms: 6, 8, 10, 12, 14, 16, 18, 20, 22, 24, 29, 30

Activity Limitation: 1, 2, 3, 4, 5, 11, 19, 25, 28, 31, 32

Emotional Function: 7, 13, 15, 21, 27

Environmental Stimuli: 9, 17, 23, 26

Appendix C – St. George’s Respiratory Questionnaire

ST. GEORGE’S RESPIRATORY QUESTIONNAIRE ORIGINAL ENGLISH VERSION

ST. GEORGE’S RESPIRATORY QUESTIONNAIRE (SGRQ)

This questionnaire is designed to help us learn much more about how your breathing is troubling you and how it affects your life. We are using it to find out which aspects of your illness cause you most problems, rather than what the doctors and nurses think your problems are.

Please read the instructions carefully and ask if you do not understand anything. Do not spend too long deciding about your answers.

Before completing the rest of the questionnaire:

Please tick in one box to show how you describe your current health:

Very good Good Fair Poor Very poor

Copyright reserved
P.W. Jones, PhD FRCP
Professor of Respiratory Medicine,
St. George’s University of London,
Jenner Wing,
Cranmer Terrace,
London SW17 ORE, UK.

Tel. +44 (0) 20 8725 5371
Fax +44 (0) 20 8725 5955

UK/ English (original) version

1

continued...

f:\institute\culturaldep\project\gsk1881\question\final\version\siagrqr1q.doc 14/03/03

St. George's Respiratory Questionnaire PART 1

Questions about how much chest trouble you have had over the past 3 months.

Please tick (✓) one box for each question.

- | | most
days
a week | several
days
a week | a few
days
a month | only with
chest
infections | not
at
all |
|---|--------------------------|---------------------------|--------------------------|----------------------------------|--------------------------|
| 1. Over the past 3 months, I have coughed: | <input type="checkbox"/> | <input type="checkbox"/> | <input type="checkbox"/> | <input type="checkbox"/> | <input type="checkbox"/> |
| 2. Over the past 3 months, I have brought up phlegm (sputum): | <input type="checkbox"/> | <input type="checkbox"/> | <input type="checkbox"/> | <input type="checkbox"/> | <input type="checkbox"/> |
| 3. Over the past 3 months, I have had shortness of breath: | <input type="checkbox"/> | <input type="checkbox"/> | <input type="checkbox"/> | <input type="checkbox"/> | <input type="checkbox"/> |
| 4. Over the past 3 months, I have had attacks of wheezing: | <input type="checkbox"/> | <input type="checkbox"/> | <input type="checkbox"/> | <input type="checkbox"/> | <input type="checkbox"/> |
| 5. During the past 3 months how many severe or very unpleasant attacks of chest trouble have you had? | | | | | |

Please tick (✓) one:

- more than 3 attacks
- 3 attacks
- 2 attacks
- 1 attack
- no attacks

6. How long did the worst attack of chest trouble last?
(Go to question 7 if you had no severe attacks)

Please tick (✓) one:

- a week or more
- 3 or more days
- 1 or 2 days
- less than a day

7. Over the past 3 months, in an average week, how many good days (with little chest trouble) have you had?

Please tick (✓) one:

- No good days
- 1 or 2 good days
- 3 or 4 good days
- nearly every day is good
- every day is good

8. If you have a wheeze, is it worse in the morning?

Please tick (✓) one:

- No
- Yes

St. George's Respiratory Questionnaire PART 2

Section 1

How would you describe your chest condition?

Please tick (✓) one:

- The most important problem I have
- Causes me quite a lot of problems
- Causes me a few problems
- Causes no problem

If you have ever had paid employment.

Please tick (✓) one:

- My chest trouble made me stop work altogether
- My chest trouble interferes with my work or made me change my work
- My chest trouble does not affect my work

Section 2

Questions about what activities usually make you feel breathless these days.

Please tick (✓) in *each box* that applies to you *these days*:

	True	False
Sitting or lying still	<input type="checkbox"/>	<input type="checkbox"/>
Getting washed or dressed	<input type="checkbox"/>	<input type="checkbox"/>
Walking around the home	<input type="checkbox"/>	<input type="checkbox"/>
Walking outside on the level	<input type="checkbox"/>	<input type="checkbox"/>
Walking up a flight of stairs	<input type="checkbox"/>	<input type="checkbox"/>
Walking up hills	<input type="checkbox"/>	<input type="checkbox"/>
Playing sports or games	<input type="checkbox"/>	<input type="checkbox"/>

St. George's Respiratory Questionnaire PART 2

Section 3

Some more questions about your cough and breathlessness these days.

Please tick (✓) in each box that applies to you these days:

	True	False
My cough hurts	<input type="checkbox"/>	<input type="checkbox"/>
My cough makes me tired	<input type="checkbox"/>	<input type="checkbox"/>
I am breathless when I talk	<input type="checkbox"/>	<input type="checkbox"/>
I am breathless when I bend over	<input type="checkbox"/>	<input type="checkbox"/>
My cough or breathing disturbs my sleep	<input type="checkbox"/>	<input type="checkbox"/>
I get exhausted easily	<input type="checkbox"/>	<input type="checkbox"/>

Section 4

Questions about other effects that your chest trouble may have on you these days.

Please tick (✓) in each box that applies to you these days:

	True	False
My cough or breathing is embarrassing in public	<input type="checkbox"/>	<input type="checkbox"/>
My chest trouble is a nuisance to my family, friends or neighbours	<input type="checkbox"/>	<input type="checkbox"/>
I get afraid or panic when I cannot get my breath	<input type="checkbox"/>	<input type="checkbox"/>
I feel that I am not in control of my chest problem	<input type="checkbox"/>	<input type="checkbox"/>
I do not expect my chest to get any better	<input type="checkbox"/>	<input type="checkbox"/>
I have become frail or an invalid because of my chest	<input type="checkbox"/>	<input type="checkbox"/>
Exercise is not safe for me	<input type="checkbox"/>	<input type="checkbox"/>
Everything seems too much of an effort	<input type="checkbox"/>	<input type="checkbox"/>

Section 5

Questions about your medication, if you are receiving no medication go straight to section 6.

Please tick (✓) in each box that applies to you these days:

	True	False
My medication does not help me very much	<input type="checkbox"/>	<input type="checkbox"/>
I get embarrassed using my medication in public	<input type="checkbox"/>	<input type="checkbox"/>
I have unpleasant side effects from my medication	<input type="checkbox"/>	<input type="checkbox"/>
My medication interferes with my life a lot	<input type="checkbox"/>	<input type="checkbox"/>

St. George's Respiratory Questionnaire PART 2

Section 6

These are questions about how your activities might be affected by your breathing.

Please tick (✓) in *each box* that applies to you *because of your breathing*:

	True	False
I take a long time to get washed or dressed	<input type="checkbox"/>	<input type="checkbox"/>
I cannot take a bath or shower, or I take a long time	<input type="checkbox"/>	<input type="checkbox"/>
I walk slower than other people, or I stop for rests	<input type="checkbox"/>	<input type="checkbox"/>
Jobs such as housework take a long time, or I have to stop for rests	<input type="checkbox"/>	<input type="checkbox"/>
If I walk up one flight of stairs, I have to go slowly or stop	<input type="checkbox"/>	<input type="checkbox"/>
If I hurry or walk fast, I have to stop or slow down	<input type="checkbox"/>	<input type="checkbox"/>
My breathing makes it difficult to do things such as walk up hills, carrying things up stairs, light gardening such as weeding, dance, play bowls or play golf	<input type="checkbox"/>	<input type="checkbox"/>
My breathing makes it difficult to do things such as carry heavy loads, dig the garden or shovel snow, jog or walk at 5 miles per hour, play tennis or swim	<input type="checkbox"/>	<input type="checkbox"/>
My breathing makes it difficult to do things such as very heavy manual work, run, cycle, swim fast or play competitive sports	<input type="checkbox"/>	<input type="checkbox"/>

Section 7

We would like to know how your chest usually affects your daily life.

Please tick (✓) in *each box* that applies to you *because of your chest trouble*:

	True	False
I cannot play sports or games	<input type="checkbox"/>	<input type="checkbox"/>
I cannot go out for entertainment or recreation	<input type="checkbox"/>	<input type="checkbox"/>
I cannot go out of the house to do the shopping	<input type="checkbox"/>	<input type="checkbox"/>
I cannot do housework	<input type="checkbox"/>	<input type="checkbox"/>
I cannot move far from my bed or chair	<input type="checkbox"/>	<input type="checkbox"/>

St. George's Respiratory Questionnaire

Here is a list of other activities that your chest trouble may prevent you doing. (You do not have to tick these, they are just to remind you of ways in which your breathlessness may affect you):

- Going for walks or walking the dog
- Doing things at home or in the garden
- Sexual intercourse
- Going out to church, pub, club or place of entertainment
- Going out in bad weather or into smoky rooms
- Visiting family or friends or playing with children

Please write in any other important activities that your chest trouble may stop you doing:

.....
.....
.....
.....

Now would you tick in the box (one only) which you think best describes how your chest affects you:

- It does not stop me doing anything I would like to do
- It stops me doing one or two things I would like to do
- It stops me doing most of the things I would like to do
- It stops me doing everything I would like to do

Thank you for filling in this questionnaire. Before you finish would you please check to see that you have answered all the questions.

Appendix D – MRI and CT Lung Biomarkers: Towards an *In Vivo* Understanding of Lung Biomechanics

This review paper presents the historical and current use of MRI and CT for in vivo studies of lung biomechanics.

The contents of this chapter were previously published in Clinical Biomechanics: HM Young, RL Eddy and G Parraga. MRI and CT lung biomarkers: Towards an in vivo understanding of lung biomechanics. Invited Review, Clinical Biomechanics. In Press. doi: 10.1016/j.clinbiomech.2017.09.016. Permission to reproduce this article was granted by Elsevier and is provided in Appendix E.

1. Introduction

The respiratory system, dominated by the working of the lungs, is necessarily elastic, undergoing complex biomechanical changes to enable breathing for efficient gas exchange. The lungs are over-engineered for day-to-day tasks, making detection and deep understanding of lung diseases and their biomechanical mechanisms extremely challenging. The lungs are composed of different tissues and compartments including the large and small airways, blood vessels and parenchymal tissue. The biomechanical properties of the respiratory system are therefore interdependent and derive from these complex structures.

As shown in Figure 1, the overarching function of the respiratory system and the lungs is to deliver oxygen to the bloodstream and to remove CO₂; this functionality can be measured in part by evaluating ventilation. Total lung ventilation is the rate of air expiration from the lungs (mL/min), while alveolar ventilation is the rate at which fresh air enters the respiratory zone and is made available for gas exchange.¹ This is achieved through the biomechanical process of breathing whereby muscle contraction and relaxation and thoracic cavity pressure changes allow air to flow in and out of the lungs.¹ The relationship between volume, pressure and flow can be described using the mechanical properties of the lung tissue, which include the parenchyma, airways and airspaces. Many diseases of the lung are a result of inflammation, fibrosis, airway constriction and parenchymal destruction. These processes change its mechanical properties and understanding the biomechanical properties of the lung is essential when evaluating its function in order to understand the disease.²

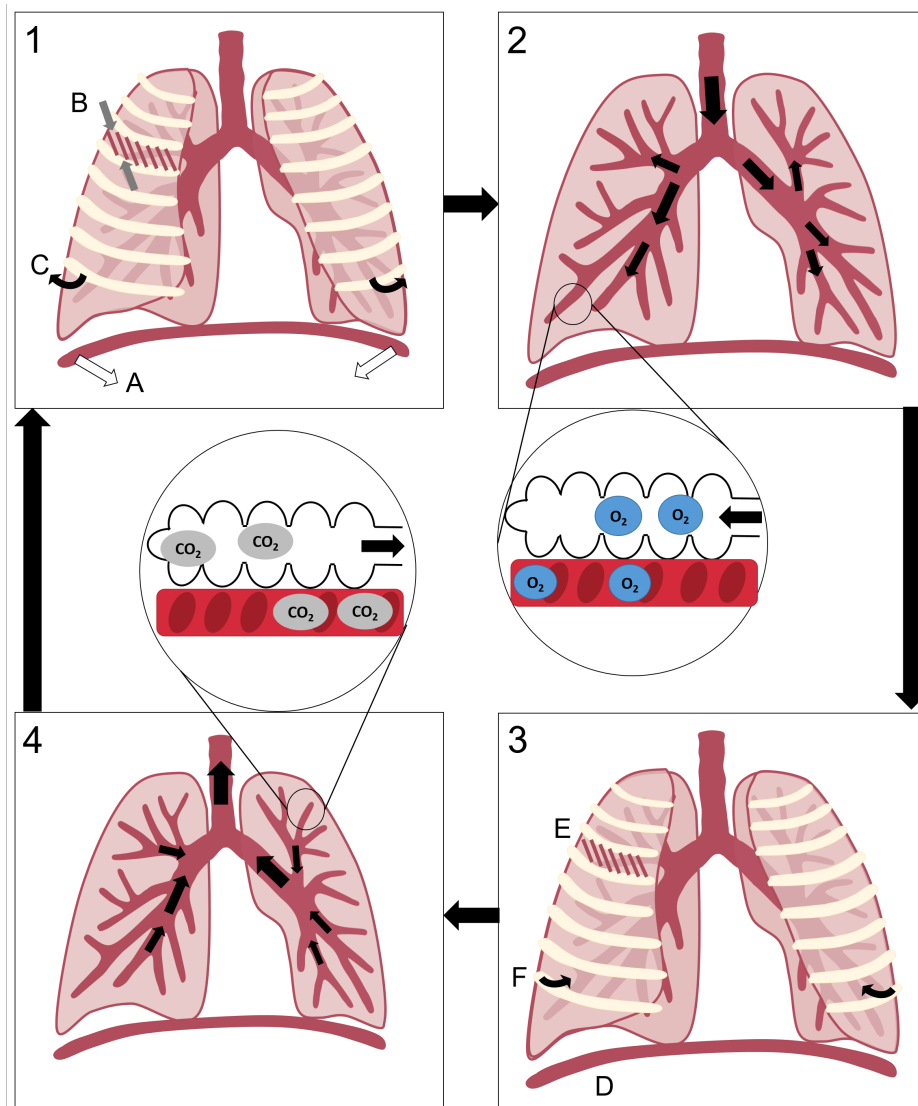


Figure 4-1. Respiratory System Mechanics and Function

1. Through the contraction of the diaphragm (A) and the intercostal muscles (B), the thoracic cavity expands via the outward motion of the ribcage and the downward motion of the diaphragm, decreasing the air pressure within the thoracic cavity. 2. Fresh air flows into the lungs through the airways and reaches the alveoli, where oxygen diffuses into the bloodstream. 3. The diaphragm (D) and the intercostal muscles (E) relax causing the ribcage to move inward, increasing the pressure in the thoracic cavity. 4. Carbon dioxide has diffused from the bloodstream into the alveoli, and is removed as air flows back out of the lungs through the airways.

1.1 Clinical Measurements of Lung Biomechanics: Strengths and Limitations

In clinical evaluations, the biomechanics of the lung are quantified through measurements of volume, flow and pressure of air, usually taken at the mouth. These measurements are

simple and inexpensive to acquire, and are therefore widely used. The primary clinical biomarker of lung function is the spirometry measurement of forced expiratory volume in one second (FEV₁). This measurement is highly variable,³ and in asthma and chronic obstructive lung disease, FEV₁ correlates weakly with quality of life and other patient outcomes.⁴ It also provides little information about the biomechanical cause of airflow limitation, in part because FEV₁ provides a global lung measure and cannot capture regional information. Other tools for measuring lung biomechanics include multiple-breath inert gas wash-in and wash-out⁵ for the lung clearance index (LCI),⁵ measuring ventilation heterogeneity,^{6,7} and the forced oscillation technique (FOT).⁸ FOT measures resistance and elastance of the central and peripheral airways independently and has been validated using direct measures of impedance.⁹ While these tools provide important information related to lung biomechanics and are well understood, they cannot distinguish the regional contributions of different lung components. For this information, novel lung imaging tools are required.

1.2 Solutions Provided by Pulmonary Imaging

Pulmonary imaging provides a way to visualize and quantify lung structure and function with high spatial and temporal resolution in order to better understand *in vivo* regional lung biomechanics. Pulmonary disease is heterogeneously distributed throughout the lung and pulmonary imaging is uniquely able to quantify the severity and distribution of disease in a way that directly reflects lung function and pathophysiology. As summarized in Table 1, a number of pulmonary imaging techniques can be used to measure numerous biomechanical properties of the lung. These imaging tools can be classified into three main categories: microstructural, anatomical and functional imaging. In this review, we summarize and discuss imaging methods required to generate imaging biomarkers of lung biomechanics, and how these measurements may be used to provide a greater understanding of pulmonary function. As summarized in the schematic in Figure 2, a wide variety of lung biomechanical measurements can be derived using both x-ray based and magnetic resonance imaging (MRI) methods.

Table 4-1. Pulmonary Imaging-Derived Biomechanical Measurements

Method	Imaging Biomarker*	Biomechanical Property
Microstructural Imaging	Alveolar diameter ¹⁰⁻¹²	Acinar deformation
	Surface-to-volume ratio ¹³⁻¹⁵	Microstructural elasticity
Anatomical Imaging	Volume change	Tissue expansion
	Jacobian determinant ¹⁶⁻²¹	Tissue deformation, compliance
	4DCT Jacobian determinant ²²⁻²⁴	Deformation hysteresis
	Deformation anisotropy ^{24, 25}	Forces and strain in tissue
	Lobar deformation ²⁶	Lobar mechanics
Functional Imaging	Wash-in and washout time constants ^{27, 28}	Airflow distribution
	Ventilation ²⁹⁻³³	Ventilation heterogeneity
	Specific ventilation ³⁴⁻³⁶	Tissue expansion
	Apparent diffusion coefficient, airspace morphometry ³⁷	Transpulmonary pressure, elasticity

*Citations are included in Reference section

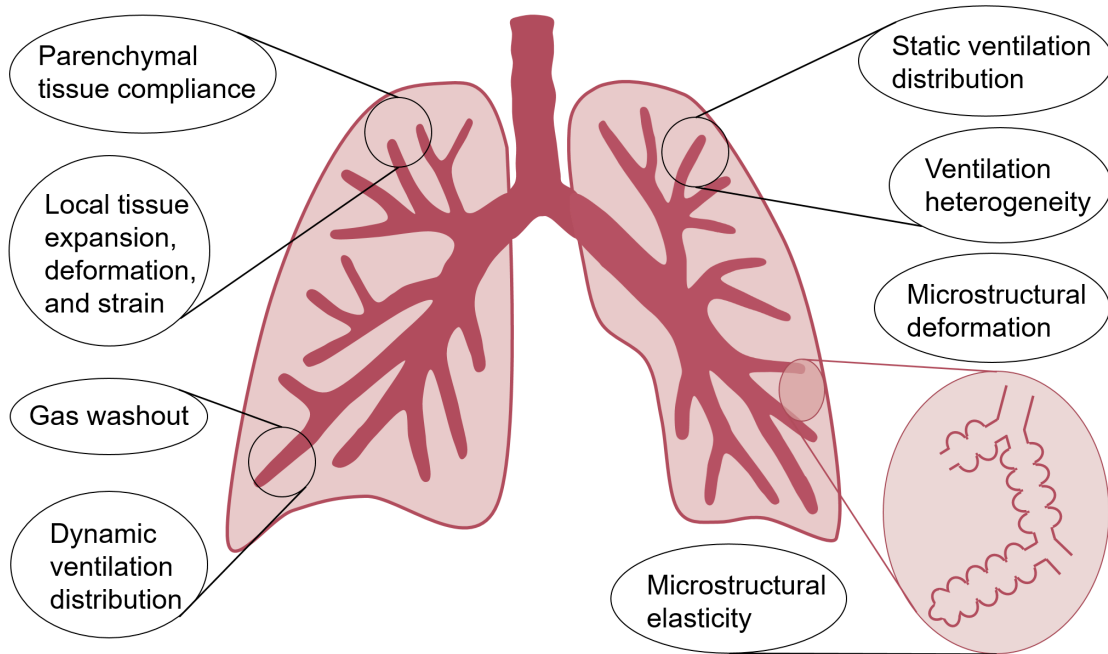


Figure 4-2. Pulmonary Imaging Biomarkers of Lung Biomechanics

1.2.1 Micro-CT and Synchrotron x-ray Microscopy

The functional units of the lung, including the terminal airways and the alveoli, are too small (ranging from 100-600 μm in diameter)¹ and too deeply positioned in the body to be resolved using clinical imaging methods. However, they play a vital mechanical role, so it is very important to be able to measure and understand these structures. Our understanding of the geometry and features of the acinar ducts was generated from lung tissue samples and *ex vivo* histology measurements, pioneered by pulmonary pathologists and stereologists over the past decades.³⁸⁻⁴⁰ These measurements and approaches have provided a deeper understanding of normal tissue³⁹ and tissues from asthmatics and COPD patients,⁴¹ but such methods are dependent on lung tissue excision and *ex vivo* analyses. The potential for *in vivo* measurements in animal models and patients was first demonstrated using micro-computed tomography (micro-CT), and exploited by Hogg and collaborators.^{42, 43} The concept of micro-CT was reduced to practice and commercialized between 1994-2001⁴⁴ and was initially used for geological core sample evaluations^{45, 46} and small animal bone studies.^{47, 48} Micro-CT generates high-resolution 3D images of small samples, providing direct, non-invasive measurements of lung anatomy and microstructure. This technique has been used to study the destruction and remodeling that occurs in the small airways in COPD,⁴³ and confirmed the narrowing and loss of small conducting airways in COPD as compared to healthy controls.⁴⁹ Current micro-CT methods have been used for hypothesis driven pulmonary research in *ex vivo*⁵⁰ and *in vivo*¹⁴ small animal studies and to image excised samples of human lung tissue.⁴² In these studies, the first *in vivo* visualization and quantification of the microstructure of the lung parenchyma were performed.^{14, 51}

Synchrotron x-ray tomographic microscopy (SRXTM) is another example of high-resolution micro-CT imaging using synchrotron radiation x-rays as a monochromatic, coherent radiation source, providing even greater image resolution than can be achieved with conventional micro-CT (approximately 1 μm) and the ability to perform phase contrast imaging⁵². Recent advancements have enabled the use of this technique for serial imaging studies without adverse effects,⁵³ and larger beamlines will enable application of SRXTM in larger animal studies.⁵⁴ While SRXTM shows promise for *in vivo* studies of large

animals and humans in the future, these studies are currently performed using dedicated clinical imaging techniques.

1.2.2 *Clinical CT*

The discovery of x-ray Computed Tomography (CT)⁵⁵ heralded a true paradigm shift in medicine and research. Soon after its development in the 1970s, this groundbreaking technology was applied to pulmonary imaging.⁵⁶ Early studies identified the utility of CT for studying structure, function, and biomechanics of the lungs through studies of ventilation in an animal model,⁵⁷ and in imaging studies of breathing mechanics.⁵⁸⁻⁶⁰ During this time, the first evaluations of lung biomechanics in humans were also made.⁶¹ This marked the first use of pulmonary imaging for measurements and analysis of lung biomechanics, a field that has continued to develop as image acquisition and analysis techniques have evolved. During this time, advancements in CT imaging provided the ability to image the anatomy, structure, and function of the lung with high spatial and temporal resolution. Pulmonary CT has been used to study many pathologies, and is now the clinically accepted standard for the evaluation of severe emphysema in COPD⁶² and alpha-1 antitrypsin deficiency.⁶³ CT provides regional lung tissue structural information and high-resolution methods that may be used to measure the airways and blood vessels, and to quantify emphysema or air trapping in the lung parenchyma with well-established radiodensity thresholds.⁶³⁻⁶⁵ The anatomical and structural information provided by CT can also be used to evaluate deformation and strain in the lung using CT images acquired at more than one lung volume.⁶⁶ These measurements provide *in vivo* visualization and quantification of the kinematics of breathing, and how this may differ in some disease states. From these measurements, information about structural and functional changes in the lung such as specific volume, which is correlated with specific ventilation, can be ascertained.⁶⁷

1.2.3 *Magnetic Resonance Imaging*

Magnetic resonance imaging (MRI) provides soft tissue contrast that is not achievable using x-ray based methods like CT and does not carry the risk of ionizing radiation exposure. However, its use was previously limited, as very little signal intensity is

measurable from lung parenchymal tissue due to very low proton density (and substantial gas density) and the millions of air-tissue interfaces in the lung parenchyma.⁶⁸ In the early 1990s, the application of ultra-short echo time (UTE) MRI in lung imaging was investigated and used to increase the signal intensity measured in the lung tissue.⁶⁹ UTE MRI enabled the acquisition of higher quality images of lung tissue and parenchyma, and represented the first application of advanced proton MRI techniques to anatomical lung imaging. The other critical advancement in pulmonary MRI was the introduction of inhaled contrast agents for the assessment of lung function. Using inhaled noble gases, such as hyperpolarized ^3He and ^{129}Xe , pulmonary ventilation may be visualized and quantified. This was first demonstrated using hyperpolarized ^{129}Xe ,⁷⁰ shortly followed by *in vivo* human lung imaging using both ^3He ⁷¹ and ^{129}Xe .⁷² This functional imaging technique has since been widely applied in pulmonary imaging research. Inhaled hyperpolarized noble gas MRI can also be used to derive microstructural information from the diffusion of gas within the small airways and alveoli.⁷³

Since the first use of UTE MRI in lung imaging, other advanced proton MRI methods have been developed, including oxygen-enhanced MRI and Fourier decomposition (FD) MRI. Oxygen-enhanced MRI measures the effect of paramagnetic dissolved oxygen on the ^1H signal⁷⁴ and has been acquired in both static (breath-hold) and dynamic (free-breathing) conditions to evaluate oxygenated air flow and the impact of this on signal relaxation in the lungs. FDMRI, another free-breathing ^1H MRI method, depends on the accurate co-registration of images acquired throughout the breathing cycle. The Fourier transform is used to transform the data in order to measure the ^1H signal intensity changes in each voxel. These changes are due to the mechanics of breathing as the parenchyma expands and contracts with each breath. Using the signal fluctuation at the respiratory rate, ventilation-weighted images can be generated, whereas the signal fluctuations at the cardiac frequency (roughly 4 times greater than the respiratory rate) is used to generate perfusion maps.

1.2.4 Overarching Rationale for Review

Here we summarize recently developed pulmonary imaging tools and studies that were aimed at developing biomarkers and/or a deeper understanding of the biomechanics of

breathing and the respiratory system. As shown in Table 2, where the key publications are summarized, numerous studies have been performed in large and small animal models, *ex vivo* in lung tissue samples as well as *in vivo*, in healthy volunteers and patients with respiratory disease. Overall, this approach may be considered as an emerging field that will continue to evolve as imaging methods become less dependent upon physics expertise and image processing skills and more broadly used as standalone, turnkey systems for physiological investigations. It is important to acknowledge that we focus necessarily on x-ray and MRI based methods in order to provide a review of the pulmonary imaging techniques that are applied most widely to studies of pulmonary structure, function and biomechanics, and are poised for application in physiological investigations outside of imaging research.

Table 4-2. Recent Pulmonary Imaging Studies of Biomechanics

Method	Investigation Model	Imaging Biomarker	Biomechanics Measurement	Citation*
Micro-Computed Tomography				
Synchrotron radiation-based x-ray tomographic microscopy (SRXTM)	Mouse	Surface area, Volume, pressure	Acinar Deformation	Sera et al. J Appl Physiol. 2013 ¹³
Synchrotron radiation-based x-ray tomographic microscopy (SRXTM)	Mouse	Airspace morphometry	Image-derived flow simulation	Sznitman et al. J Vis 2010 ¹¹
Synchrotron radiation-based x-ray tomographic microscopy (SRXTM)	Mouse	Airspace morphometry	Image-derived flow simulation	Sera et al. Comput Methods Biomech Biomed Engin 2015 ¹²
Micro Computed Tomography	Rat	Airway diameter, Volume	Local Compliance	Sera et al. J Appl Physiol. 2004 ¹⁰
Micro Computed Tomography	Mouse	Surface area, Volume	Morphology and Function	Ford et al. J Appl Physiol 2007 ¹⁴
Micro-Computed Tomography	Mouse	Surface-to-volume ratio at different pressures	Acinar Deformation	Kumar et al. J Appl Physiol. 2013 ¹⁵
X-Ray Computed Tomography				
Xenon-enhanced Dual-energy CT	Human- asthma	Xenon wash-in and washout	Airflow	Kim et al. Am J Roentgenol. 2012 ²⁷
Xenon-enhanced Dual-energy CT	Human- COPD	Xenon wash-in (WI) and washout (WO)	WI and WO relationship to tissue expansion	Lee et al. Eur Radiol 2017 ²⁸
Inspiration-Expiration CT	Canine	Jacobian determinant	Compliance	Kaczka et al. Ann Biomed Eng 2011 ²⁰
Inspiration-Expiration CT	Human- healthy	Lobar Deformation	Lobar mechanics	Ding et al. MICCAI 2009 ²⁶
Inspiration-Expiration CT	Human- healthy and asthma	Volume change, Jacobian determinant	Deformation	Choi et al. J Appl Physiol. 2013 ¹⁶
Inspiration-Expiration CT	Human- COPD	Jacobian determinant, Deformation anisotropy	Deformation, strain	Bodduluri et al. Acad Radiol 2013 ¹⁷
Multi-volume CT	Human- healthy	Volume change, Jacobian determinant	Deformation, strain	Jahani et al. J Biomech. 2014 ²³
Inspiration-Expiration CT	Human- COPD	Jacobian determinant	Deformation	Bhatt et al. Am J Respir Crit Care Med. 2017 ¹⁹

Inspiration-Expiration CT	Human- COPD	Jacobian determinant	Deformation	Bodduluri et al. Thorax. 2017 ¹⁸
4DCT	Human- healthy	Jacobian determinant, Deformation anisotropy	Deformation, hysteresis	Jahani et al. J Appl Physiol 2015 ²⁴
4DCT	Human- healthy and asthma	Jacobian determinant, Deformation anisotropy	Deformation, hysteresis	Jahani et al. J Biomech 2017 ²⁵
Magnetic Resonance Imaging (MRI)				
Grid-tagged hyperpolarized ³ He MRI	Human- healthy, asthma, and pulmonary fibrosis	Deformation	Deformation, strain	Tustison et al, J Magn Reson Imaging. 2010 ²¹
Static Hyperpolarized ³ He ventilation	Human- healthy, asthma	Ventilation	Airflow and its relationship to mechanics	Campana et al. J Appl Physiol 2009 ³⁰
Static Hyperpolarized ³ He ventilation	Human- healthy, asthma	Ventilation	Airflow and its relationship to mechanics	Lui et al. PLoS One 2015 ²⁹
Static Hyperpolarized ³ He ventilation	Human- healthy, asthma	Ventilation	Airflow and its relationship to mechanics	Leary et al. Physiol Rep 2016 ³¹
Hyperpolarized noble gas diffusion-weighted MRI	Human- COPD	Apparent diffusion coefficient, surface area, volume	Transpulmonary pressure, elasticity	Choy et al. J Appl Physiol. 2017 ³⁷
Dynamic Hyperpolarized gas washout	Human- healthy, COPD	Specific Ventilation, alveolar oxygen tension	Airflow	Hamedani et al. Magn Reson Med 2016 ³⁴
Fourier Decomposition (FDMRI)	Human- COPD	Ventilation	Tissue Expansion	Capaldi et al. Acad Radiol 2015 ³²
Fourier Decomposition (FDMRI)	Human- asthma	Ventilation	Tissue Expansion	Capaldi et al. Acad Radiol 2107 ³³
Oxygen enhanced (OEMRI)	Human- asthma	Specific Ventilation	Airflow	Ohno et al. Radiology 2014 ³⁶
Oxygen enhanced (OEMRI)	Human- healthy	Specific Ventilation	Airflow distribution, gravitational dependence	Sa et al. J Appl Physiol 2010 ³⁵

*Citations are included in Reference section

2. Anatomical and Microstructural Imaging Biomarkers of Lung Biomechanics

As shown in Table 1 and Figure 2, the structural/anatomical and fine details of the lung airways and parenchyma can be visualized and quantified using both x-ray based and MRI-based imaging methods. Imaging provides the advantage of scalability from the laboratory

bench including *ex vivo* tissue samples and *in vivo* in small animal models to clinical research and investigations *in vivo* in individual patients. Anatomical and microstructural lung biomarkers may be dynamically acquired during tidal breathing or in static breath-hold to provide biomarkers of lung airways and parenchyma morphology. Biomarkers related to the size, shape, and morphology of the airways and parenchyma may be used in combination with computational models^{75, 76} to generate biomechanical measurements of volume, pressure, and flow of air in the lung,³⁷ and the forces generated in the process.³⁷

2.1 Biomarkers of Alveolar Morphology and Distension

Figure 2 provides an overview of lung microstructural and micromechanical measurements and how these may be combined to better understand the relationship between larger-scale mechanical properties and the mechanics of the lung microstructure. For example, high resolution (up to 2 μ m/voxel) micro-computed tomography (micro-CT) of lung tissue can be acquired using either cone beam^{48, 77} or fan-beam micro-CT systems as well using synchrotron radiation x-ray tomographic microscopy (SRXTM), which uses a linear, monochromatic beam. Using micro-CT, murine acinar ducts and alveoli may be visualized and directly measured, providing measurements acinar duct morphometry and deformation,¹⁵ as shown in Figure 3. Early *ex vivo* studies,^{10, 78} which were used to probe local tissue compliance, preceded *in vivo* studies that required respiratory and cardiac gating techniques to overcome image artefacts and blurring due to the respiratory motion of tidal or ventilated breathing.^{14, 51} Retrospective and prospective respiratory gating techniques⁷⁹ were later generated to systematically reduce motion blurring. With the development of these methods, *in vivo* micro-CT in ventilated animals⁷⁹ and small animal models of pulmonary disease¹⁴ have been performed to extend the findings revealed using *ex vivo* micro-CT of excised samples of human lung tissue.⁴² In these *in vivo* studies, the morphology and function of the lung microstructure were further studied in ventilated mice.¹⁴ Micro-CT imaging has also been exploited to investigate animal models of emphysema,⁵¹ and using xenon gas contrast enhancement to measure ventilation⁸⁰ as well as provide a detailed picture of lung microstructure^{81, 82} and mechanics in mouse models.¹⁵

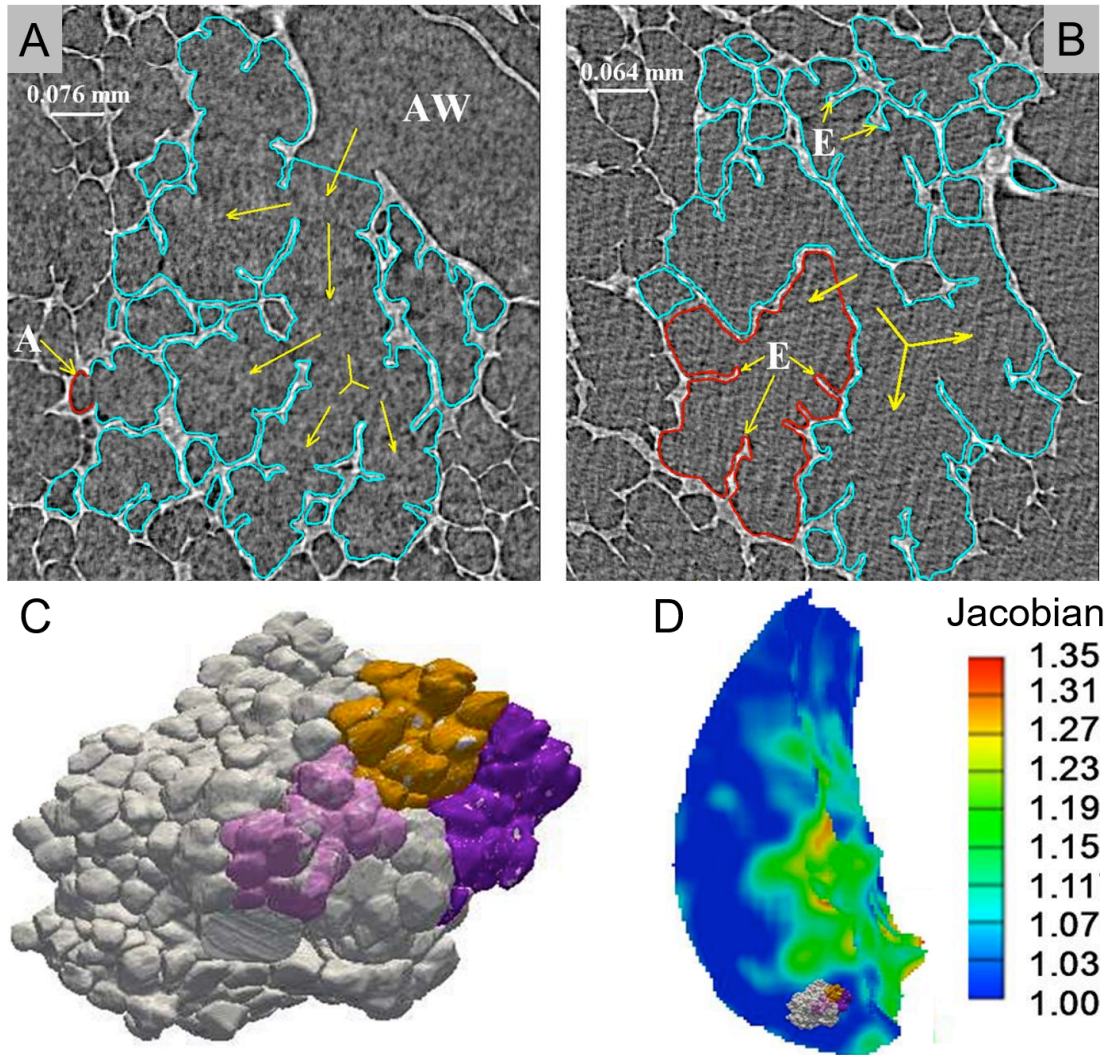


Figure 4-3. Mouse Lung Micro-CT

(A,B) Segmented micro-CT slices. In the white text, A indicates a single alveolus highlighted in red, AW indicates the airway. E indicates interalveolar septal edges. The boundary of the acinus is indicated in cyan. (C) 3D reconstruction of the acinus, with substructures highlighted in pink, orange, and purple. (D) Map of the Jacobian determinant with the acinus overlaid. (Adapted with permission from Kumar *et al.* J Appl Physiol. 2013;114(8):971-8.)¹⁵

While SRXTM has not yet been demonstrated for *in vivo* patient studies, it provides greater spatial resolution ($\sim 1 \mu\text{m}$) than micro-CT and has been used for small animal studies of lung morphometry.^{83, 84} In addition, the coherence of the synchrotron beam enables the acquisition of x-ray phase contrast imaging. The use of phase contrast provides more sensitivity to airway structure, and increases the signal-to-noise ratio of the resulting

images.⁵² Phase contrast imaging also enables imaging measurements of ventilation, which have been validated with plethysmography.⁸⁵ Rapid tomographic imaging has also been demonstrated which can have the potential to be used for 4D tomographic imaging.⁸⁶ This has been applied to mammalian studies of ventilation in the airways and the parenchyma *in vivo*.⁸⁷ As shown in Figure 4, high-resolution SRXTM images have been used in combination with computational fluid dynamics studies of aerosol deposition,^{11, 12} and in studies of lung mechanics. For example, Figure 4 shows SRXTM and volume rendered images of a mouse lung at two inflation levels,¹³ where tissue deformation can clearly be visualized and quantified. Moreover, morphometric SRXTM imaging of the mouse lung has been used to calculate the surface-to-volume ratio (S/V) at a known pressure, and deformable registration techniques were used to show that deformation of the acinus is anisotropic.¹⁵ SRXTM has also been used to image the kinematics of lung microstructure during breathing in a murine model, demonstrating directly that alveolar expansion is a heterogeneous process.¹³

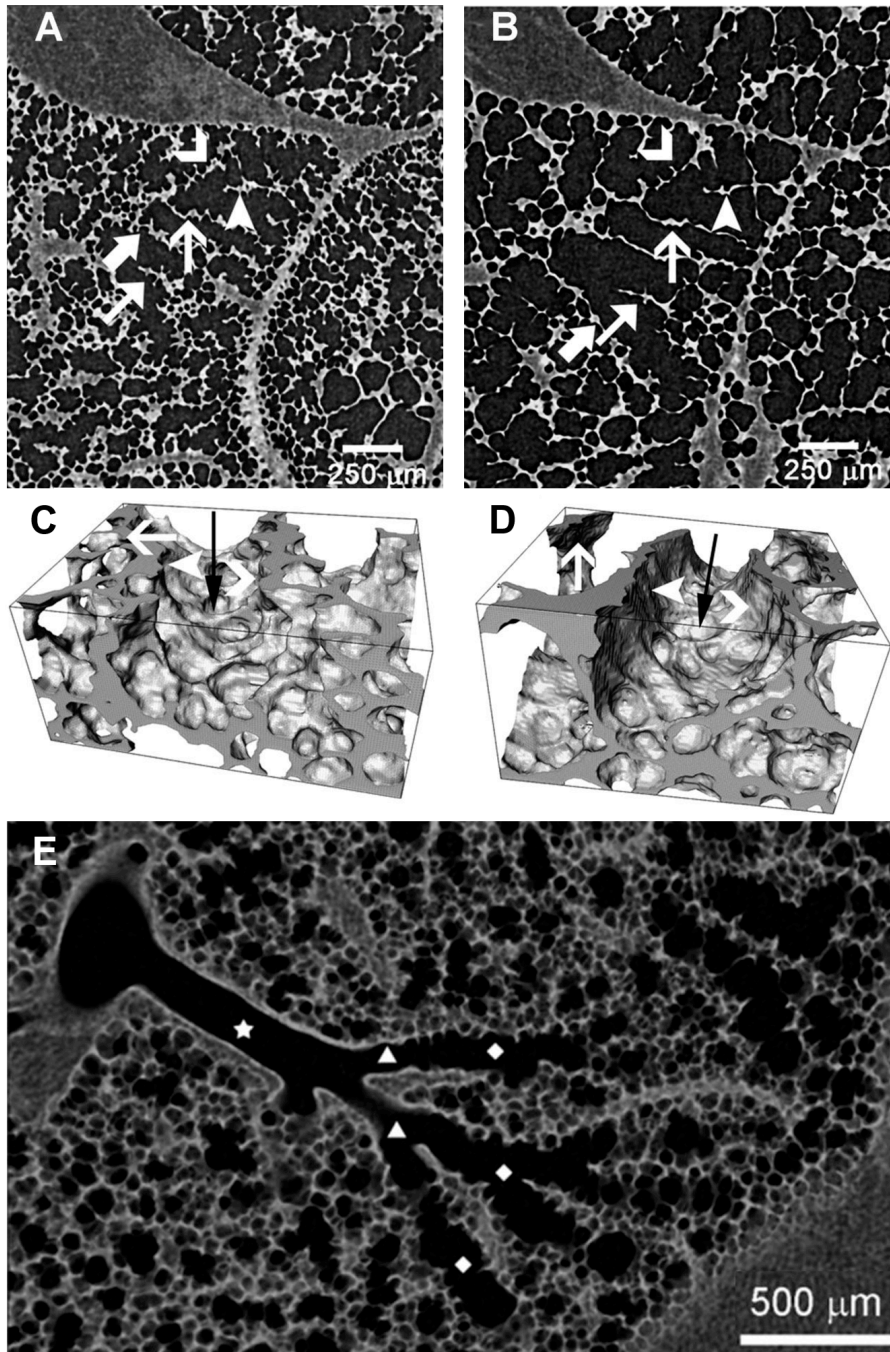


Figure 4-4 Synchrotron Radiation X-ray Micro-CT of Mouse Lung Microstructure Deformation.

Images of micro-CT (top) and volume rendering (center) of a mouse lung at FRC (A,C) and FRC+0.2L (B, D) showing deformation due to lung inflation. Arrows indicate the alveolar ducts and septa in the right and left images. (E) A volume-rendering image of a mouse lung showing a conducting airway (star), bronchioles (triangle), and alveolar ducts (diamond). (Adapted with permission from Sera *et al. J Appl Physiol.* 115, 219-28 (2013).)¹³

Recently, a technique called dark-field imaging, in which absorption, phase and dark-field images can be acquired simultaneously, has been applied in lung imaging. Dark-field image contrast is dependent on the scattering power of the sample, and it is therefore very sensitive to small structural changes in lung tissue. It has been applied in emphysematous and healthy mice,⁸⁸ and maps of emphysema generated with this technique have been verified with histology.⁸⁹ It has also shown promise for the evaluation of pulmonary fibrosis in a murine model.⁹⁰ Most recently, this technique has been applied in a living pig using clinically acceptable imaging parameters, showing the promise of dark-field imaging in human studies of lung disease.⁹¹ SRXTM and micro-CT are unique in their ability to provide non-invasive visualization and quantification of lung microstructure in small animals that would otherwise only be possible using histology. This provides the ability to study the micromechanical processes involved in breathing *in vivo*, which are implicated in important processes such as particle deposition.^{11, 12}

2.2 Biomarkers from Regional Pressure-Volume Curves

Inhaled hyperpolarized gas MRI can also be used to probe the microstructure of the lung by measuring the restricted Brownian motion of the inhaled gas in order to derive information about the size and shape of airspaces, which are abnormal in emphysema.^{73, 92, 93} This is quantified by the apparent diffusion coefficient (ADC) of the inhaled gas. This measurement has been shown to be strongly correlated with CT and histological measures of emphysema.⁹⁴ Diffusion-weighted MRI has been used to measure local ADC gradients in healthy and diseased lung. This measurement is sensitive to disease severity in COPD, providing additional insight to how COPD affects the mechanical properties of the tissue throughout the lung.⁹⁵

Using multiple b-values (related to specific gradients applied during MR imaging), other morphological values can be determined, such as the surface-to-volume ratio, airway radius, depth of the alveolar sleeve, and mean linear intercept. MRI estimates of mean linear intercept have been verified using histological measurements of the same parameter in excised tissue,^{96, 97} which is a standard measure used to evaluate emphysema.⁹⁸ Therefore, diffusion-weighted pulmonary MRI provides a way to noninvasively quantify

airspace morphometry, and *in vivo* regional quantification of emphysema severity as has been accomplished using both $^3\text{He}^{99}$ and ^{129}Xe MRI.¹⁰⁰ Figure 5 illustrates the quantification of ADC and mean linear intercept using both ^3He and ^{129}Xe imaging in an elderly never-smoker and ex-smokers with COPD, demonstrating that both ADC and mean linear intercept are elevated in COPD compared to elderly never-smokers.

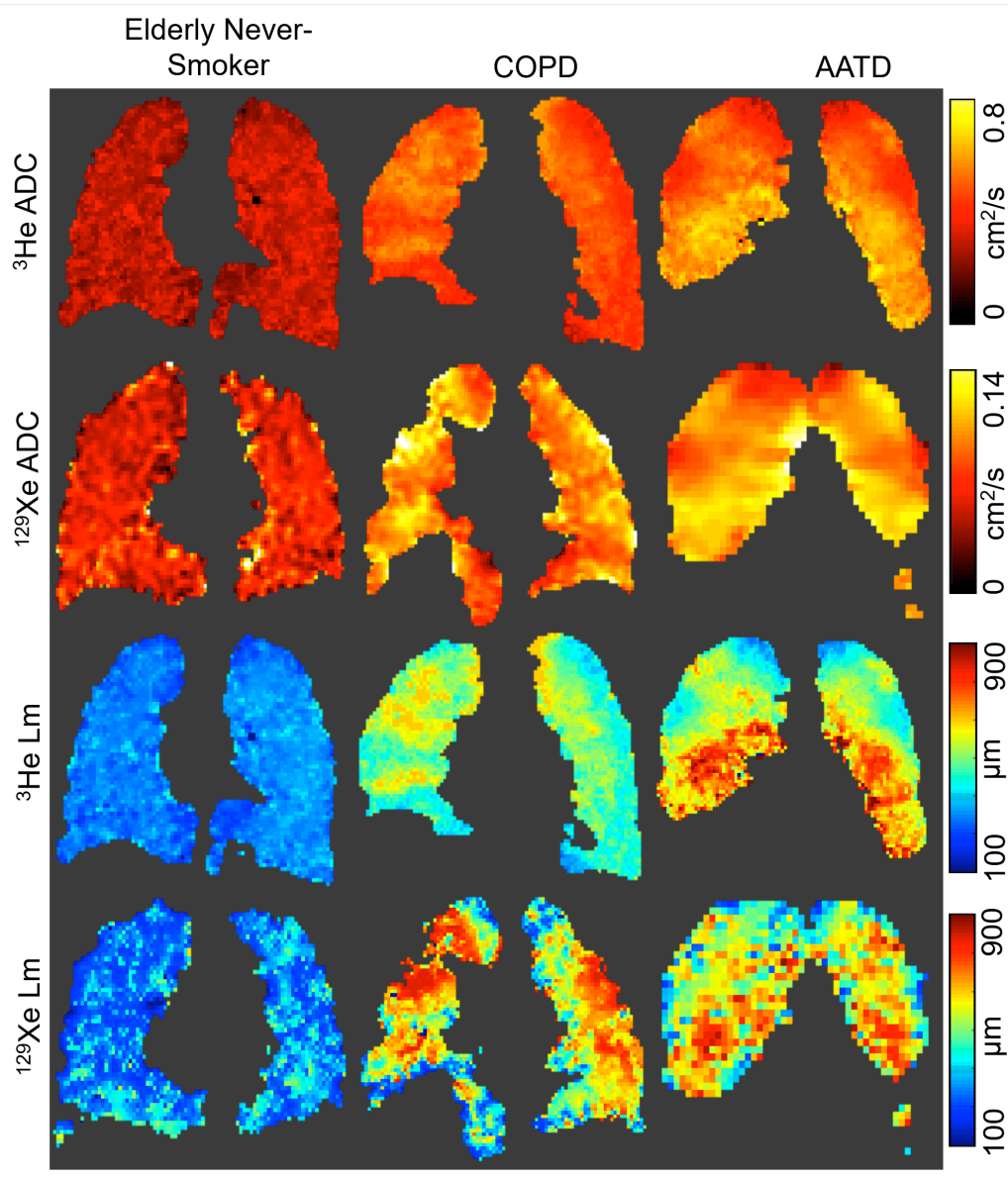


Figure 4-5. Diffusion-Weighted ^3He and ^{129}Xe MRI Mean Linear Intercept and ADC Maps

Apparent diffusion coefficient (ADC) (top) and mean linear intercept (Lm) (bottom) maps generated using hyperpolarized ^3He (upper) and ^{129}Xe (lower) measurements in an elderly never-smoker (left), an ex-smoker with COPD (center), and subject with COPD caused by Alpha-1 antitrypsin deficiency (AATD) (right).

These measurements have been used to probe biomechanics of the lung, and were shown to be sensitive to COPD grade.⁹⁵ As shown in Figure 6, diffusion-weighted MRI can probe the morphology of the airspaces to measure surface area (S) and volume (V). Using micromechanical models, these measurements can be used to calculate transpulmonary pressure (P_{tp}) and pressure-volume curves using the following equation:³⁷

$$P_{tp}(V) = \frac{N F(L)L}{3V} + \frac{2 \gamma(S)S}{3V} + \frac{n F(l) l}{3V} \quad (4.1)$$

where surface area (S) and volume (V) are derived from MRI, and the following parameters describe the model tissue network: $F(L)$ is the force exerted by the stretching of N (computed using FRC+1L lung volume) distinct line elements of length L (estimated from ADC measurements) in the parenchymal tissue, $\gamma(S)$ describes the alveolar surface tension and $F(l)$ represents the force exerted by n alveolar ducts of circumference l ^{75, 101}. The above parameters were calculated using data and relationships described by Ingenito *et al.*¹⁰¹ These microstructural and micromechanical measurements are unique in their ability to provide insight into structures too small to be directly measured *in vivo*. Using these model-derived pressure-volume curves, a ‘shape factor’ (k) can be calculated by fitting the following equation to the experimental data using an iterative least squares method:³⁷

$$V(P) = V_{max} - (V_{max} - V_{min})e^{-kP} \quad (4.2)$$

This ‘shape factor’ (k) is a volume-independent measure of pulmonary elasticity.⁷⁶ The combination of pulmonary imaging and micromechanical modeling enables *in vivo* measurements of mechanical properties of parenchymal tissue. The ability to combine these techniques provides the opportunity to further probe the relationships between pulmonary imaging biomarkers and lung biomechanics.

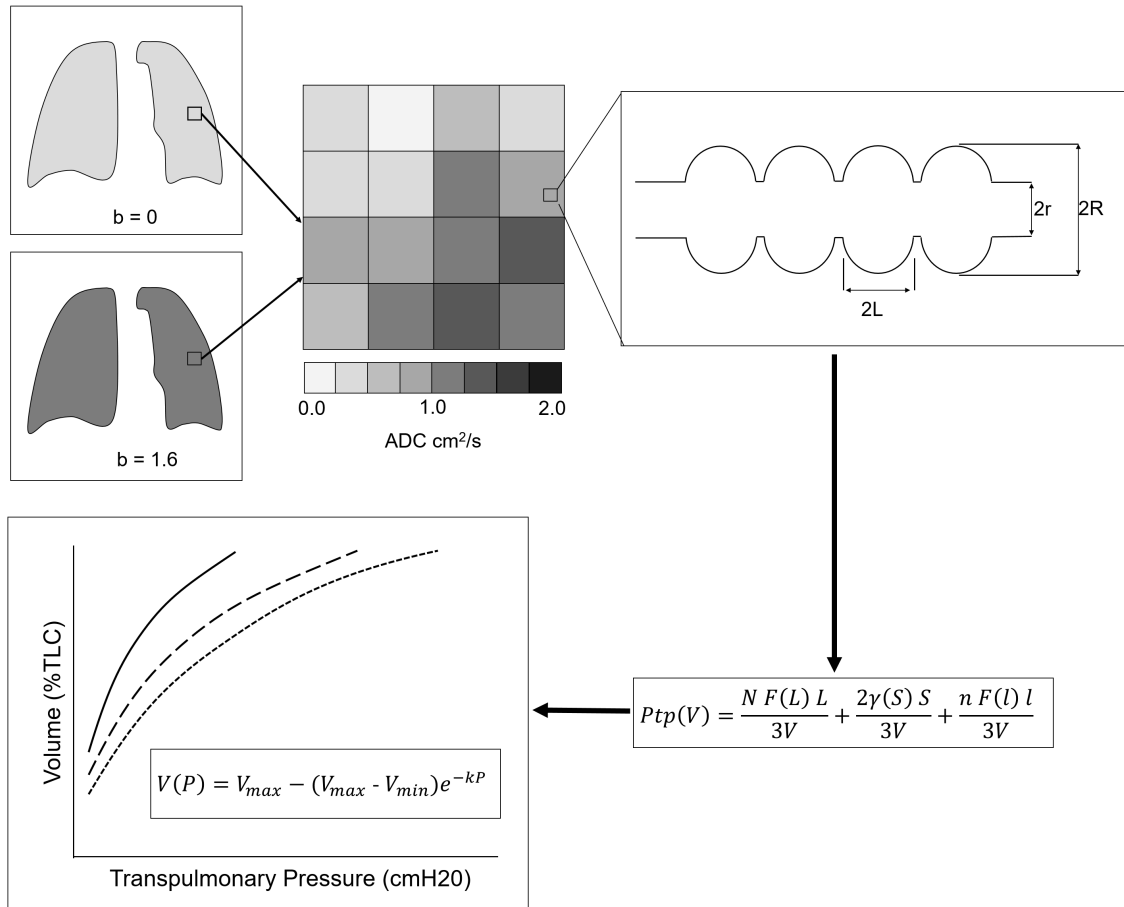


Figure 4-6. Diffusion-weighted MRI Derived Regional Pressure-Volume Curves

³He MRI was acquired with two diffusion weightings and the change in the measured signal intensity was used to calculate the apparent diffusion coefficient (ADC) on a voxel by voxel basis. ADC values were used to calculate geometric parameters of the airway, including surface area and volume, assuming the geometry shown below on the right. Using these parameters, the transpulmonary pressure (P_{tp}) was calculated using the equation shown on the bottom right, derived from micromechanical models. In this way, pulmonary pressure-volume curves (bottom left) can be derived from imaging data to probe regional pulmonary elasticity. Choy *et al.* 2010.³⁷

2.3 Biomarkers of Pulmonary Deformation during Breathing

In contrast to small animal studies, the microstructure of the human lung cannot be directly imaged *in vivo*, due to the ionizing radiation dose and size constraints associated with micro-CT. Human studies and clinical evaluations rely on the imaging of large-scale anatomical features and advanced image processing techniques to evaluate the mechanics of the lungs. CT has been used for over 30 years to evaluate the mechanics of the lung and during breathing, first in animals,^{58, 60} and later in humans.⁶¹ It was also used for early *in*

in vivo evaluations of the geometry and kinematics of breathing motion.^{57, 61, 102} As image acquisition and processing techniques have advanced, so have the imaging-derived metrics used to study mechanics. Figure 7 summarizes a number of CT-derived metrics that are currently used to evaluate lung mechanics. These include measurements of airway structure and geometry, gas trapping, global lung structure, and registration-based mechanical measurements of volume change and tissue deformation. These measurements can be used to identify imaging phenotypes, which are correlated with clinical characteristics.¹⁰³ In addition, airway measurements such as total airway length and branch count made using CT have been correlated with pulmonary function tests of lung biomechanics.^{104, 105}

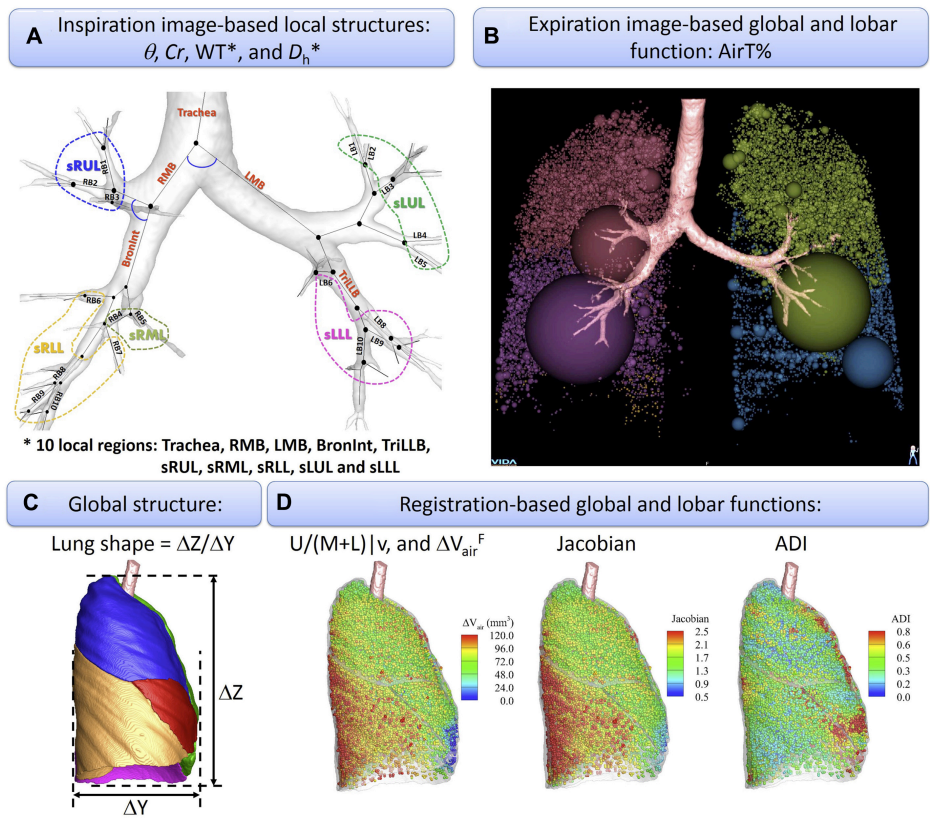


Figure 4-7. Clinical CT Measurements of Pulmonary Structure and Function

(A) An airway tree identifying structural components such as airway length and branching diameter. (B) A map of low-attenuating clusters (LAC) in an expiration CT image. (C) A segmented image identifying the size and shape of each lobe. (D) Maps of CT-derived functional biomechanical measurements. From left to right, the ratio of air-volume change in the upper lobes (U) to the middle and lower lobes (M+L), the Jacobian determinant, and the anisotropic deformation index (ADI). (Adapted with permission from Choi *et al.* J Allergy Clin Immunol (2017).)¹⁰³

By acquiring thoracic CT images at different phases in the breathing cycle (i.e. full inspiration and full expiration), anatomical biomarkers may be generated and used to quantify forces and strain within the lung. Using non-rigid or deformable image registration methods,¹⁰⁶⁻¹⁰⁸ lung deformations during the breathing cycle can be evaluated.⁶⁶ Biomarkers of lung deformation also include measures of local volume change, estimates of tissue compliance and deformation biomarkers during breathing. For example, upon co-registration of images acquired at different phases in the breathing cycle, vector maps can be created to describe local tissue deformation related to the differences in the two original images. A Jacobian matrix can be applied to this vector field (D) using the following:

$$J(x, y, z) = \begin{vmatrix} 1 + \frac{\partial D_x}{\partial x} & \frac{\partial D_x}{\partial y} & \frac{\partial D_x}{\partial z} \\ \frac{\partial D_y}{\partial x} & 1 + \frac{\partial D_y}{\partial y} & \frac{\partial D_y}{\partial z} \\ \frac{\partial D_z}{\partial x} & \frac{\partial D_z}{\partial y} & 1 + \frac{\partial D_z}{\partial z} \end{vmatrix} \quad (4.3)$$

where D_x is the x component of the vector field D, and $\partial D_x / \partial x$ is the partial derivative of D with respect to x. The determinant of the Jacobian matrix (called the Jacobian determinant) is a measure related to the change in specific volume,⁶⁷ which has been shown to reflect regional ventilation.²² Thus, the Jacobian determinant is a biomechanical measure that is directly related to lung function.

Using multi-volume CT, Jacobian biomarkers of lung deformation have been evaluated in patients with obstructive lung disease including severe asthmatics^{16, 25} and COPD participants in the COPDgene study.¹⁷⁻¹⁹ Differences and abnormal lung biomechanical properties have been quantified in severe asthmatics including a diminished volume change during breathing, suggestive of gas-trapping.¹⁶ In COPD patients, CT-derived biomarkers of lung biomechanics are sensitive to GOLD stage,¹⁷ disease progression,¹⁹ and clinical outcomes.¹⁸ Figure 8 provides an example of deformable registration of multi-volume CT whereby the Jacobian determinant of voxels within 2mm of emphysema voxels were

shown to be related to disease progression. This finding strongly suggests that biomechanical lung measurements made using CT provide a way to identify lung abnormalities that are not yet detected as emphysema.¹⁹ CT-derived deformation maps have also been used to evaluate the biomechanics of the lung lobes independently in order to gain a deeper understanding of how the lobar surfaces slide against each other during breathing.²⁶ While these techniques have been primarily applied to static images acquired at inspiration and expiration, they have recently been applied to images acquired under free-breathing conditions, as discussed further in section 3.2

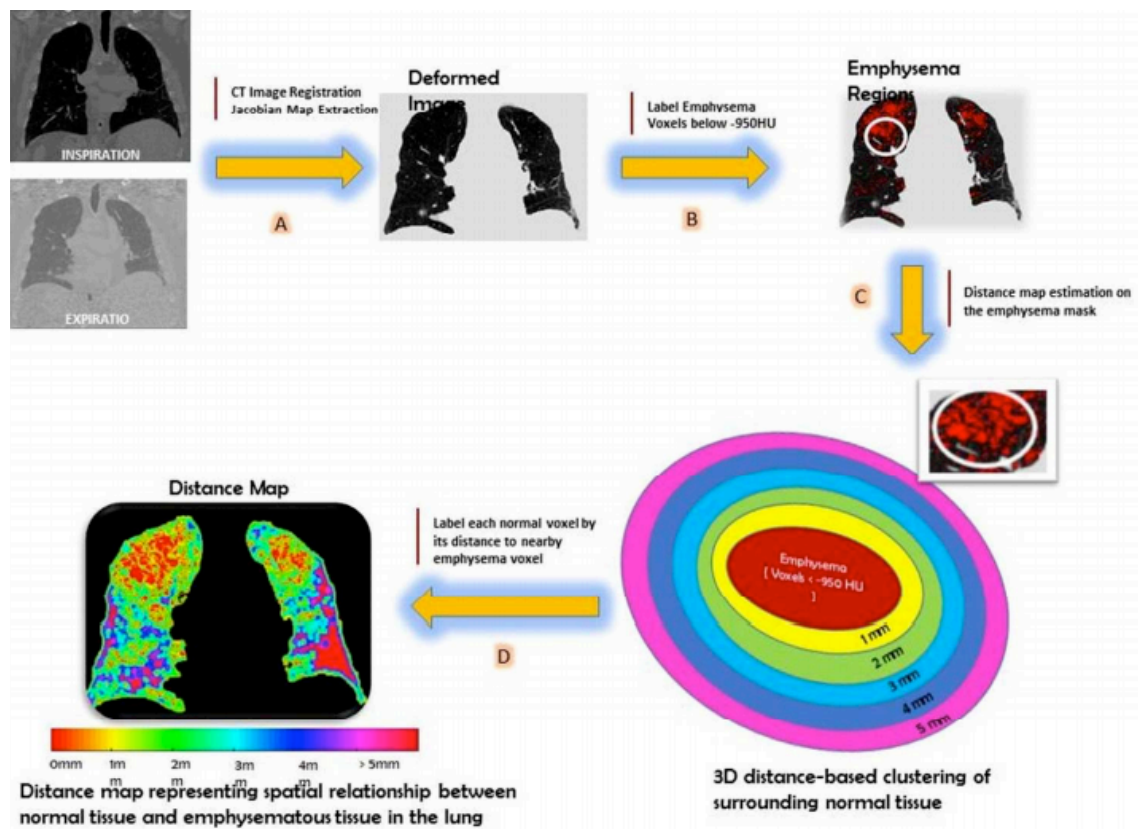


Figure 4-8. Mapping the Distance between Healthy and Emphysematous Voxels
 (A) Inspiration and expiration images are deformably co-registered. (B) Emphysematous regions in the inspiration image are identified (voxels with attenuation <-950 HU). (C) Normal tissue voxels are clustered based on their Euclidean distance to the nearest emphysema voxel. (D) Color map showing the distance of each normal voxel to the nearest emphysema voxel. (Reproduced with permission from Bhatt *et al.* Am J Respir Crit Care Med. 2017.)¹⁹

3. Functional Imaging Biomarkers of Pulmonary Biomechanics

While the primary function of the lungs is to facilitate gas exchange, the biomechanical properties of the lungs are defined by the interdependent relationships between pressure and volume that drive lung ventilation. This process can be studied using both static and dynamic imaging approaches. Here, we summarize multiple ways in which pulmonary imaging can be used to visualize and quantify ventilation.

3.1 Breath-hold Ventilation Imaging Biomarkers as Predictors of Airway Resistance

Hyperpolarized noble gas MRI is used to capture a static image of ventilation. To acquire this image, patients are instructed to inhale a known volume of hyperpolarized noble gas, and images are acquired during a 10-16 second breath-hold. Well-ventilated regions fill with hyperpolarized gas, and a bright signal is measured. However, in regions where airflow is obstructed or filling constants are longer than the 10-16 seconds necessary for image acquisition, little signal is measured and these areas appear as a dark void in the image. These dark voids are called ventilation defects, and correspond to regions of the lung that are poorly ventilated.¹⁰⁹ In this way, inhaled hyperpolarized gas MRI can be used to visualize and quantify the distribution of inhaled gas within the lungs. The normalized volume of ventilation defects in the lung is called the ventilation defect percent (VDP), and is a sensitive imaging biomarker used in research to evaluate diseases such as asthma and COPD. Figure 9 shows ^3He and ^{129}Xe static ventilation maps for a healthy never-smoker, a subject with COPD, and a subject with asthma. Pulmonary MRI can be used to identify the size, shape, and distribution of ventilation defects throughout the lung. This measurement has been validated in many disease states, and is sensitive to changes due to provocation^{110, 111} or treatment. Static ventilation measurements using hyperpolarized ^3He MRI have been used to show response to bronchodilator treatment in asthma^{112, 113} and COPD,¹¹⁴ and MRI ventilation heterogeneity has been shown to be an independent predictor of asthma control.¹¹⁵ As shown in Figure 9, ^3He and ^{129}Xe provide very similar imaging information. However, differences have been observed in both COPD¹¹⁶ and asthma.¹¹³ These differences are important for researchers to be aware of during the ongoing transition from ^3He to ^{129}Xe MRI due to restricted supply and rising costs of ^3He .¹¹⁷

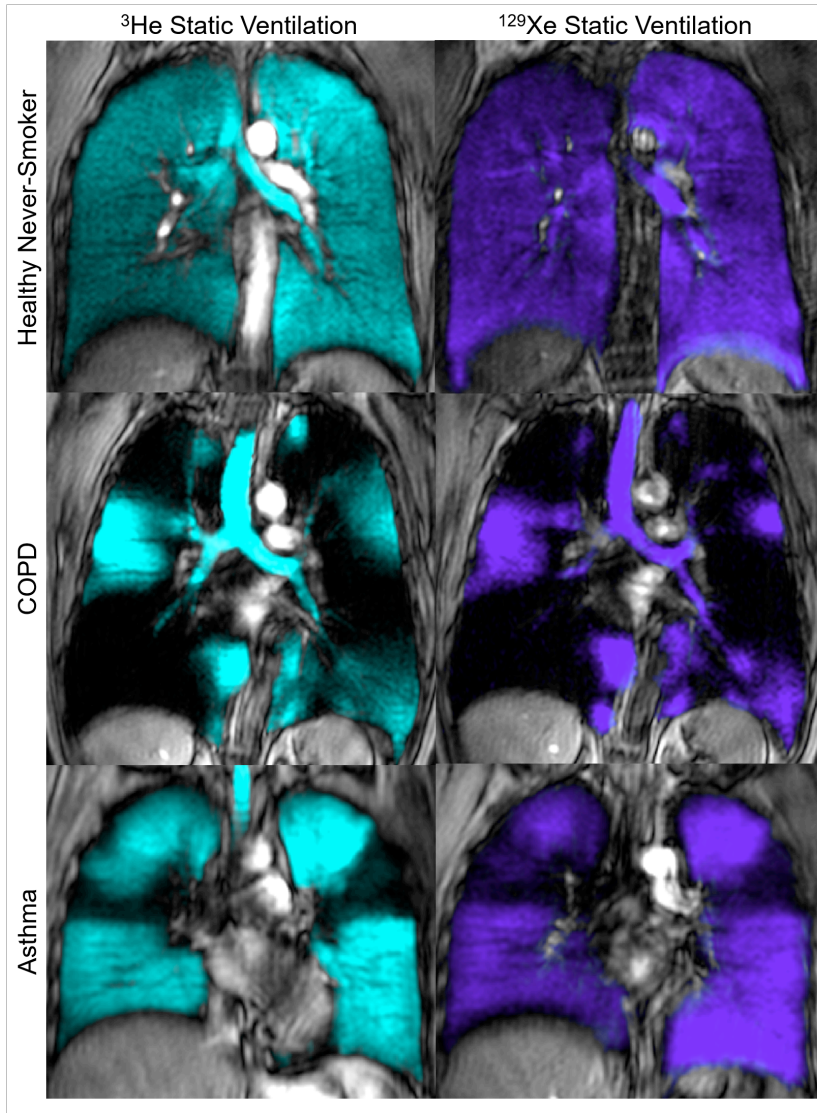


Figure 4-9. Static Breath-hold ^3He and ^{129}Xe Ventilation MRI

Hyperpolarized ^3He (left) and ^{129}Xe (right) static ventilation magnetic resonance images of a healthy never-smoker (top), an ex-smoker with COPD (center), and a subject with asthma (bottom). Helium is shown in cyan and Xenon is shown in violet co-registered to a greyscale anatomical image.

The information derived from ventilation MRI is complementary to the biomechanical information that is acquired using pulmonary function tests. In order to understand the biomechanical measurements derived from the forced oscillation technique (FOT), recent studies have used combinations of measured and model-derived lung impedance estimates and measures of MRI-derived ventilation heterogeneity in order to probe the relationships between them. Lui *et al.* demonstrated that the coefficient of variation of ^3He MRI

ventilation is significantly correlated with respiratory impedance, as well as airway hyperresponsiveness in asthma.²⁹ Hyperpolarized ³He MRI and image functional modeling have been used to study the relationship between airway closure and model-predicted ventilation distributions; these results support the hypothesis that small airway dysfunction is a crucial component of airway narrowing in ventilation defects.³⁰ In another recent study, model-predicted ventilation distributions were used to support the hypothesis that the heterogeneity of intrinsic properties of lung tissue likely contributes to heterogeneous ventilation.¹¹⁸ Patient-specific ventilation maps derived from ³He MRI have also been used with an asymmetric-branching airway tree model to generate estimates of airway impedance in asthma.³¹ The combination of ventilation MRI and computational modelling of airway mechanics provide complementary information that may provide a better understanding of the underlying biomechanical mechanisms that cause ventilation defects in obstructive lung disease.

3.2 Dynamic Ventilation Imaging of Biomechanical Changes During the Respiratory Cycle

Ventilation is a dynamic process, and this aspect of its nature can be captured in dynamic ventilation images using dual-energy xenon CT, multi-breath hyperpolarized gas MRI, oxygen-enhanced MRI, and Fourier Decomposition MRI. Xenon-enhanced CT (Xe-CT) is a free-breathing technique used to measure the wash-in and washout of inhaled xenon. Animal studies performed using this technique have shown that the time for washout is greater than for wash-in.¹¹⁹ This technique has been applied in human studies to evaluate asthma,²⁷ and has been shown to be feasible for the diagnosis of pulmonary embolism.¹²⁰ In a recent COPD study, wash-in and washout times were shown to be correlated with measures of lung tissue expansion derived from virtual, non-contrast CT images at inspiration and expiration.²⁸

Hyperpolarized noble gas MRI can also be used to acquire dynamic images of ventilation. In multi-breath wash-in MRI, the signal increase is measured as the subject inhales multiple doses of hyperpolarized ³He gas.¹²¹ In multi-breath inert gas washout imaging, the subject breathes normally after inhaling a single volume of hyperpolarized noble gas and the

decrease in signal intensity is measured as the gas is washed out of the subject's lungs.^{122,}
¹²³ Recently, both wash-in and washout imaging were combined in a single protocol, and used to evaluate healthy subjects, asymptomatic smokers, and subjects with COPD.³⁴ Using this protocol, COPD subjects and smokers were shown to have reduced mean specific ventilation as compared to healthy never-smokers. Dynamic ventilation imaging may be able to differentiate between slow-filling regions of the lung and regions where absolutely no ventilation is present, which is unattainable with static breath-hold imaging. The techniques applied to multi-volume CT imaging in section 2.3 can also be applied to images at different points in the respiratory cycle, which enables measurements of lung deformation throughout the cycle rather than only at end inspiration and end expiration²³. Using four-dimensional CT (4DCT), images are reconstructed at many points throughout the breathing cycle, and changes in volume can be measured throughout the entire process. This technique was used to show that deformation throughout the respiratory cycle is nonlinear, and demonstrates hysteresis.²⁴ This non-linearity and hysteresis have been shown to be greater in asthmatics than in healthy subjects.²⁵ 4DCT images have also been used in the development of computational fluid dynamics models to study the mechanics and dynamics of the lungs *in silico*.¹²⁴

CT deformation techniques provide unique information that is complementary to measurements derived from the forced oscillation technique in an animal model of lung injury.²⁰ In this animal study, transrespiratory pressure was also measured, and a Jacobian-based estimate for total respiratory compliance (C_{TOT}^{Jac}) was determined using the equation below.

$$C_{TOT}^{Jac} = \sum_{n=1}^N \frac{V_n}{\Delta P_{ao}} (|J_n| - 1) \quad (4.4)$$

In the above equation, n denotes a single voxel, V_n is the volume of the voxel element, ΔP_{ao} is the overall transrespiratory pressure change, and J_n is the Jacobian. Using a combination of direct mechanical measurements and pulmonary imaging, voxel-wise measurements of mechanical properties of the tissue can be made.

Using MRI, lung deformations have been measured using hyperpolarized $^3\text{He}^{71}$ and grid-tagging methods adapted from cardiac imaging.¹²⁵ First demonstrated at very low field strength (0.15T) in a healthy volunteer,¹²⁶ this was later demonstrated at clinical field strengths in healthy volunteers.^{127, 128} This technique has been adapted for 3D image acquisition and analysis, and can be used to quantify kinematics and mechanics regionally in both healthy and diseased lung.²¹ This imaging tool has been used in the development of computational modeling of respiratory motion, providing the physiological information needed to advance computational models.¹²⁹

MRI methods may also be employed that rely on the change in pulmonary proton signal measured during breathing, including oxygen-enhanced MRI (OEMRI)⁷⁴ and Fourier decomposition MRI (FDMRI).¹³⁰ Static OE imaging can be used to identify ventilation defects, or areas of low signal enhancement.⁷⁴ Recently, the feasibility of 3D isotropic OEMR imaging was demonstrated in healthy adults using an ultra-short echo time (UTE) pulse sequence.¹³¹ Dynamic OEMRI is used to measure the wash-in and washout of gas in a two-dimensional slice over time. Dynamic OEMRI measures of wash-in and washout are correlated with diffusing capacity (DL_{CO}) and FEV_1 ,¹³² and demonstrate the gravitational dependence of specific ventilation in a supine subject.³⁵ Oxygen enhanced MRI has been used to evaluate ventilation in cystic fibrosis,¹³³ COPD,¹³⁴ and asthma,³⁶ and has comparable effectiveness to CT for clinical staging and evaluation of asthma.¹³⁵ FDMRI has been investigated in several diseases including COPD, bronchiectasis and severe asthma.^{32, 33} FDMRI ventilation measurements at 3T are correlated with ^3He measurements of ventilation in COPD³² and asthma,^{32, 33} demonstrating the relationship between the signal observed in ventilation-weighted FDMRI and the ventilation distribution observed using ^3He MRI. Both of these techniques are able to probe functional changes that occur in asthma and COPD as a result of structural and mechanical changes such as tissue destruction and airway remodeling.

Figure 10 shows FDMRI in subjects with asthma, bronchiectasis, and COPD. Hyperpolarized ^3He ventilation and CT images are shown for each subject, and it is clear that ventilation defects identified using FDMRI and hyperpolarized noble gas MRI are

spatially related. This technique is particularly interesting for the study of ventilation and biomechanics because the measurements of ventilation are directly related to the mechanical expansion of the lungs.¹³⁶ This highlights the fundamental relationship between ventilation and other biomechanical properties in the lung.

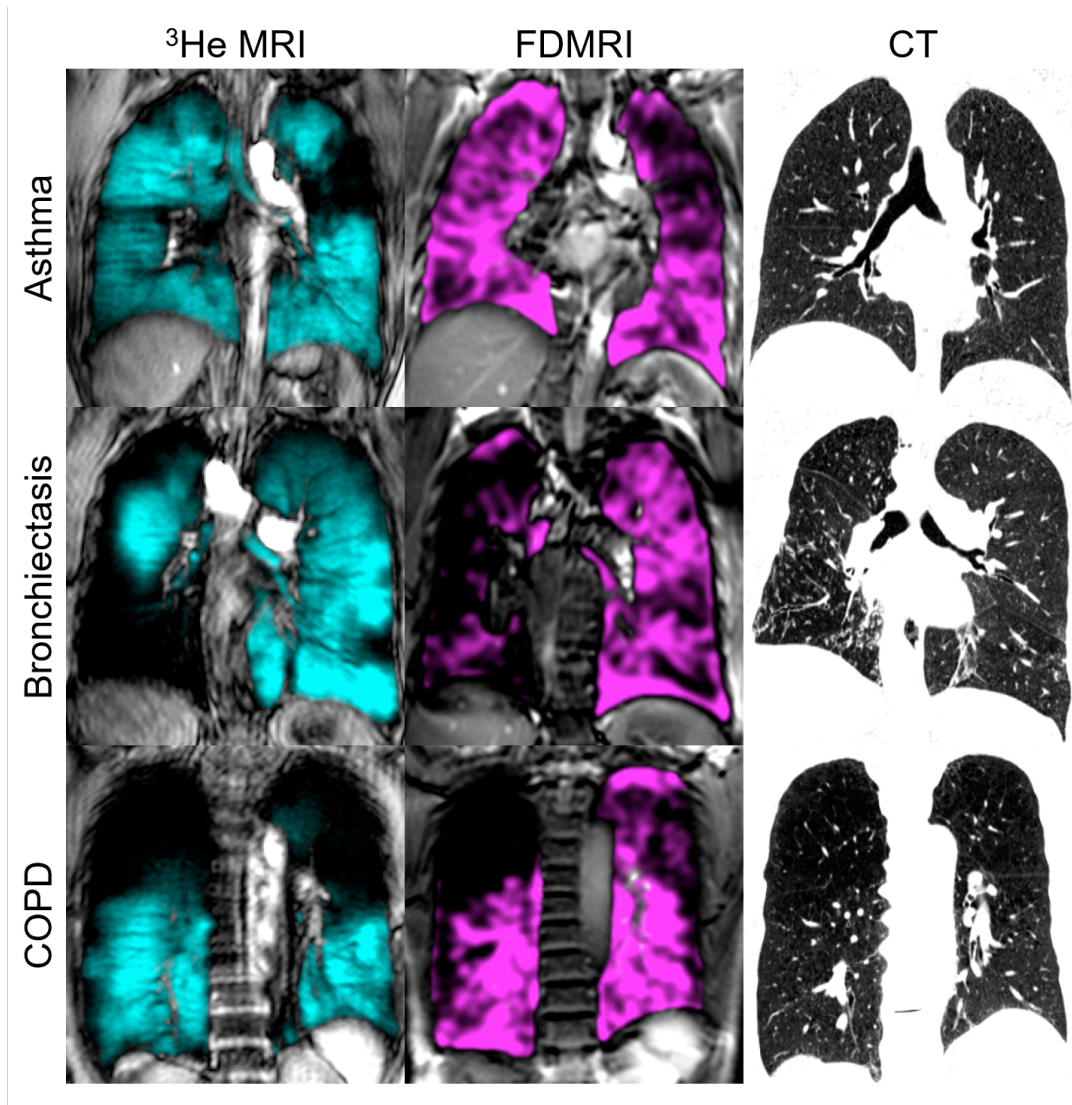


Figure 4-10. Ventilation MRI and CT of Obstructive Lung Disease

Hyperpolarized ^3He MRI (left), Fourier decomposition (FD) MRI (center) and x-ray CT of subjects with asthma (top), bronchiectasis (center), and COPD (bottom). Helium in cyan and FDMRI ventilation in magenta are co-registered to a greyscale anatomical image.

4. Discussion and Future Work

Over the past five decades, pulmonary x-ray and MRI-based imaging tools and biomarkers have been developed and applied to the study of lung biomechanics. As summarized in

Table 2, these methods have provided biomarkers and measurements stemming from *ex vivo* tissue and animal studies as well as *in vivo* investigations in small animal models and patients or healthy volunteers. In combination, functional and structural lung imaging provides a wealth of information that can be used to generate a deeper understanding of lung biomechanics. As shown in Figure 11 in 3D, co-registered functional MRI and anatomical CT images can be used to quantify abnormal airways and parenchymal tissue, identifying abnormal regions of the lung where either or both structure and function are impacted. Together, with measurements of biomechanics made at the mouth and the imaging biomarkers themselves, there is the potential for regional insights that cannot be derived by any one measurement alone. This is important because lung disease is spatially heterogeneous, and pulmonary imaging helps to identify and measure regional and local lung structure and function abnormalities. These include microstructural techniques such as micro-CT and diffusion-weighted hyperpolarized MRI, and anatomical imaging techniques such as multi-volume CT and MRI. There have also been several functional techniques developed, including static and dynamic ventilation CT and MRI techniques with or without inhaled contrast agents. More work is required and future studies will likely include the development of advanced image acquisition and processing techniques in order to develop new biomarkers that may provide a deeper understanding of lung biomechanics in health and disease. As pulmonary imaging technologies continue to improve, so should our ability to probe the relationships between the biomechanical properties of the lung tissue and structural and functional changes *in vivo*. This is important as we embark on new cell and scaffold-based therapies of lung disease that require a deeper understanding of how lung biomechanics relates to lung structure-function.

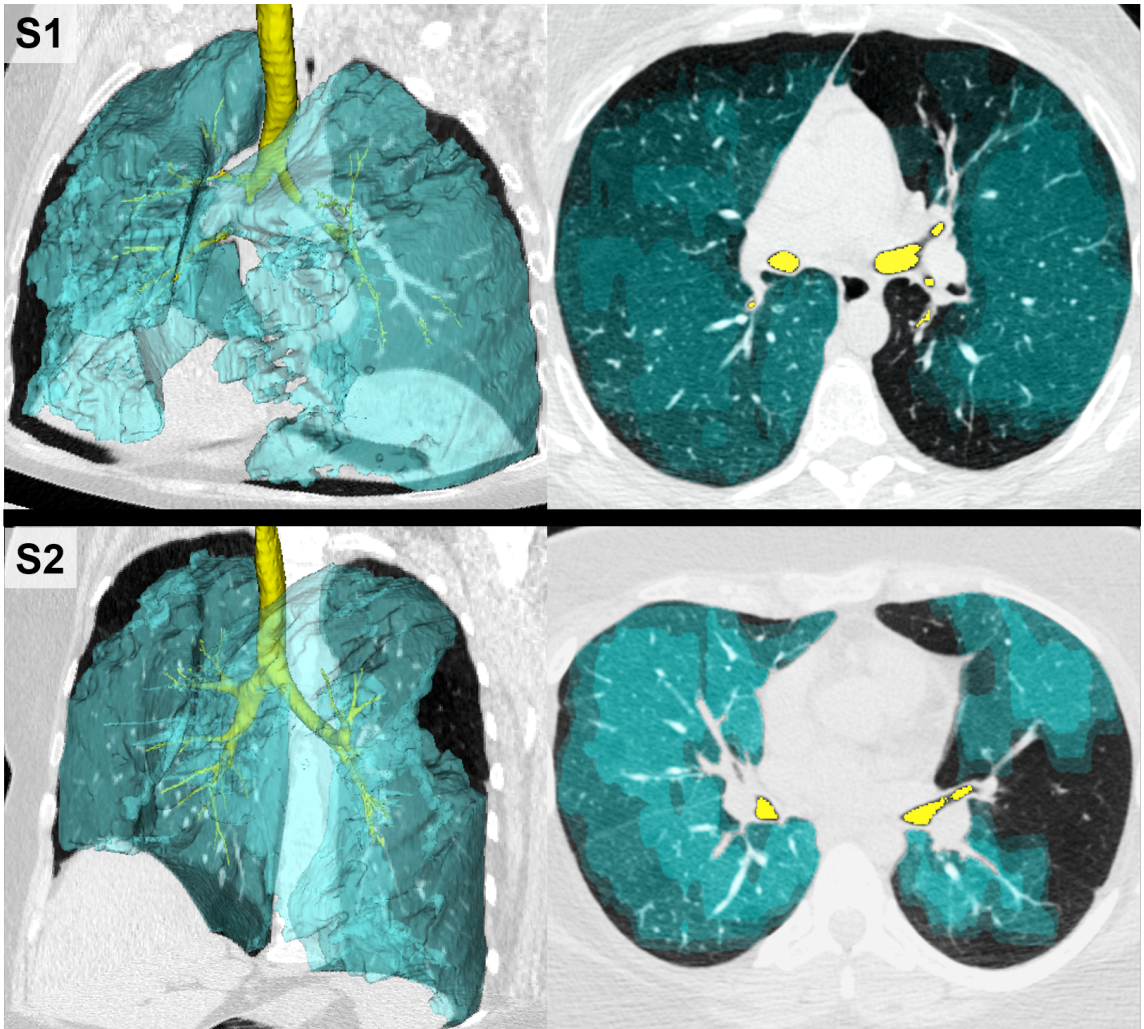


Figure 4-11. MR and CT Imaging of Lung Structure and Function

Function hyperpolarized ^3He MRI (cyan) is shown co-registered to structural CT (greyscale) with a 3D rendering of the airway tree (yellow) for two asthmatic subjects. (S1) Subject 1: female, age=30yrs, $\text{FEV1}=71\%_{\text{pred}}$, $\text{R}(5\text{Hz})=10\text{cmH}_2\text{O}^*\text{s/L}$, $\text{R}(5-19\text{Hz})=4\text{cmH}_2\text{O}^*\text{s/L}$. (S2) Subject 2: female, age=34yrs, $\text{FEV1}=50\%_{\text{pred}}$, $\text{R}(5\text{Hz})=6\text{cmH}_2\text{O}^*\text{s/L}$, $\text{R}(5-19\text{Hz})=3\text{cmH}_2\text{O}^*\text{s/L}$.

5. Conclusions

Recent advancements in thoracic imaging including x-ray based methods (micro-CT, clinical CT) as well as conventional and inhaled gas MRI provide a way to generate never-before possible biomarkers of lung structure and function. This imaging data may be acquired in tissue samples, animal models and patients and include high spatial and temporal resolution biomarkers and biomechanical information. Beyond the measurements that pulmonary function tests, multiple breath washout studies and FOT

provide, lung imaging can localize lung biomechanical abnormalities. As pulmonary imaging continues to develop and is translated into clinical use, it will continue to provide new and critically-needed insights into the relationships between lung structure, function and biomechanics.

6. References

- (1) West, J.B. *Respiratory Physiology: The Essentials* (Lippincott Williams & Wilkins, 2012).
- (2) Bates, J.H. *Lung Mechanics: An Inverse Modeling Approach* (Cambridge University Press, 2009).
- (3) Miller, M.R. et al. Standardisation of spirometry. *Eur Respir J* **26**, 319-38 (2005).
- (4) Jones, P.W. Health status and the spiral of decline. *COPD* **6**, 59-63 (2009).
- (5) Robinson, P.D. et al. Consensus statement for inert gas washout measurement using multiple- and single- breath tests. *Eur Respir J* **41**, 507-22 (2013).
- (6) Lutchen, K.R. & Gillis, H. Relationship between heterogeneous changes in airway morphometry and lung resistance and elastance. *J Appl Physiol* (1985) **83**, 1192-201 (1997).
- (7) Kaczka, D.W., Ingenito, E.P., Israel, E. & Lutchen, K.R. Airway and lung tissue mechanics in asthma. Effects of albuterol. *Am J Respir Crit Care Med* **159**, 169-78 (1999).
- (8) Oostveen, E. et al. The forced oscillation technique in clinical practice: methodology, recommendations and future developments. *Eur Respir J* **22**, 1026-41 (2003).
- (9) Tomioka, S., Bates, J.H. & Irvin, C.G. Airway and tissue mechanics in a murine model of asthma: alveolar capsule vs. forced oscillations. *J Appl Physiol* (1985) **93**, 263-70 (2002).
- (10) Sera, T. et al. Localized compliance of small airways in excised rat lungs using microfocal X-ray computed tomography. *J Appl Physiol* (1985) **96**, 1665-73 (2004).
- (11) Sznitman, J. et al. Visualization of respiratory flows from 3D reconstructed alveolar airspaces using X-ray tomographic microscopy. *J Vis* **13**, 337-345 (2010).
- (12) Sera, T., Uesugi, K., Yagi, N. & Yokota, H. Numerical simulation of airflow and microparticle deposition in a synchrotron micro-CT-based pulmonary acinus model. *Comput Methods Biomech Biomed Engin* **18**, 1427-35 (2015).
- (13) Sera, T. et al. Murine pulmonary acinar mechanics during quasi-static inflation using synchrotron refraction-enhanced computed tomography. *J Appl Physiol* (1985) **115**, 219-28 (2013).

- (14) Ford, N.L. et al. In vivo characterization of lung morphology and function in anesthetized free-breathing mice using micro-computed tomography. *J Appl Physiol (1985)* **102**, 2046-2055 (2007).
- (15) Kumar, H. et al. Multiscale imaging and registration-driven model for pulmonary acinar mechanics in the mouse. *J Appl Physiol (1985)* **114**, 971-8 (2013).
- (16) Choi, S. et al. Registration-based assessment of regional lung function via volumetric CT images of normal subjects vs. severe asthmatics. *J Appl Physiol (1985)* **115**, 730-42 (2013).
- (17) Bodduluri, S., Newell, J.D., Jr., Hoffman, E.A. & Reinhardt, J.M. Registration-based lung mechanical analysis of chronic obstructive pulmonary disease (COPD) using a supervised machine learning framework. *Acad Radiol* **20**, 527-36 (2013).
- (18) Bodduluri, S. et al. Biomechanical CT metrics are associated with patient outcomes in COPD. *Thorax* **72**, 409-414 (2017).
- (19) Bhatt, S.P. et al. CT Measure of Lung At-risk and Lung Function Decline in Chronic Obstructive Pulmonary Disease. *Am J Respir Crit Care Med* (2017).
- (20) Kaczka, D.W., Cao, K., Christensen, G.E., Bates, J.H. & Simon, B.A. Analysis of regional mechanics in canine lung injury using forced oscillations and 3D image registration. *Ann Biomed Eng* **39**, 1112-24 (2011).
- (21) Tustison, N.J. et al. Pulmonary kinematics from tagged hyperpolarized helium-3 MRI. *J Magn Reson Imaging* **31**, 1236-41 (2010).
- (22) Fuld, M. et al. CT-measured regional specific volume change reflects regional ventilation in supine sheep. *J Appl Physiol (1985)* **104**, 1177-84 (2008).
- (23) Jahani, N., Yin, Y., Hoffman, E.A. & Lin, C.L. Assessment of regional non-linear tissue deformation and air volume change of human lungs via image registration. *J Biomech* **47**, 1626-33 (2014).
- (24) Jahani, N. et al. Assessment of regional ventilation and deformation using 4D-CT imaging for healthy human lungs during tidal breathing. *J Appl Physiol (1985)* **119**, 1064-74 (2015).
- (25) Jahani, N. et al. A four-dimensional computed tomography comparison of healthy and asthmatic human lungs. *J Biomech* **56**, 102-110 (2017).
- (26) Ding, K. et al. Evaluation of Lobar Biomechanics during Respiration Using Image Registration. *Medical Image Computing and Computer-Assisted Intervention – MICCAI 2009: 12th International Conference, London, UK, September 20-24, 2009, Proceedings, Part I*, 739-746 (2009).

- (27) Kim, W.W. et al. Xenon-enhanced dual-energy CT of patients with asthma: dynamic ventilation changes after methacholine and salbutamol inhalation. *AJR Am J Roentgenol* **199**, 975-81 (2012).
- (28) Lee, S.M. et al. Assessment of regional emphysema, air-trapping and Xenon-ventilation using dual-energy computed tomography in chronic obstructive pulmonary disease patients. *Eur Radiol* **27**, 2818-2827 (2017).
- (29) Lui, J.K., Parameswaran, H., Albert, M.S. & Lutchen, K.R. Linking Ventilation Heterogeneity Quantified via Hyperpolarized ³He MRI to Dynamic Lung Mechanics and Airway Hyperresponsiveness. *PLoS One* **10**, e0142738 (2015).
- (30) Campana, L. et al. Probing airway conditions governing ventilation defects in asthma via hyperpolarized MRI image functional modeling. *J Appl Physiol (1985)* **106**, 1293-300 (2009).
- (31) Leary, D. et al. Hyperpolarized ³He magnetic resonance imaging ventilation defects in asthma: relationship to airway mechanics. *Physiol Rep* **4**, e12761 (2016).
- (32) Capaldi, D.P. et al. Free-breathing pulmonary ¹H and Hyperpolarized ³He MRI: comparison in COPD and bronchiectasis. *Acad Radiol* **22**, 320-9 (2015).
- (33) Capaldi, D.P.I. et al. Free-breathing Functional Pulmonary MRI: Response to Bronchodilator and Bronchoprovocation in Severe Asthma. *Acad Radiol* (2017).
- (34) Hamedani, H. et al. A hybrid multibreath wash-in wash-out lung function quantification scheme in human subjects using hyperpolarized ³ He MRI for simultaneous assessment of specific ventilation, alveolar oxygen tension, oxygen uptake, and air trapping. *Magn Reson Med* (2016).
- (35) Sa, R.C. et al. Vertical distribution of specific ventilation in normal supine humans measured by oxygen-enhanced proton MRI. *J Appl Physiol (1985)* **109**, 1950-9 (2010).
- (36) Ohno, Y. et al. Asthma: comparison of dynamic oxygen-enhanced MR imaging and quantitative thin-section CT for evaluation of clinical treatment. *Radiology* **273**, 907-16 (2014).
- (37) Choy, S., Wheatley, A., McCormack, D.G. & Parraga, G. Hyperpolarized (³)He magnetic resonance imaging-derived pulmonary pressure-volume curves. *J Appl Physiol (1985)* **109**, 574-85 (2010).
- (38) Weibel, E.R. & Gomez, D.M. A principle for counting tissue structures on random sections. *J Appl Physiol (1985)* **17**, 343-348 (1962).
- (39) Weibel, E.R. & Gomez, D.M. Architecture of the human lung. *Science* **137**, 577-585 (1962).

- (40) Ochs, M. A brief update on lung stereology. *J Microsc* **222**, 188-200 (2006).
- (41) Thurlbeck, W.M. et al. A comparison of three methods of measuring emphysema. *Hum Pathol* **1**, 215-226 (1970).
- (42) Watz, H., Breithecker, A., Rau, W.S. & Kriete, A. Micro-CT of the human lung: imaging of alveoli and virtual endoscopy of an alveolar duct in a normal lung and in a lung with centrilobular emphysema—initial observations. *Radiology* **236**, 1053-1058 (2005).
- (43) Hogg, J.C. et al. Micro-computed tomography measurements of peripheral lung pathology in chronic obstructive pulmonary disease. *Proc Am Thorac Soc* **6**, 546-9 (2009).
- (44) Elliott, J.C. & Dover, S.D. X-ray microtomography. *J Microsc* **126**, 211-3 (1982).
- (45) Dunsmuir, J.H., Ferguson, S., D'Amico, K. & Stokes, J. in SPE annual technical conference and exhibition (Society of Petroleum Engineers, 1991).
- (46) Coles, M., Spanne, P., Muegge, E. & Jones, K. in Proceedings of the 1994 Annual SCA Meeting 12-14 (1994).
- (47) Kapadia, R.D. et al. Applications of micro- CT and MR microscopy to study pre-clinical models of osteoporosis and osteoarthritis. *Technol Health Care* **6**, 361-372 (1998).
- (48) Rügsegger, P., Koller, B. & Müller, R. A microtomographic system for the nondestructive evaluation of bone architecture. *Calcif Tissue Int* **58**, 24-29 (1996).
- (49) McDonough, J.E. et al. Small-airway obstruction and emphysema in chronic obstructive pulmonary disease. *N Engl J Med* **365**, 1567-75 (2011).
- (50) Badea, C.T. et al. Dual-energy micro-CT of the rodent lung. *Am J Physiol Lung Cell Mol Physiol* **302**, L1088-L1097 (2012).
- (51) Ford, N. et al. Quantifying lung morphology with respiratory-gated micro-CT in a murine model of emphysema. *Phys Med Biol* **54**, 2121 (2009).
- (52) Lewis, R.A. et al. Dynamic imaging of the lungs using x-ray phase contrast. *Phys Med Biol* **50**, 5031-40 (2005).
- (53) Donnelley, M. et al. Tracking extended mucociliary transport activity of individual deposited particles: longitudinal synchrotron X-ray imaging in live mice. *J Synchrotron Radiat* **21**, 768-73 (2014).
- (54) Murrie, R.P. et al. Live small-animal X-ray lung velocimetry and lung microtomography at the Australian Synchrotron Imaging and Medical Beamline. *J Synchrotron Radiat* **22**, 1049-55 (2015).

- (55) Hounsfield, G.N. Computerized transverse axial scanning (tomography): Part 1. Description of system. *Br J Radiol* **46**, 1016-1022 (1973).
- (56) Ritman, E.L. et al. Three-dimensional imaging of heart, lungs, and circulation. *Science* **210**, 273-280 (1980).
- (57) Hubmayr, R.D., Rodarte, J.R., Walters, B.J. & Tonelli, F. Regional ventilation during spontaneous breathing and mechanical ventilation in dogs. *J Appl Physiol (1985)* **63**, 2467-2475 (1987).
- (58) Hoffman, E.A., Behrenbeck, T., Chevalier, P.A. & Wood, E.H. Estimation of regional pleural surface expansile forces in intact dogs. *J Appl Physiol (1985)* **55**, 935-948 (1983).
- (59) Hoffman, E.A. & Ritman, E.L. Effect of body orientation on regional lung expansion in dog and sloth. *J Appl Physiol (1985)* **59**, 481-91 (1985).
- (60) Rodarte, J.R., Hubmayr, R.D., Stamenovic, D. & Walters, B.J. Regional lung strain in dogs during deflation from total lung capacity. *J Appl Physiol (1985)* **58**, 164-172 (1985).
- (61) Wilson, T. et al. Geometry and respiratory displacement of human ribs. *J Appl Physiol (1985)* **62**, 1872-1877 (1987).
- (62) Coxson, H.O. et al. Computed tomography assessment of lung volume changes after bronchial valve treatment. *Eur Respir J* **32**, 1443-50 (2008).
- (63) Chapman, K.R. et al. Intravenous augmentation treatment and lung density in severe alpha1 antitrypsin deficiency (RAPID): a randomised, double-blind, placebo-controlled trial. *Lancet* **386**, 360-8 (2015).
- (64) Hayhurst, M.D. et al. Diagnosis of pulmonary emphysema by computerised tomography. *Lancet* **2**, 320-2 (1984).
- (65) Zach, J.A. et al. Quantitative computed tomography of the lungs and airways in healthy nonsmoking adults. *Invest Radiol* **47**, 596-602 (2012).
- (66) Li, B., Christensen, G.E., Hoffman, E.A., McLennan, G. & Reinhardt, J.M. Pulmonary CT image registration and warping for tracking tissue deformation during the respiratory cycle through 3D consistent image registration. *Med Phys* **35**, 5575-83 (2008).
- (67) Reinhardt, J.M. et al. Registration-based estimates of local lung tissue expansion compared to xenon CT measures of specific ventilation. *Med Image Anal* **12**, 752-63 (2008).
- (68) Wild, J.M. et al. MRI of the lung (1/3): methods. *Insights Imaging* **3**, 345-53 (2012).

- (69) Bergin, C., Pauly, J. & Macovski, A. Lung parenchyma: projection reconstruction MR imaging. *Radiology* **179**, 777-781 (1991).
- (70) Albert, M.S. et al. Biological magnetic resonance imaging using laser-polarized ^{129}Xe . *Nature* **370**, 199-201 (1994).
- (71) Ebert, M. et al. Nuclear magnetic resonance imaging with hyperpolarised helium-3. *Lancet* **347**, 1297-1299 (1996).
- (72) Mugler, J.P., 3rd et al. MR imaging and spectroscopy using hyperpolarized ^{129}Xe gas: preliminary human results. *Magn Reson Med* **37**, 809-15 (1997).
- (73) Yablonskiy, D.A. et al. Quantitative in vivo assessment of lung microstructure at the alveolar level with hyperpolarized ^3He diffusion MRI. *Proc Natl Acad Sci U S A* **99**, 3111-6 (2002).
- (74) Edelman, R.R., Hatabu, H., Tadamura, E., Li, W. & Prasad, P.V. Noninvasive assessment of regional ventilation in the human lung using oxygen-enhanced magnetic resonance imaging. *Nat Med* **2**, 1236-9 (1996).
- (75) Stamenovic, D. Micromechanical foundations of pulmonary elasticity. *Physiol Rev* **70**, 1117-34 (1990).
- (76) Eidelman, D.H., Ghezzi, H. & Bates, J.H. Exponential fitting of pressure-volume curves: confidence limits and sensitivity to noise. *J Appl Physiol (1985)* **69**, 1538-41 (1990).
- (77) Holdsworth, D., Drangova, M. & Fenster, A. A high-resolution XR-II based quantitative volume CT scanner. *Med Phys* **20**, 449-462 (1993).
- (78) Langheinrich, A.C. et al. Acute rat lung injury: feasibility of assessment with micro-CT. *Radiology* **233**, 165-71 (2004).
- (79) Ford, N.L., Wheatley, A.R., Holdsworth, D.W. & Drangova, M. Optimization of a retrospective technique for respiratory-gated high speed micro-CT of free-breathing rodents. *Phys Med Biol* **52**, 5749 (2007).
- (80) Lam, W.W. et al. Micro-CT imaging of rat lung ventilation using continuous image acquisition during xenon gas contrast enhancement. *J Appl Physiol (1985)* **103**, 1848-1856 (2007).
- (81) Kizhakke Puliyakote, A.S. et al. Morphometric differences between central vs. surface acini in A/J mice using high-resolution micro-computed tomography. *J Appl Physiol (1985)* **121**, 115-22 (2016).
- (82) Vasilescu, D.M. et al. Assessment of morphometry of pulmonary acini in mouse lungs by nondestructive imaging using multiscale microcomputed tomography. *Proc Natl Acad Sci U S A* **109**, 17105-10 (2012).

- (83) Haberthur, D. et al. Visualization and stereological characterization of individual rat lung acini by high-resolution X-ray tomographic microscopy. *J Appl Physiol (1985)* **115**, 1379-87 (2013).
- (84) Xiao, L., Sera, T., Koshiyama, K. & Wada, S. Morphological Characterization of Acinar Cluster in Mouse Lung Using a Multiscale-based Segmentation Algorithm on Synchrotron Micro-CT Images. *Anat Rec (Hoboken)* **299**, 1424-34 (2016).
- (85) Kitchen, M.J. et al. Dynamic measures of regional lung air volume using phase contrast x-ray imaging. *Phys Med Biol* **53**, 6065-77 (2008).
- (86) Lovric, G., Mokso, R., Schleputz, C.M. & Stampanoni, M. A multi-purpose imaging endstation for high-resolution micrometer-scaled sub-second tomography. *Phys Med* **32**, 1771-1778 (2016).
- (87) Dubsky, S., Hooper, S.B., Siu, K.K. & Fouras, A. Synchrotron-based dynamic computed tomography of tissue motion for regional lung function measurement. *J R Soc Interface* **9**, 2213-24 (2012).
- (88) Schleede, S. et al. Emphysema diagnosis using X-ray dark-field imaging at a laser-driven compact synchrotron light source. *Proc Natl Acad Sci U S A* **109**, 17880-5 (2012).
- (89) Yaroshenko, A. et al. Pulmonary emphysema diagnosis with a preclinical small-animal X-ray dark-field scatter-contrast scanner. *Radiology* **269**, 427-33 (2013).
- (90) Hellbach, K. et al. X-ray dark-field radiography facilitates the diagnosis of pulmonary fibrosis in a mouse model. *Sci Rep* **7**, 340 (2017).
- (91) Gromann, L.B. et al. In-vivo X-ray Dark-Field Chest Radiography of a Pig. *Sci Rep* **7**, 4807 (2017).
- (92) Snider, G.L., Kleinerman, J., Thurlbeck, W.M. & Bengali, Z.H. The definition of emphysema. Report of a National Heart, Lung, and Blood Institute, Division of Lung Diseases workshop. *Am Rev Respir Dis* **132**, 182-5 (1985).
- (93) Sukstanskii, A.L. & Yablonskiy, D.A. In vivo lung morphometry with hyperpolarized ³He diffusion MRI: theoretical background. *J Magn Reson* **190**, 200-10 (2008).
- (94) Thomen, R.P. et al. Direct comparison of ¹²⁹Xe diffusion measurements with quantitative histology in human lungs. *Magn Reson Med* **77**, 265-272 (2017).
- (95) Evans, A., McCormack, D.G., Santyr, G. & Parraga, G. Mapping and quantifying hyperpolarized ³He magnetic resonance imaging apparent diffusion coefficient gradients. *J Appl Physiol (1985)* **105**, 693-9 (2008).

- (96) Woods, J.C. et al. Hyperpolarized ^3He diffusion MRI and histology in pulmonary emphysema. *Magn Reson Med* **56**, 1293-300 (2006).
- (97) Yablonskiy, D.A. et al. Quantification of lung microstructure with hyperpolarized ^3He diffusion MRI. *J Appl Physiol (1985)* **107**, 1258-65 (2009).
- (98) Weibel, E.R., Hsia, C.C. & Ochs, M. How much is there really? Why stereology is essential in lung morphometry. *J Appl Physiol (1985)* **102**, 459-67 (2007).
- (99) Paulin, G.A. et al. Noninvasive quantification of alveolar morphometry in elderly never- and ex-smokers. *Physiol Rep* **3** (2015).
- (100) Ouriadov, A. et al. Lung morphometry using hyperpolarized (^{129}Xe) apparent diffusion coefficient anisotropy in chronic obstructive pulmonary disease. *Magn Reson Med* **70**, 1699-706 (2013).
- (101) Ingenito, E.P., Tsai, L.W., Majumdar, A. & Suki, B. On the role of surface tension in the pathophysiology of emphysema. *Am J Respir Crit Care Med* **171**, 300-4 (2005).
- (102) Margulies, S., Rodarte, J. & Hoffman, E. Geometry and kinematics of dog ribs. *J Appl Physiol (1985)* **67**, 707-712 (1989).
- (103) Choi, S. et al. Quantitative computed tomographic imaging-based clustering differentiates asthmatic subgroups with distinctive clinical phenotypes. *J Allergy Clin Immunol* (2017).
- (104) Karayama, M. et al. Respiratory impedance is correlated with morphological changes in the lungs on three-dimensional CT in patients with COPD. *Sci Rep* **7**, 41709 (2017).
- (105) Pu, J. et al. Three-dimensional airway tree architecture and pulmonary function. *Acad Radiol* **19**, 1395-401 (2012).
- (106) Yin, Y., Hoffman, E.A. & Lin, C.L. Mass preserving nonrigid registration of CT lung images using cubic B-spline. *Med Phys* **36**, 4213-4222 (2009).
- (107) Guerrero, T. et al. Quantification of regional ventilation from treatment planning CT. *Int J Radiat Oncol Biol Phys* **62**, 630-634 (2005).
- (108) Guerrero, T. et al. Dynamic ventilation imaging from four-dimensional computed tomography. *Phys Med Biol* **51**, 777 (2006).
- (109) Parraga, G. et al. Hyperpolarized ^3He ventilation defects and apparent diffusion coefficients in chronic obstructive pulmonary disease: preliminary results at 3.0 Tesla. *Invest Radiol* **42**, 384-91 (2007).

- (110) Costella, S. et al. Regional pulmonary response to a methacholine challenge using hyperpolarized (3)He magnetic resonance imaging. *Respirology* **17**, 1237-46 (2012).
- (111) Tzeng, Y.S., Lutchen, K. & Albert, M. The difference in ventilation heterogeneity between asthmatic and healthy subjects quantified using hyperpolarized 3He MRI. *J Appl Physiol (1985)* **106**, 813-22 (2009).
- (112) Altes, T.A. et al. Hyperpolarized 3He MR lung ventilation imaging in asthmatics: preliminary findings. *J Magn Reson Imaging* **13**, 378-84 (2001).
- (113) Svenningsen, S. et al. Hyperpolarized (3) He and (129) Xe MRI: differences in asthma before bronchodilation. *J Magn Reson Imaging* **38**, 1521-30 (2013).
- (114) Kirby, M. et al. Chronic obstructive pulmonary disease: quantification of bronchodilator effects by using hyperpolarized (3)He MR imaging. *Radiology* **261**, 283-92 (2011).
- (115) Svenningsen, S., Nair, P., Guo, F., McCormack, D.G. & Parraga, G. Is ventilation heterogeneity related to asthma control? *Eur Respir J* **48**, 370-9 (2016).
- (116) Kirby, M. et al. Hyperpolarized 3He and 129Xe MR imaging in healthy volunteers and patients with chronic obstructive pulmonary disease. *Radiology* **265**, 600-10 (2012).
- (117) Shea, D.A. & Morgan, D. (Congressional Research Service, Library of Congress, 2010).
- (118) Swan, A.J., Clark, A.R. & Tawhai, M.H. A computational model of the topographic distribution of ventilation in healthy human lungs. *J Theor Biol* **300**, 222-31 (2012).
- (119) Chon, D. et al. Differences in regional wash-in and wash-out time constants for xenon-CT ventilation studies. *Respir Physiol Neurobiol* **148**, 65-83 (2005).
- (120) Zhang, L.J. et al. Dual-energy CT lung ventilation/perfusion imaging for diagnosing pulmonary embolism. *Eur Radiol* **23**, 2666-75 (2013).
- (121) Hamedani, H. et al. Regional Fractional Ventilation by Using Multibreath Wash-in (3)He MR Imaging. *Radiology* **279**, 917-24 (2016).
- (122) Horn, F.C., Deppe, M.H., Marshall, H., Parra-Robles, J. & Wild, J.M. Quantification of regional fractional ventilation in human subjects by measurement of hyperpolarized 3He washout with 2D and 3D MRI. *J Appl Physiol (1985)* **116**, 129-39 (2014).
- (123) Horn, F.C., Rao, M., Stewart, N.J. & Wild, J.M. Multiple breath washout of hyperpolarized 129 Xe and 3 He in human lungs with three-dimensional balanced steady-state free-precession imaging. *Magn Reson Med* (2016).

- (124) Miyawaki, S., Choi, S., Hoffman, E.A. & Lin, C.-L. A 4DCT imaging-based breathing lung model with relative hysteresis. *J Comput Phys* **326**, 76-90 (2016).
- (125) Fischer, S.E., McKinnon, G., Maier, S. & Boesiger, P. Improved myocardial tagging contrast. *Magn Reson Med* **30**, 191-200 (1993).
- (126) Owers-Bradley, J.R. et al. MR tagging of human lungs using hyperpolarized ³He gas. *J Magn Reson Imaging* **17**, 142-6 (2003).
- (127) Cai, J. et al. MR grid-tagging using hyperpolarized helium-3 for regional quantitative assessment of pulmonary biomechanics and ventilation. *Magn Reson Med* **58**, 373-80 (2007).
- (128) Cai, J. et al. Dynamic MRI of grid-tagged hyperpolarized helium-3 for the assessment of lung motion during breathing. *Int J Radiat Oncol Biol Phys* **75**, 276-84 (2009).
- (129) Cui, T. Evaluation of Lung Ventilation Maps with Hyperpolarized Gas Tagged Magnetic Resonance Imaging and its Application towards Respiratory Motion Modeling. *Duke University* (2015).
- (130) Bauman, G. et al. Non-contrast-enhanced perfusion and ventilation assessment of the human lung by means of fourier decomposition in proton MRI. *Magn Reson Med* **62**, 656-664 (2009).
- (131) Kruger, S.J., Fain, S.B., Johnson, K.M., Cadman, R.V. & Nagle, S.K. Oxygen-enhanced 3D radial ultrashort echo time magnetic resonance imaging in the healthy human lung. *NMR Biomed* **27**, 1535-41 (2014).
- (132) Ohno, Y. et al. Dynamic oxygen-enhanced MRI reflects diffusing capacity of the lung. *Magn Reson Med* **47**, 1139-44 (2002).
- (133) Jakob, P.M. et al. Assessment of human pulmonary function using oxygen-enhanced T(1) imaging in patients with cystic fibrosis. *Magn Reson Med* **51**, 1009-16 (2004).
- (134) Ohno, Y. et al. Oxygen-enhanced magnetic resonance imaging versus computed tomography: multicenter study for clinical stage classification of smoking-related chronic obstructive pulmonary disease. *Am J Respir Crit Care Med* **177**, 1095-102 (2008).
- (135) Ohno, Y. et al. Oxygen-enhanced MRI vs. quantitatively assessed thin-section CT: pulmonary functional loss assessment and clinical stage classification of asthmatics. *Eur J Radiol* **77**, 85-91 (2011).
- (136) Zapke, M. et al. Magnetic resonance lung function--a breakthrough for lung imaging and functional assessment? A phantom study and clinical trial. *Respir Res* **7**, 106 (2006).

Appendix E – Permission for Reproduction of Scientific Articles

ELSEVIER LICENSE TERMS AND CONDITIONS

Dec 11, 2017

This Agreement between Ms. Heather Young ("You") and Elsevier ("Elsevier") consists of your license details and the terms and conditions provided by Elsevier and Copyright Clearance Center.

License Number	4245951011047
License date	Dec 11, 2017
Licensed Content Publisher	Elsevier
Licensed Content Publication	The Lancet
Licensed Content Title	Pathophysiology of airflow limitation in chronic obstructive pulmonary disease
Licensed Content Author	James C Hogg
Licensed Content Date	21–27 August 2004
Licensed Content Volume	364
Licensed Content Issue	9435
Licensed Content Pages	13
Start Page	709
End Page	721
Type of Use	reuse in a thesis/dissertation
Portion	figures/tables/illustrations
Number of figures/tables/illustrations	1
Format	both print and electronic
Are you the author of this Elsevier article?	No
Will you be translating?	No
Original figure numbers	Figure 4
Title of your thesis/dissertation	Evaluating Small Airways Disease in Asthma and COPD using the Forced Oscillation Technique and Magnetic Resonance Imaging
Expected completion date	Dec 2017
Estimated size (number of pages)	150
Requestor Location	
Total	0.00 CAD
Terms and Conditions	



Title: MRI and CT lung biomarkers:
Towards an in vivo
understanding of lung
biomechanics

Author: Heather M. Young, Rachel L.
Eddy, Grace Parraga

Publication: Clinical Biomechanics

Publisher: Elsevier

Date: Available online 29 September
2017

© 2017 Elsevier Ltd. All rights reserved.

Please note that, as the author of this Elsevier article, you retain the right to include it in a thesis or dissertation, provided it is not published commercially. Permission is not required, but please ensure that you reference the journal as the original source. For more information on this and on your other retained rights, please visit: <https://www.elsevier.com/about/our-business/policies/copyright#Author-rights>

BACK

CLOSE WINDOW

Copyright © 2017 Copyright Clearance Center, Inc. All Rights Reserved. [Privacy statement](#). [Terms and Conditions](#).
Comments? We would like to hear from you. E-mail us at customer@copyright.com

Appendix F – Health Science Research Ethics Board Approval Notices



**Western
Research**

Research Ethics

**Western University Health Science Research Ethics Board
HSREB Amendment Approval Notice**

Principal Investigator: Dr. Grace Parraga
Department & Institution: Schulich School of Medicine and Dentistry\Imaging,Robarts Research Institute

Review Type: Full Board
HSREB File Number: 6014
Study Title: Longitudinal Study of Helium-3 Magnetic Resonance Imaging of COPD (REB #15930)
Sponsor: UWO Internal Research Fund

HSREB Amendment Approval Date: June 07, 2017
HSREB Expiry Date: February 10, 2018

Documents Approved and/or Received for Information:

Document Name	Comments	Version Date
Revised Western University Protocol		2017/05/02
Letter of Information & Consent		2017/05/02

The Western University Health Science Research Ethics Board (HSREB) has reviewed and approved the amendment to the above named study, as of the HSREB Initial Approval Date noted above.

HSREB approval for this study remains valid until the HSREB Expiry Date noted above, conditional to timely submission and acceptance of HSREB Continuing Ethics Review.

The Western University HSREB operates in compliance with the Tri-Council Policy Statement Ethical Conduct for Research Involving Humans (TCPS2), the International Conference on Harmonization of Technical Requirements for Registration of Pharmaceuticals for Human Use Guideline for Good Clinical Practice Practices (ICH E6 R1), the Ontario Personal Health Information Protection Act (PHIPA, 2004), Part 4 of the Natural Health Product Regulations, Health Canada Medical Device Regulations and Part C, Division 5, of the Food and Drug Regulations of Health Canada.

Members of the HSREB who are named as Investigators in research studies do not participate in discussions related to, nor vote on such studies when they are presented to the REB.

The HSREB is registered with the U.S. Department of Health & Human Services under the IRB registration number IRB 00000940.

Ethics Officer on behalf of Dr. Joseph Gilbert, HSREB Chair

[Redacted Signature Line]

[Redacted Signature Line]



**Western
Research**

**Western University Health Science Research Ethics Board
HSREB Amendment Approval Notice**

Principal Investigator: Dr. Grace Parraga
Department & Institution: Schulich School of Medicine and Dentistry/Imaging, Robarts Research Institute

Review Type: Full Board
HSREB File Number: 103516
Study Title: Structure and Function MRI of Asthma

HSREB Amendment Approval Date: May 19, 2017
HSREB Expiry Date: February 19, 2018

Documents Approved and/or Received for Information:

Document Name	Comments	Version Date
Other	Attestation Form	2017/05/04
Increase in number of local Participants	PDF Protocol ROB0037	2017/05/04
Revised Letter of Information & Consent	Clean Copy	2017/05/19
Revised Western University Protocol	Clean Copy	2017/05/19

The Western University Health Science Research Ethics Board (HSREB) has reviewed and approved the amendment to the above named study, as of the HSREB Initial Approval Date noted above.

HSREB approval for this study remains valid until the HSREB Expiry Date noted above, conditional to timely submission and acceptance of HSREB Continuing Ethics Review.

The Western University HSREB operates in compliance with the Tri-Council Policy Statement Ethical Conduct for Research Involving Humans (TCPS2), the International Conference on Harmonization of Technical Requirements for Registration of Pharmaceuticals for Human Use Guideline for Good Clinical Practice Practices (ICH E6 R1), the Ontario Personal Health Information Protection Act (PHIPA, 2004), Part 4 of the Natural Health Product Regulations, Health Canada Medical Device Regulations and Part C, Division 5, of the Food and Drug Regulations of Health Canada.

Members of the HSREB who are named as Investigators in research studies do not participate in discussions related to, nor vote on such studies when they are presented to the REB.

The HSREB is registered with the U.S. Department of Health & Human Services under the IRB registration number IRB.00000940

Ethics Officer on behalf of Dr. Marcelo Kremenchutzky, HSREB Vice Chair



**Western University Health Science Research Ethics Board
HSREB Amendment Approval Notice**

Principal Investigator: Dr. Grace Parraga
Department & Institution: Schulich School of Medicine and Dentistry\Imaging, Robarts Research Institute

Review Type: Full Board
HSREB File Number: 104200
Study Title: Hyperpolarized Magnetic Resonance Imaging in Asthma Pre- and Post-Bronchial Thermoplasty
Sponsor: Lawson Health Research Institute

HSREB Amendment Approval Date: June 26, 2017
HSREB Expiry Date: September 03, 2017

Documents Approved and/or Received for Information:

Document Name	Comments	Version Date
Revised Western University Protocol		2017/06/26
Revised Letter of Information & Consent		2017/06/05
Other	Site Protocol Version 5	2017/06/08

The Western University Health Science Research Ethics Board (HSREB) has reviewed and approved the amendment to the above named study, as of the HSREB Initial Approval Date noted above.

HSREB approval for this study remains valid until the HSREB Expiry Date noted above, conditional to timely submission and acceptance of HSREB Continuing Ethics Review.

The Western University HSREB operates in compliance with the Tri-Council Policy Statement Ethical Conduct for Research Involving Humans (TCPS2), the International Conference on Harmonization of Technical Requirements for Registration of Pharmaceuticals for Human Use Guideline for Good Clinical Practice Practices (ICH E6 R1), the Ontario Personal Health Information Protection Act (PHIPA, 2004), Part 4 of the Natural Health Product Regulations, Health Canada Medical Device Regulations and Part C, Division 5, of the Food and Drug Regulations of Health Canada.

Members of the HSREB who are named as Investigators in research studies do not participate in discussions related to, nor vote on such studies when they are presented to the REB.

The HSREB is registered with the U.S. Department of Health & Human Services under the IRB registration number IRB 00000940.

Ethics Officer, on behalf of Dr. Marcelo Kremenchutzky, HSREB Vice Chair

Appendix G – Curriculum Vitae

EDUCATION

- 2016- Present Master of Science in Medical Biophysics (Candidate)
Department of Medical Biophysics
The University of Western Ontario, London, Canada
Supervisor: Dr. Grace Parraga
- 2011-2016 Bachelor of Science (Honours Physics, Co-operative Program)
Department of Physics
The University of Waterloo, Waterloo, Canada

POSITIONS

- 2016- Present Robarts Research Institute
London, Ontario
Graduate Research Assistant, MSc Candidate
Department of Medical Biophysics, University of Western Ontario
Supervisor: Dr. Grace Parraga
- 2015-2016 University of Waterloo
Waterloo, Ontario
Undergraduate Research Assistant
Supervisor: Dr. Melanie Campbell
Project: ‘Polarization Properties of Amyloid Beta in the Retina in
an Animal Model of Alzheimer’s Disease’
- Sept-Dec 2014,
May-Aug 2015 London Regional Cancer Program
London, Ontario
Undergraduate Co-op Student
Supervisors: Dr. Stewart Gaede, Dr. Slav Yartsev
- 2013-2014 North East Cancer Centre
Sudbury, Ontario
Undergraduate Co-op Student
Supervisor: Dr. Daniel Provost
- Jan-April 2013 SNOLAB
Lively, Ontario
Undergraduate Research Assistant
Supervisor: Dr. Chris Jillings

HONOURS AND AWARDS

- September 2017 AC Groom Graduate Seminar Award
Department of Medical Biophysics, University of Western Ontario

Awarded for the most effective presentation in Medical Biophysics Seminars given on the student's research topic.

April 2017	Trainee Stipend ISMRM 25th Annual Meeting & Exhibition (declined)
2016 - Present	Western Graduate Research Scholarship Department of Medical Biophysics, University of Western Ontario Awarded to a full time graduate student for stipend support who has maintained an average of 80% or more. Institutional (\$1,500 per term)
June 2016	Dean's Honours List University of Waterloo Awarded to a student who completed an honours undergraduate degree with an average of 80% or more. Institutional

PUBLICATIONS AND PRESENTATIONS

A Peer-Reviewed Journal Manuscripts (4)

Submitted for Publication (1)

1. HM Young, FGuo, RL Eddy, G Maksym, and G Parraga. Oscillometry and Pulmonary MRI Measurements of Ventilation Heterogeneity in Obstructive Lung Disease: Relationship to Quality of Life and Disease Control. *Submitted November 2017. J Appl Physiol.*

Published and in Press (3)

1. HM Young, RL Eddy, and G Parraga. MRI and CT Lung Biomarkers: Towards an In Vivo Understanding of Lung Biomechanics. Invited Review, Clinical Biomechanics. In Press. doi: 10.1016/j.clinbiomech.2017.09.016.
2. E Lessard, HM Young, A Bhalla, D Pike, K Sheikh, DG McCormack, A Ouriadov and G. Parraga. Pulmonary Magnetic Resonance Imaging Biomarkers of Regional Airspace Enlargement in Alpha-1 Antitrypsin Deficiency. In Press. Acad Radiol.
3. K Sheikh, A Bhalla, A Ouriadov, HM Young, CM Yamashita, TM Luu, S Katz and G Parraga. Pulmonary magnetic resonance imaging biomarkers of lung structure and function in adult survivors of bronchopulmonary dysplasia with COPD. *Cogent Medicine*, 4(1), 1282033. <https://doi.org/10.1080/2331205X.2017.1282033>

B Proffered Oral Presentations (2)

1. HM Young, DPI Capaldi, K Sheikh, DG McCormack, CM Yamashita, and G Parraga. Ultra-Short Echo Time MRI Quantification of Airspace Enlargement in Bronchopulmonary Dysplasia and Alpha-1 Antitrypsin Deficiency: Parenchyma Destruction, Air trapping or Both? Imaging Network of Ontario (ImNO), 15th Annual Imaging Network Ontario Symposium, London, Canada, March 15-16, 2017.
2. H Young, M Mulligan, K Jordan, S Gaede. Patient-Specific QA of Respiratory-Gated VMAT using a Programmable Cylindrical Respiratory Motion Insert for the

ArcCHECK™ Phantom. World Congress on Medical Physics and Biomedical Engineering 2015 Toronto ON June 7-12, 2015

C Proffered Poster Presentations (9)

1. HM Young, F Guo, RL Eddy, C Church, G Maksym and G Parraga. Forced oscillation technique and MRI predictions of airway reactance in moderate-severe asthma. ERS International Congress, Milan, Italy, September 9-13 2017.
2. HM Young, DPI Capaldi, K Sheikh, DM McCormack, CM Yamashita, and G Parraga. Quantifying Airspace Enlargement in Bronchopulmonary Dysplasia and Alpha-1 Antitrypsin Deficiency Using Ultra-Short Echo Time MRI. Robarts Research Retreat 2017. Robarts Research Institute, Western University June 20 2017.
3. A Bhalla, K Sheikh, HM Young, RL Eddy, DG McCormack, TM Luu, S Katz, G Parraga. Asthma Phenotypes in Adult Survivors of Premature Birth Using Functional Magnetic Resonance Imaging. ATS International Conference (2017).
4. Alexei Ouriadov, E Lessard, F Guo, HM Young, A Bhalla, M Kirby, H Coxson, DG. McCormack and G Parraga. Biomarkers of Emphysema in COPD and Alpha-1 Antitrypsin Deficiency: 129Xe MRI Morphomics. ATS International Conference (2017).
5. HM Young, DPI Capaldi, K Sheikh, DM McCormack, CM Yamashita, and G Parraga. Ultra-Short Echo Time MRI Quantification of Airspace Enlargement in Bronchopulmonary Dysplasia and Alpha-1 Antitrypsin Deficiency: Parenchyma Destruction, Air trapping or Both?. ISMRM 25th Annual Meeting, 6799 (2017).
6. A Ouriadov, E Lessard, F Guo, HM Young, A Bhalla, DG McCormack, and G Parraga. Accelerated Diffusion-weighted 129Xe MRI Morphometry of Emphysema in COPD and Alpha-1 Antitrypsin Deficiency Patients. ISMRM 25th Annual Meeting, 2664 (2017).
7. HM Young, DPI Capaldi, K Sheikh, DM McCormack, CM Yamashita, and G Parraga. Quantifying Airspace Enlargement in Bronchopulmonary Dysplasia and Alpha-1 Antitrypsin Deficiency Using Ultra-Short Echo Time MRI. London Health Research Day 2017. Schulich School of Medicine and Dentistry, Western University March 28 2017.
8. A. Ouriadov, E. Lessard, F. Guo, HM. Young, A. Bhalla, D.G. McCormack and G. Parraga. Accelerated Diffusion-weighted 129Xe MRI Morphometry of Emphysema. Imaging Network of Ontario (ImNO), 15th Annual Imaging Network Ontario Symposium, London, Canada, March 15-16, 2017.
9. S Gaede, HM Young, M Mulligan, K Jordan, A Programmable Moving Insert for the ArcCHECK™ Phantom for Dose Verification of Respiratory-Gated VMAT. American Association of Physicists in Medicine Annual Meeting 2016 Anaheim CA Jul 12-16, 2015.

D Submitted Abstracts (17)

1. **HM Young**, F Guo, RL Eddy, GN Maksym and G Parraga. Pulmonary MRI Measurements of Ventilation Heterogeneity in Obstructive Lung Disease: Relationship to Oscillometry, Quality of Life and Disease Control. International Society of Magnetic Resonance in Medicine Annual Scientific Meeting 2018 Paris, France June 16-21, 2018.

2. A Westcott, RL Eddy, DPI Capaldi, **HM Young**, DG McCormack and G Parraga. Quantification of Hyperpolarized 3He MRI Ventilation Heterogeneity in Asthmatics: Surface Area of Ventilation Clusters. International Society of Magnetic Resonance in Medicine Annual Scientific Meeting 2018 Paris, France June 16-21, 2018.
3. RL Eddy, **HM Young**, A Kassay, DPI Capaldi, S Svenningsen, DG McCormack and G Parraga. Contributions of Large Versus Small Airways to MRI Ventilation Heterogeneity in Asthmatics. International Society of Magnetic Resonance in Medicine Annual Scientific Meeting 2018 Paris, France June 16-21, 2018.
4. C Church, **HM Young**, G Parraga and GN Maksym. Improvements in Functional Image Impedance Modelling of Asthmatic Lungs Using K-means Clustering. ATS 2018 International Conference San Diego, CA, May 18-23, 2018.
5. A Ouriadov, DPI Capaldi, **HM Young**, M Kirby, HO Coxson, DG McCormack and G Parraga. Imaging Biomarkers of Emphysema in COPD and Alpha-1 Antitrypsin Deficiency Patients using Accelerated 129Xe MRI. ATS 2018 International Conference San Diego, CA, May 18-23, 2018.
6. HM Young, DPI Capaldi, K Sheikh, DM McCormack, CM Yamashita, and G Parraga. Quantifying Airspace Enlargement in Bronchopulmonary Dysplasia and Alpha-1 Antitrypsin Deficiency Using Ultra-Short Echo Time MRI. Robarts Research Retreat 2017. Robarts Research Institute, Western University June 20 2017.
7. HM Young, F Guo, R Eddy, C Church, G Maksym and G Parraga. Forced oscillation technique and MRI predictions of airway reactance in moderate-severe asthma. ERS International Congress, Milan, Italy, September 9-13 2017.
8. F Guo, DPI Capaldi, HM Young, A Fenster and G Parraga. Pulmonary imaging platform: towards broad clinical applications of quantitative pulmonary imaging. European Respiratory Society. ERS International Congress, Milan, Italy, September 9-13 2017.
9. HM Young, DPI Capaldi, K Sheikh, DG McCormack, CM Yamashita, and G Parraga. Ultra-Short Echo Time MRI Quantification of Airspace Enlargement in Bronchopulmonary Dysplasia and Alpha-1 Antitrypsin Deficiency: Parenchyma Destruction, Air trapping or Both? Imaging Network of Ontario (ImNO), 15th Annual Imaging Network Ontario Symposium, London, Canada, March 15-16, 2017.
10. A. Ouriadov, E. Lessard, F. Guo, HM. Young, A. Bhalla, D.G. McCormack and G. Parraga. Accelerated Diffusion-weighted 129Xe MRI Morphometry of Emphysema. Imaging Network of Ontario (ImNO), 15th Annual Imaging Network Ontario Symposium, London, Canada, March 15-16, 2017.
11. HM Young, DPI Capaldi, K Sheikh, DM McCormack, CM Yamashita, and G Parraga. Quantifying Airspace Enlargement in Bronchopulmonary Dysplasia and Alpha-1 Antitrypsin Deficiency Using Ultra-Short Echo Time MRI. London Health Research Day 2017. Schulich School of Medicine and Dentistry, Western University March 28 2017
12. HM Young, DPI Capaldi, K Sheikh, DM McCormack, CM Yamashita, and G Parraga. Ultra-Short Echo Time MRI Quantification of Airspace Enlargement in

- Bronchopulmonary Dysplasia and Alpha-1 Antitrypsin Deficiency: Parenchyma Destruction, Air trapping or Both?. ISMRM 25th Annual Meeting, 6799 (2017).
13. A Ouriadov, E Lessard, F Guo, HM Young, A Bhalla, DG McCormack, and G Parraga. Accelerated Diffusion-weighted ^{129}Xe MRI Morphometry of Emphysema in COPD and Alpha-1 Antitrypsin Deficiency Patients. ISMRM 25th Annual Meeting, 2664 (2017).
 14. A Ouriadov, E Lessard, F Guo, HM Young, A Bhalla, M Kirby, H Coxson, DG McCormack and G Parraga. Biomarkers of Emphysema in COPD and Alpha-1 Antitrypsin Deficiency: ^{129}Xe MRI Morphomics. ATS International Conference (2017)
 15. A Bhalla, K Sheikh, HM Young, RL Eddy, DG McCormack, TM Luu, S Katz, G Parraga. Asthma Phenotypes in Adult Survivors of Premature Birth Using Functional Magnetic Resonance Imaging. ATS International Conference (2017)
 16. S Gaede, HM Young, M Mulligan, K Jordan, A Programmable Moving Insert for the ArcCHECK™ Phantom for Dose Verification of Respiratory-Gated VMAT. American Association of Physicists in Medicine Annual Meeting 2016 Anaheim CA Jul 12-16, 2015.
 17. H Young, M Mulligan, K Jordan, S Gaede. Patient-Specific QA of Respiratory-Gated VMAT using a Programmable Cylindrical Respiratory Motion Insert for the ArcCHECK™ Phantom. World Congress on Medical Physics and Biomedical Engineering 2015 Toronto ON June 7-12, 2015.

COMMITTEES AND PROFESSIONAL ACTIVITIES

- 2017- Inspiring Young Women in STEM Conference 2018
Graduate Program Expo Planning Committee- Member
- 2013-2015 University of Waterloo
Undergraduate Student Representative
Department of Physics

PROFESSIONAL SOCIETIES

- 2016- American Thoracic Society
Student Member
- 2016- International Society for Magnetic Resonance in Medicine
Student Member
- 2015-2017 Canadian Association of Physicists
Student Member

LEADERSHIP, VOLUNTEER and COMMUNITY ACTIVITIES

- 2017- Planning Committee Member, Inspiring Young Women in STEM Conference 2018
- 2016-present Member, Robarts Association of Trainees
- 2015-2016 Mentor, Physics Interconnected, University of Waterloo

2015 Team Captain, University of Waterloo Orientation Week, University of Waterloo

2012-2015 Orientation Leader, University of Waterloo Orientation Week, University of Waterloo